



저작자표시-변경금지 2.0 대한민국

이용자는 아래의 조건을 따르는 경우에 한하여 자유롭게

- 이 저작물을 복제, 배포, 전송, 전시, 공연 및 방송할 수 있습니다.
- 이 저작물을 영리 목적으로 이용할 수 있습니다.

다음과 같은 조건을 따라야 합니다:



저작자표시. 귀하는 원저작자를 표시하여야 합니다.



변경금지. 귀하는 이 저작물을 개작, 변형 또는 가공할 수 없습니다.

- 귀하는, 이 저작물의 재이용이나 배포의 경우, 이 저작물에 적용된 이용허락조건을 명확하게 나타내어야 합니다.
- 저작권자로부터 별도의 허가를 받으면 이러한 조건들은 적용되지 않습니다.

저작권법에 따른 이용자의 권리는 위의 내용에 의하여 영향을 받지 않습니다.

이것은 [이용허락규약\(Legal Code\)](#)을 이해하기 쉽게 요약한 것입니다.

[Disclaimer](#)

이학박사 학위논문

Controlled ROMP
for the synthesis of polymer
having precise structures

정확한 구조를 가지는 고분자 합성을 위한
제어된 고리개환복분해중합

2014 년 8 월

서울대학교 대학원

화학과 유기화학 전공

김 경 오

Controlled ROMP
for the synthesis of polymer
having precise structures

지도 교수 최 태 립

이 논문을 이학박사 학위논문으로 제출함
2014 년 8 월

서울대학교 대학원
화학과 유기화학 전공
김 경 오

김경오의 이학박사 학위논문을 인준함
2014 년 8 월

위 원 장 홍 순 혁 (인)

부위원장 최 태 립 (인)

위 원 손 병 혁 (인)

위 원 이 연 (인)

위 원 Rudolf. Zentel (인)

Abstract

Ring opening metathesis polymerization (ROMP) is one of the most popular polymerization technique for the synthesis of well-defined polymers with diverse functionalities. One of the attractive point of ROMP is that living (controlled) polymerization is possible. Using this point, extensive research has been done to prepare various polymers having precise structures. However, still there are many challenges to be improved such like introducing new functional monomers and development of more complex nanostructures.

This thesis describes the synthesis of polymers having precise structures by controlled ROMP and possible features as a nano-sized material. Firstly, the conformation control of dendronized polymer was done by changing the generation of dendrons, linker moiety, and back bone structure. The single chain conformation was analyzed by MALLS analysis and visualized by AFM imaging technique. As a result, rigid rod-like conformation was obtained using high generation (G5) of dendrons or TD based macromonomers, and all these homopolymerization showed living manner. Using this living ROMP of NB and TD monomers, block and gradient copolymerization could be achieved by conventional sequential addition method and batch method, respectively. Resulting two copolymers showed clear structural difference, existence of boundary, from the AFM image. This successful and first example of synthesis of gradient copolymer by batch method via ROMP was possible because of different reactivity between two monomers. According to the kinetic study, TD monomer does faster initiation and slower propagation compare with conventional monomer NB. It increase the k_i/k_p ratio and enable the controlled ROMP even with

slow initiating but stable 2nd generation Grubbs and Hoveyda–Grubbs catalysts. With this advantage, three–arm star polymer was synthesized by core first method via ROMP for the first time. In addition, controlled ROMP of monomer containing alkyne moiety was achieved without protection group due to the fast initiation of TD monomers. Lastly, various block copolymers (BCP) were prepared using living ROMP of NB and TD based monomers, to fabricate polymer nanostructures. Large size domain structure was obtained from dendronized BCPs under the comparatively mild condition due to the extended conformation and large size of dendrons. In the case of BCP with PA block, thermally/mechanically stable nanocaterpillar structure was obtained during the polymerization by strong $\pi - \pi$ interaction between conjugated polymers. Also, redox responsive self–assembly was demonstrated from the BCP containing ferrocene moiety.

Keywords

ring opening metathesis polymerization (ROMP),
living polymerization, dendronized polymer,
polymer single chain structure, polymer nanostructure

Student Number

2010–30089

Contents

Abstract	i
Contents	iii
List of Schemes	v
List of Tables.....	vii
List of Figures.....	ix
Chapter 1 : Introduction	
1.1 Ring opening metathesis polymerization (ROMP)	1
1.2 Thesis research	5
1.3 References	7
Chapter 2 : Conformation Control of Polymer and Single-chain Analysis	
2.1 Introduction	9
2.2 Experimental	12
2.3 Results and Discussion	
2.3.1 Different generation of ester type dendron	19
2.3.2 Different backbone structure	30
2.3.3 <i>endo</i> -tricyclo[4.2.2.0 ^{2,5}]deca-3,9-diene monomer	34
2.4 Conclusion	42
2.5 References	43
Chapter 3 : Structural Analysis of Copolymers using 1D Rod-like Dendronized Polymer	
3.1 Introduction	46
3.2 Experimental	48
3.3 Results and Discussion	
3.3.1 Diblock copolymerization.....	50
3.3.2 Gradient copolymerization	54
3.3.3 Comparison the structure of two copolymers	60
3.4 Conclusion	62

3.5 References	63
Chapter 4 : Controlled ROMP of TD Based Monomers	
4.1 Introduction	64
4.2 Experimental	68
4.3 Results and Discussion	
4.3.1 Living ROMP using 2 nd generation Grubbs and 2 nd generation Hoveyda–Grubbs catalysts	75
4.3.2 Three–arm star polymer	86
4.3.3 Controlled ROMP of monomer containing alkyne moiety	90
4.4 Conclusion	100
4.5 References	101
Chapter 5 : Fabrication of Polymer Nanostructure using ROMP polymer	
5.1 Introduction	104
5.2 Experimental	106
5.3 Results and Discussion	
5.3.1 BCP with two kinds of dendrons	110
5.3.2 Insitu nanoparticlization of conjugated polymer (INCP)	116
5.3.3 Self–assembly behavior of BCP containing ferrocene	126
5.4 Conclusion	133
5.5 References	134
Abstract in Korean	136
Abstract in German	138
Acknowledgement	140

List of Schemes

Scheme 1–1. Mechanism of ROMP	1
Scheme 1–2. Chain transfer reaction during ROMP	3
Scheme 2–1. Synthesis route for NB macromonomers with ester type dendrons	14
Scheme 2–2. Synthesis route for TD macromonomers with ester type dendrons	15
Scheme 2–3. Synthesis route for NB macromonomers with fr�chet type dendrons	16
Scheme 2–4. ROMP of NB macromonomers	19
Scheme 2–5. Synthesis of brush polymers	27
Scheme 2–6. Backbone controlled polymerization of NB macromonomers	31
Scheme 2–7. ROMP of TD macromonomers	34
Scheme 3–1. Synthesis of diblock copolymers	51
Scheme 3–2. Synthesis of gradient copolymers	54
Scheme 4–1. Competition between alkenes and alkynes for reaction with a metathesis catalyst	67
Scheme 4–2. Synthesis of tri–functionalized catalyst	72
Scheme 4–3. ROMP of TD monomers 14–16	75
Scheme 4–4. Synthesis of three–arm polymers	86

Scheme 4–5. Result of three–arm diblock copolymerization	88
Scheme 4–6. Structure of NB monomers containing alkyne moiety and scheme for polymerization and post– functionalization	90
Scheme 4–7. ROMP of TD monomers containing alkyne moiety.	93
Scheme 5–1. Synthesis route for TD macromonomers with ether type dendrons	107
Scheme 5–2. ROMP of COT and undesired benzene formation.	116
Scheme 5–3. Polymerization scheme for (a) block copolymer and (b) gradient copolymer containing ferrocene	126

List of Tables

Table 2–1. ROMP of NB based macromonomers	21
Table 2–2. Molecular weight control of poly(4)	22
Table 2–3. The shape parameter data of poly(1)–(5)	24
Table 2–4. Result of backbone controlled polymerization	32
Table 2–5. ROMP of TD based macromonomers	35
Table 3–1. Results of block copolymerization	52
Table 3–2. Results of gradient copolymerization	56
Table 4–1. ROMP of monomers using catalyst II–IV	76
Table 4–2. Kinetic parameter for monomers by three catalysts.	79
Table 4–3. ROMP of various TD monomers using catalyst IV ...	83
Table 4–4. Results of diblock copolymerization	84
Table 4–5. Results of three–arm polymerization	86
Table 4–6. ROMP result of NB monomers containing alkyne moiety	91
Table 4–7. Result of post–functionalization of poly(26) by click reaction	92
Table 4–8. ROMP of TD monomers containing alkyne moiety ..	94
Table 4–9. Post–functionalization of poly(28) via Cu–catalyzed azide–alkyne cycloaddition	98

Table 5–1. Molecular weight information of dendronized BCPs	111
Table 5–2. ROMP of COT for PA BCPs	117
Table 5–3. Molecular weight information of copolymers containing ferrocene.....	127

List of Figures

Figure 1–1. Typical monomers and ruthenium based catalysts for ROMP	2
Figure 1–2. Example of living ROMP for synthesis of block copolymer.....	4
Figure 2–1. Three kinds of synthetic route for dendronized polymer	9
Figure 2–2. The plots for M_n vs $[M]/[I]$ for poly(3)–(4)	21
Figure 2–3. GPC trace of poly(3)–(5)	24
Figure 2–4. Conformation plot and Mark–Houwink–Sakurada plot of poly(1)–(5)	25
Figure 2–5. AFM images of poly(1)–(5) on mica surface	26
Figure 2–6. AFM image of poly(NBPCL) and poly(NBPLA)	28
Figure 2–7. Conformation plot and Mark–Houwink–Sakurada plot of brush polymers	29
Figure 2–8. Possible backbone structures from NB	30
Figure 2–9. AFM image of poly(5) and poly(10)	33
Figure 2–10. GPC traces of poly(6)–(9)	36
Figure 2–11. The M_n control for poly(9)	37
Figure 2–12. Conformation plot of poly(6)–(9)	39
Figure 2–13. The plot of persistence length vs Flory exponent	39
Figure 2–14. AFM images of poly(6)–(9) on mica surface	40

Figure 3-1. Types of various copolymers	46
Figure 3-2. Conformation comparison of diblock copolymers with different block ratio	50
Figure 3-3. GPC traces of poly(13)- <i>b</i> -poly(9) and poly(8)- <i>b</i> - poly(13)	52
Figure 3-4. AFM images of poly(13)- <i>b</i> -poly(9) and poly(8)- <i>b</i> - poly(13)	53
Figure 3-5. Monomer conversion profiles for poly(14)- <i>g</i> -poly(15) and poly(9)- <i>g</i> -poly(13)	55
Figure 3-6. Determination of reactivity ratio of monomer 14 and 15 by Fineman-Ross equation	55
Figure 3-7. GPC traces of gradient copolymers	56
Figure 3-8. Plot for monomer consumption vs time during initiation step	58
Figure 3-9. Schematic explanation for the steric on NB and TD during initiation	58
Figure 3-10. AFM images of gradient copolymers	59
Figure 3-11. Structural difference between single chains of block copolymer and gradient copolymer	61
Figure 3-12. Conformation plot of diblock copolymer and gradient copolymer	61
Figure 4-1. Plots of molecular weight vs $[M]/[I]$ for monomer 14 & catalyst IV and monomer 16 & catalyst II	78
Figure 4-2. GPC traces of poly(14)-(15) polymerized by three catalysts	78
Figure 4-3. GPC traces of poly(16)	79

Figure 4-4. Determination of the rate constant for monomers 14 - 16 by three catalysts	82
Figure 4-5. Schematic explanation for the steric on NB and TD during initiation and propagation	82
Figure 4-6. GPC traces of poly(17)- <i>b</i> -(18) and poly(14)- <i>b</i> -(15)	84
Figure 4-7. AFM image of star polymers with various [M]/[I] ratio and average length of arm	88
Figure 4-8. GPC traces of three-arm diblock poly(22) ₁₀₀ - <i>b</i> -(8) ₁₀₀	89
Figure 4-9. AFM image of three-arm diblock poly(22) ₁₀₀ - <i>b</i> -(8) ₁₀₀ and its height profile	89
Figure 4-10. GPC traces and plot of reaction time vs $-\ln([M]/[M]_0)$ of poly(28)	96
Figure 4-11. ¹ H NMR spectra and IR spectra and GPC traces of poly(28) and poly(28a') and poly(28a) after the post-functionalization	99
Figure 5-1. Structure of fully dendronized BCPs	110
Figure 5-2. Morphology change of BCP(3) after thermal annealing at 70 °C for 12 h. Photomicrograph and AFM topography	111
Figure 5-3. Photomicrograph of dendronized BCPs	112
Figure 5-4. Solvent dependent solubility and micellization of BCP6	113
Figure 5-5. AFM image of BCP(6) from the various solvents ..	113
Figure 5-6. TEM image of BCP(6) from the various solvents ..	115

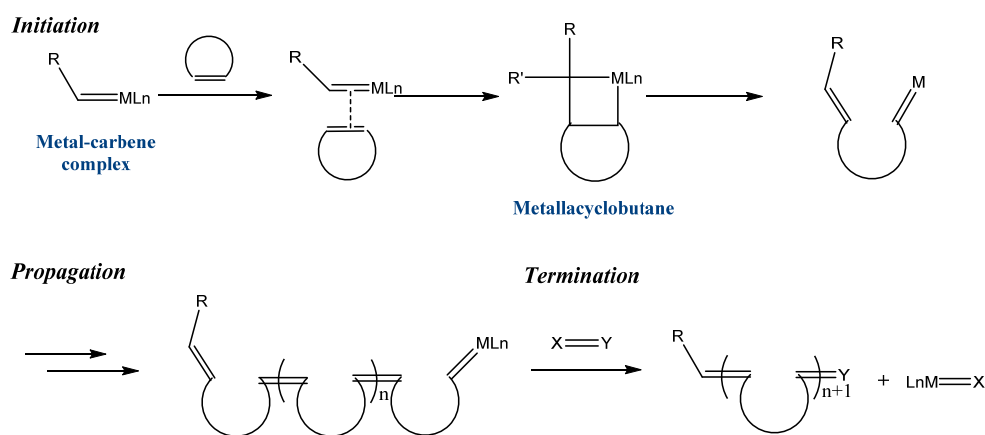
Figure 5–7. Thin film morphology of BCP(6) from THF solution by AFM and TEM after thermal annealing	115
Figure 5–8. UV/vis spectrum in chloroform and cyclic voltammogram of PA BCP(5)	120
Figure 5–9. Size comparison of PA BCPs containing various length of PA block	120
Figure 5–10. WAXS plot of PA BCP(5)	121
Figure 5–11. AFM images of the nanostructures from PA BCPs synthesized at various temperature	121
Figure 5–12. AFM images of the nanostructures with various lengths of PA block	121
Figure 5–13. AFM and TEM images of nanocaterpillar	124
Figure 5–14. Proposed mechanism for <i>in situ</i> nanoparticlization of PN- <i>b</i> -PA into nanocaterpillars (INCP)	125
Figure 5–15. GPC trace of poly(17)- <i>b</i> -(20) from THF and chloroform solution	127
Figure 5–16. Oxidation and reduction of ferrocene moiety	128
Figure 5–17. UV/vis spectrum and DLS profile of copolymers containing ferrocene in THF	129
Figure 5–18. AFM image of Fc BCPs after redox reaction	130
Figure 5–19. AFM image of poly(32)- <i>b</i> -(20) for detailed microstructure	131
Figure 5–20. TEM image of copolymers containing ferrocene after redox reaction	132

Chapter 1.

Introduction

1.1 Ring opening metathesis polymerization (ROMP)

Ring opening metathesis polymerization (ROMP), which is one of the family reaction of olefin metathesis, is a well-established polymerization technique for the synthesis of well-defined functional polymers.¹ The origins of ROMP is traced back to the middle of 1950s, but rapid progress in popularity and utility of this polymerization technique is came from extensive work on the identification of key intermediates² and well-defined catalysts³ in the late 20th century.



Scheme 1-1. Mechanism of ROMP.

The ROMP is chain-growth polymerization and the mechanism is based on olefin metathesis reaction, a metal-mediated carbon-carbon double bond exchange process (Scheme 1-1).⁴ It is

general view that the reaction progress follow by Chauvin' s proposal.⁵ The reaction is initiated primarily through the coordination of cyclic olefin monomer to the metal–carbene complex. After that, highly strained metallacyclobutane is formed as an intermediate, and new metal–carbene complex is generated to the direction for reducing the ring strain. Analogous reactions are repeated during the propagation step, and terminate by special reagent which can selectively remove and deactivate the transition metal from the end of the growing polymer chain. The driving force of ROMP is the relief of ring strain in cyclic system. The most common monomers possess large enough ring strain (> 5 kcal/mol) with cyclic olefin such like norbornene (NB), cyclobutene (Figure 1–1).⁶

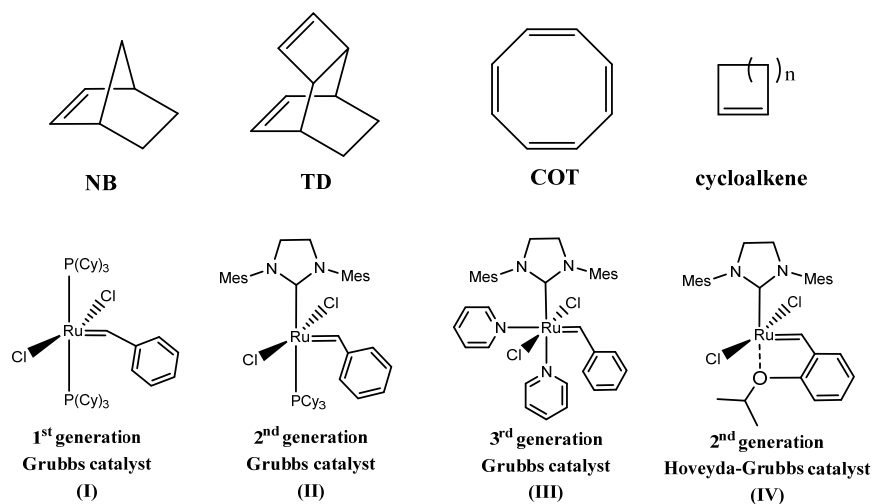
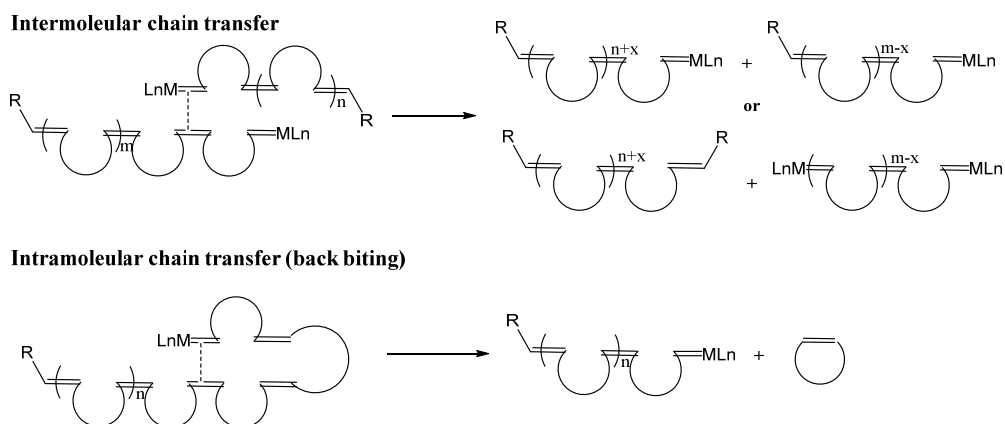


Figure 1–1. Typical monomers and ruthenium based catalysts for ROMP.

Various kinds of catalysts were developed to enhance the utility of ROMP, including titanium,⁷ tungsten,⁸ molybdenum,^{3a} ruthenium.^{3b–d} Among them, molybdenum (Mo) and ruthenium (Ru) based catalysts, developed by Schrock and Grubbs respectively, are the most popular because of the well–defined system and high reactivity with broad range of functional group tolerance. Especially,

Mo catalysts are good for stereo-selective polymerization. On the other hand, Ru catalyst is easier to handle because of high stability toward air or moisture. In addition, living polymerization, which is one of the attractive point of ROMP, is possible when a proper combination of monomer and catalyst is accomplished.⁹ For example, the ROMP of norbornene with 3rd generation Grubbs catalyst (III) or Schrock catalyst are well-known living polymerization.



Scheme 1–2. Chain transfer reaction during ROMP.

Living polymerization is defined as a polymerization process without chain transfer or termination, according to the Swarcz's first description.¹⁰ To achieve the living polymerization, initiation rate should be much faster than chain propagation rate, and every side reactions should be excluded. Possible side reactions in metathesis manner during ROMP are depicted in scheme 1–2. Those chain transfer reaction can be reduced by increasing the steric hindrance on olefin or reducing the catalyst reactivity by lowering the temperature.¹¹ As a result, the number of propagating species is maintained constantly during the polymerization. In the controlled polymerization, the synonym of living polymerization, chain transfer or termination is suppressed but not completely excluded. At any rate,

under both living/controlled condition, synthesis of desired polymers with controlled molecular weight and narrow polydispersity index (PDI) is possible.¹²

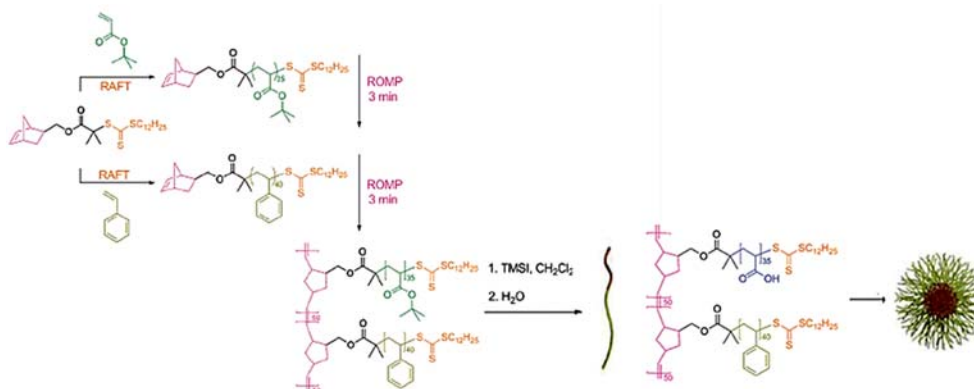


Figure 1–2. Example of living ROMP for synthesis of block copolymer.

The ROMP with these features enable to prepare well-defined copolymers including block and graft copolymers, and various other polymeric materials with useful functionalities. For example, Grubbs and Wooley reported the synthesis of graft block copolymer by combination of ROMP and radical polymerization, and its self-assembly into lamellar or micelle structures (Figure 1–2).¹³ Another example is that the synthesis of telechelic polymer using chain transfer agent (CTA) to introduce the interactive motifs and form the supramolecular polymer.¹⁴ Also, conjugated polymers like polyphenylenevinylene (PPV),¹⁵ polythienylenevinylene (PTV),¹⁶ polyacetylene (PA)¹⁷ can be prepared by living ROMP.

1.2 Thesis research

As we mentioned above, ROMP is versatile tool for synthesis of various kinds of polymers with precise structure and useful functionalities. Recent research on ROMP has been focused on obtaining more well-defined and diverse macromolecular architectures and polymer nanostructures. Following chapters describes examples for the synthesis of polymers having precise and complex structures by controlled ROMP and possible features as a nano-sized material.

Chapter 2 demonstrates the conformation control of dendronized polymer by changing the generation of dendrons, linker moiety, and back bone structure, to realize the extended polymer. The rigid rod-like conformation was obtained using high generation (G5) of dendrons or TD based macromonomers. The single chain conformation was analyzed by MALLS analysis and visualized by AFM imaging technique.

Chapter 3 describes the synthesis of block and gradient copolymers and structural comparison. The block copolymer was obtained by conventional sequential addition method, and the gradient copolymer was obtained by batch method using NB and TD as a co-monomer. This gradient copolymerization was possible because of different reactivity between two monomers. Resulting copolymers showed structural difference, existence of boundary, in AFM image.

Chapter 4 introduced the living character of TD based monomers, originated from its structural merit. Owing to the faster initiation and slower propagation compare with conventional monomer NB, living ROMP was achieved even with slow initiating but stable 2nd generation Grubbs and Hoveyda-Grubbs catalysts. Using this advantage, three-arm star polymer was synthesized by core

first method for the first time. In addition, controlled ROMP of monomer containing alkyne moiety was achieved without protection group. This polymer could do further post-functionalization via Copper-catalyzed azide-alkyne cycloaddition (CuAAC).

Chapter 5 describes the synthesis of various block copolymers (BCP) to fabricate polymer nanostructures. Large domain structure was obtained from extended dendronized BCPs under the comparatively mild condition. In the case of BCP with PA block, stable nanocaterpillar structure was obtained during the polymerization by strong $\pi-\pi$ interaction between conjugated polymers. Lastly, redox responsible self-assembly was demonstrated from the BCP containing ferrocene moiety.

1.3 References

- [1] (a) Calderon, N. *J. Macromol. Sci. Rev. Macromol. Chem.* **1972**, *7*, 105. (b) Novak, B. M.; Risse, W.; Grubbs, R. H. *Adv. Polym. Sci.*, **1992**, *102*, 47. (c) Ivin, K. J.; Mol, J. C. “*Olefin metathesis and metathesis Polymerization*” San Diego, Academic Press, **1997**. (d) Buchmeiser, M. R. *Chem. Rev.*, **2000**, *100*, 1565.
- [2] (a) Chauvin, Y. *Angew. Chem. Int. Ed.*, **2006**, *45*, 3740. (b) Schrock, R. R. *Angew. Chem. Int. Ed.*, **2006**, *45*, 3748. (c) Grubbs, R. H. *Angew. Chem. Int. Ed.*, **2006**, *45*, 3760.
- [3] (a) Schrock, R. R.; Murdzek, J. S.; Bazan, G. C.; Robbins, J.; DiMare, M.; O'Regan, M. *J. Am. Chem. Soc.*, **1990**, *112*, 3875. (b) Nguyen, S. T.; Johnson, L. K.; Grubbs, R. H.; Ziller, J. W. *J. Am. Chem. Soc.*, **1992**, *114*, 3974. (c) Bielawski, C. W.; Grubbs, R. H. *Angew. Chem. Int. Ed.*, **2000**, *39*, 2903. (d) Love, J. A.; Sanford, M. S.; Day, M. W.; Grubbs, R. H. *J. Am. Chem. Soc.*, **2003**, *125*, 10103.
- [4] (a) Calderon, N. *Acc. Chem. Res.*, **1972**, *5*, 127. (b) Calderon, N.; Ofstead, E. A.; Judy, W. A. *Angew. Chem. Int. Ed.*, **1976**, *15*, 401.
- [5] Hérisson, J. L.; Chauvin, Y. *Makromol. Chem.*, **1971**, *141*, 161.
- [6] Benson, S. W.; Cruickshank, F. R.; Golden, D. M.; Haugen, G. R.; O'Neal, H. E.; Rodgers, A. S. *Chem. Rev.*, **1969**, *69*, 279.
- [7] (a) Tebbe, F. N.; Parshall, G. W.; Reddy, G. S. *J. Am. Chem. Soc.*, **1978**, *100*, 3611. (b) Tebbe, F. N.; Parshall, G. W.; Ovenall, D. W. *J. Am. Chem. Soc.*, **1979**, *101*, 5074.
- [8] (a) Rocklage, S. M.; Fellmann, J. D.; Rupprecht, G. A.; Messerly, L. W.; Schrock, R. R. *J. Am. Chem. Soc.*, **1981**, *103*, 1440. (b) Kress, J.; Wesolek, M.; Osborn, J. A. *Chem. Commun.*, **1982**, 514.
- [9] (a) Bielawski, C. W.; Grubbs, R. H. *Prog. Polym. Sci.*, **2007**, *32*, 1. (b) Bielawski, C. W.; Grubbs, R. H. “*Controlled and living polymerizations*” Weinheim, Germany, Wiley-VCH, **2009**.
- [10] (a) Szwarc, M. *Nature*, **1956**, *178*, 1168. (b) Darling, T. R.; Davis, T. P.; Fryd, M.; Gridnec, A. A. *J. Polym. Sci. A. Polym. Chem.*, **2000**, *38*, 1706.
- [11] Choi, T. -L.; Grubbs, R. H. *Angew. Chem., Int. Ed.*, **2003**, *42*, 1743.

- [12] (a) Flory, P. J. *J. Am. Chem. Soc.*, **1940**, *62*, 1561. (b) Matyjaszewski, K. *Macromolecules*, **1993**, *26*, 1787.
- [13] (a) Xia, Y.; Olsen, B. D.; Kornfield, J. A.; Grubbs, R. H. *J. Am. Chem. Soc.*, 2009, *131*, 18525. (b) Li, A.; Ma, J.; Cheng, C.; Zhang, K.; Wooley, K. L. *Macromolecules*, **2010**, *43*, 1182.
- [14] Higley, M. N.; Pollino, J. M.; Hollembeak, E.; Weck, M. *Chem. Eur. J.*, **2005**, *11*, 2946.
- [15] (a) Conticello, V. P.; Gin, D. L.; Grubbs, R. H. *J. Am. Chem. Soc.*, **1992**, *114*, 9708. (b) Yu, C. Y.; Turner, M. L. *Angew. Chem., Int. Ed.*, **2006**, *45*, 7797.
- [16] Horie, M.; Shen, I. W.; Tuladhar, S. M.; Leventis, H.; Haque, S. A.; Nelson, J.; Saunders, B. R.; Turner, M. L. *Polymer*, **2010**, *51*, 1541.
- [17] Swager, T. M.; Dougherty, D. A.; Grubbs, R. H. *J. Am. Chem. Soc.*, **1988**, *110*, 2973.

Chapter 2.

Conformation Control of Polymer and Single-chain Analysis

2.1 Introduction

Dendronized polymers are unique macromolecules that are composed of dendrons attached to polymer backbone.¹ These polymers have many advantages because one can design a polymer with a precisely controlled molecular architecture and desired properties by tuning the polymer backbone and the dendritic wedge independently. Also, the conformation of these polymers can be controlled from entangled to extended conformation by varying the steric effect of the dendrons, and the single chains of these polymers can be easily visualized using atomic force microscopy (AFM) imaging techniques.² Hence, dendronized polymers are considered as new materials for a wide range of applications in fields of biomaterials,³ drug delivery,⁴ electronics⁵ and energy storage.⁶

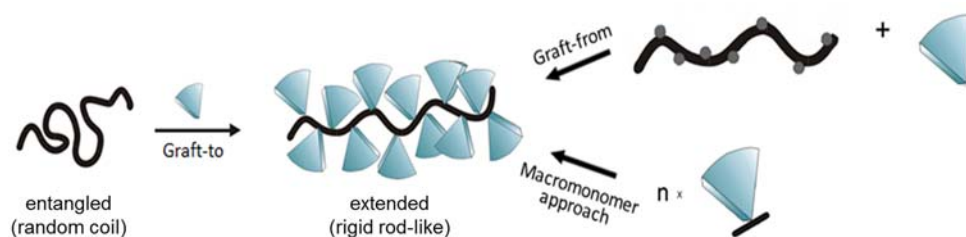


Figure 2-1. Three kinds of synthetic route for dendronized polymer.

Despite the great potential of dendronized polymers, their synthesis still proves to be challenging; hence, a more general method for both synthesis and controlling molecular weight with narrow polydispersity (PDI) of such polymers is desired. There are three synthetic routes for preparing dendronized polymers; graft-to,⁷ graft-from,⁸ and the macromonomer approach.⁹ The graft-to approach is most frequently used method and graft-from approach also good for long and high generation of dendronized polymers, but both approach inevitably contain defects, because the complete coverage of dendrons, especially for the high-generation ones is synthetically challenging. The synthesis of dendronized polymers by macromonomer approach has following advantages over alternative methods. Firstly, dendronized polymers prepared from purified macromonomers are defect-free structures. Moreover, the macromonomer approach enables the direct synthesis of block copolymers by the sequential addition of the monomers.^{9a} However, a prominent drawback of this approach is that the polymerization of macromonomers having high-generation (higher than G3) dendrons with high degree of polymerization (DP) is difficult because of their bulky side chains that hinder propagation.⁹ Moreover, the living polymerization of the macromonomers is extremely challenging because unfavorable reactions such as chain termination and chain transfer outcompete the chain propagation. For instance, dendronized polymers up to G2 were synthesized by living radical polymerization such as atom transfer radical polymerization (ATRP) and reversible addition-fragmentation transfer (RAFT) polymerization. However, from the macromonomers beyond G2, only low molecular weight polymers with broad polydispersity index (PDI) were obtained.^{9b}

Recently, ROMP has been considered as one of the most

efficient methods for synthesizing dendronized polymers and graft polymers (bottle-brush)^{9c} because the typical monomer, NB derivatives, are very reactive due to the large ring strain and highly active catalysts have been developed. For this reason, the polymers having G3 dendrons were prepared by living ROMP using 3rd generation Grubbs catalyst.¹⁰

With the high generation of dendronized polymers, we can get the highly extended polymer chain which can give different properties such like ordering, morphology, or physical behavior.¹¹ In addition, dendronized polymers have more delicate structure with stiffer polymer chain compare with cylindrical brush polymer even they are regarded as a similar kinds in terms of topology. The extension or stiffness of polymer chain depends on several parameters including generation and structure of dendrons, space between dendron and backbone, and structure of polymer backbone.¹² The control of stiffness and conformation of polymer by changing parameters was studied both in theoretically and experimentally.¹³ However, there are not many systematic studies and really extended rod-like structures were hard to obtain. The AFM image of dendronized single polymers shows aggregated or entangled structure more than expected.

2.2 Experimental

2.2.1 General considerations

All reagents which are commercially available were used without further purification. Solvents for monomer synthesis were also commercially obtained: toluene was anhydrous ($\geq 99.8\%$) grade and tetrahydrofuran (THF) was anhydrous ($\geq 99.9\%$) grade from Sigma–Aldrich®. For polymerization, THF was distilled from sodium and benzophenone. The solvents were degassed 10 minutes before using on polymerization. Thin–layer chromatography (TLC) was carried out on MERCK TLC silica gel 60 F254 and the flash column chromatography was performed using MERCK silica gel 60 (0.040~0.063 mm).

^1H –NMR and ^{13}C –NMR were recorded by Varian/Oxford As–500 (500 MHz for ^1H and 125 MHz for ^{13}C) and Bruker (300 MHz for ^1H and 75 MHz for ^{13}C) spectrometers. The molecular mass of monomers was measured by Bruker Daltonics autoflex II TOF/TOF. Dithranol and Ag–TFA 1:1 mixture in THF was used as a matrix. High resolution mass spectroscopy (HRMS) analysis were performed by the National Center for Inter–University Research Facility and elemental analyses were performed with a Perkin–Elmer 2400 Series II CHN analyzer. Gel permeation chromatography (GPC) for polymer molecular weight analysis was carried out with Waters system (1515 pump) and Shodex GPC LF–804 column eluted with THF (GPC grade, Honeywell Burdick & Jackson®). Samples in 0.001–0.003 wt% THF were filtered with a 0.45– μm PTFE filter before injection. Flow rate was 1.0 mL/min and temperature of column was maintained at 35 °C. For the conventional measurement Waters 2414 refractive index detector was used, and Wyatt triple detector, Dawn 8⁺ / Viscostar II/ Optilab T–rEX were used for the

MALLS–VIS–RI analysis. Multimode head and Nanoscope IV controller (Veeco Instrument) were used for AFM imaging. All images were obtained on tapping mode using non–contact mode tip from Nanoworld (Pointprobe® tip, NCHR type) with spring constant of 42 N m⁻¹ and tip radius of ≤8nm.

2.2.2 Synthesis of Monomers

NB–ester dendron macromonomers

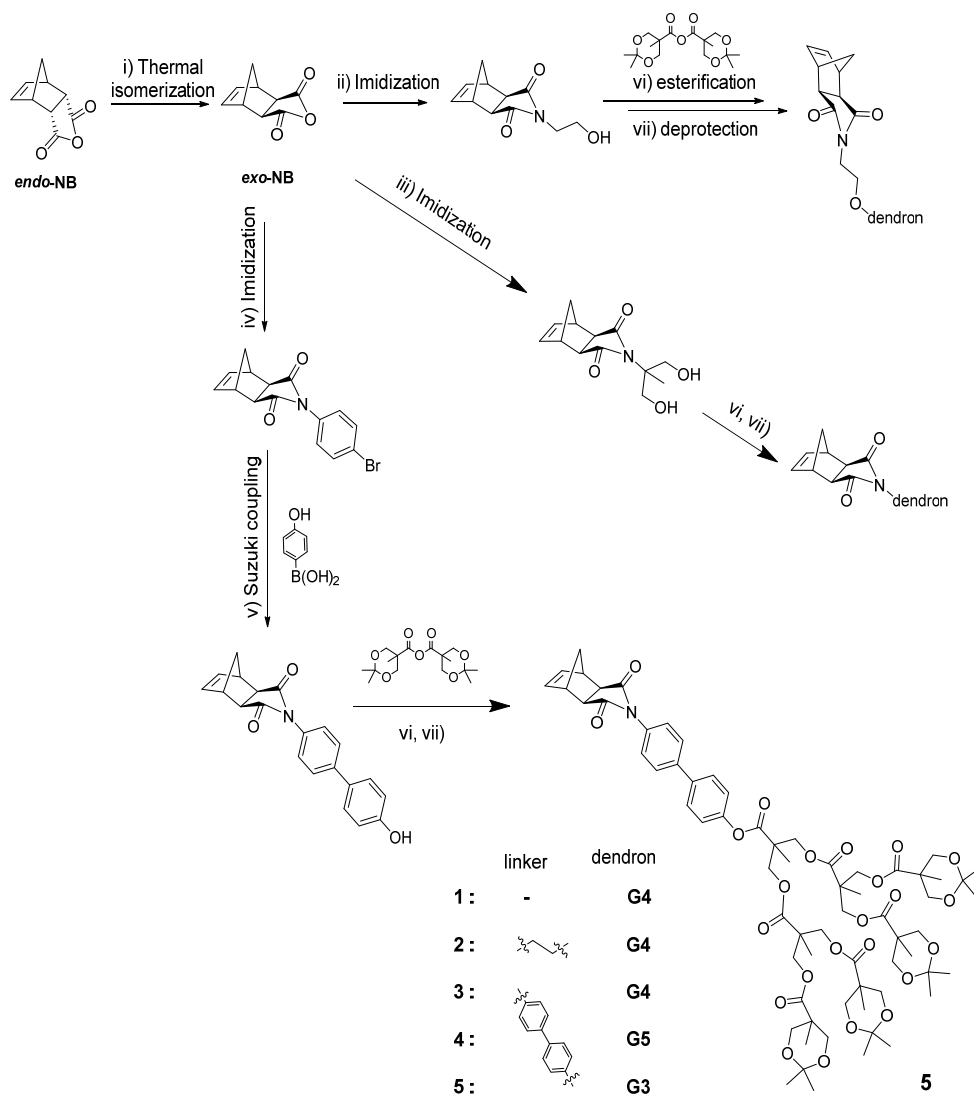
NB macromonomers with ester type dendrons were synthesized follow the Scheme 2–1.¹⁴ Only *exo*–isomer was used for the efficient ROMP which is prepared by thermal isomerization of *endo*–NB. The linker moiety was introduced by imidization, and series of dendronized macromonomers were synthesized by repetition of esterification and deprotection reaction.

TD–ester dendron macromonomers

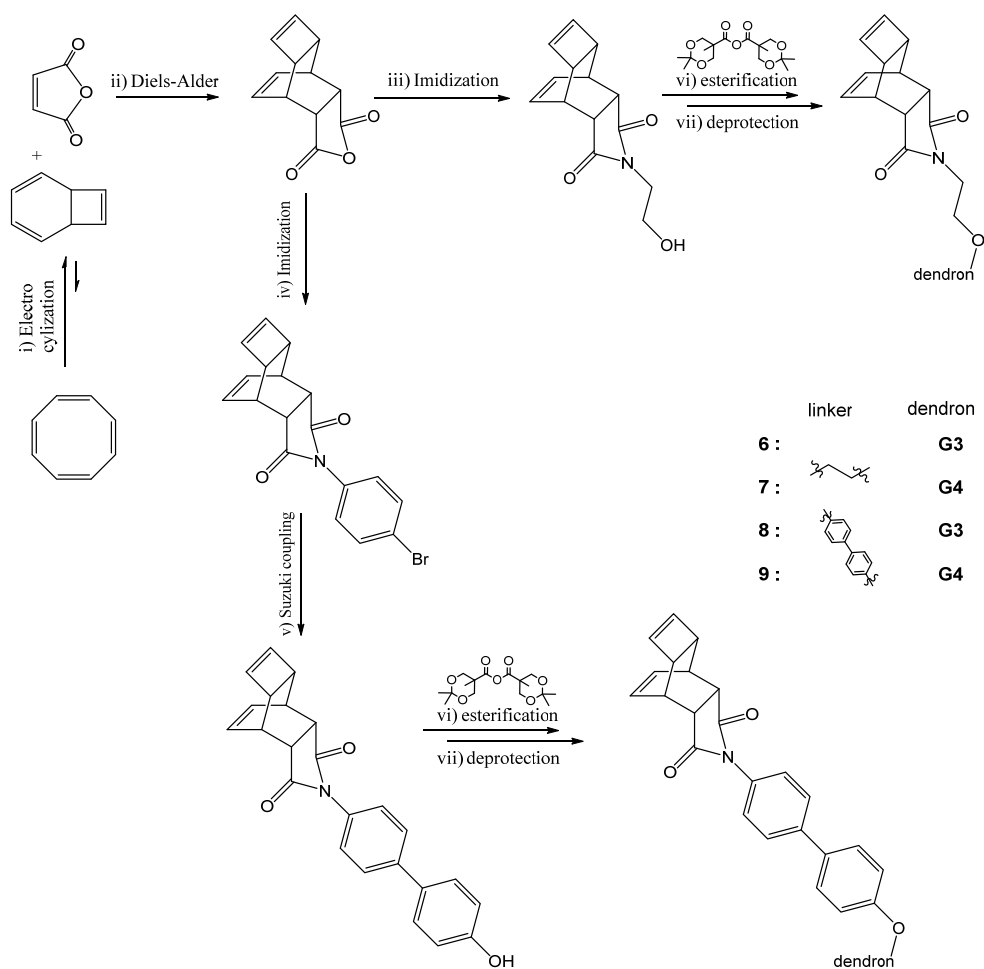
TD macromonomers with ester type dendrons were synthesized follow the Scheme 2–2.¹⁵ TD anhydride was prepared by Diels–Alder reaction of cyclooctatetraene and malic anhydride, and then imidization was performed to introduce the linker moieties. Ester dendron was synthesizes by same method with NB case.

NB–fréchet macromonomers

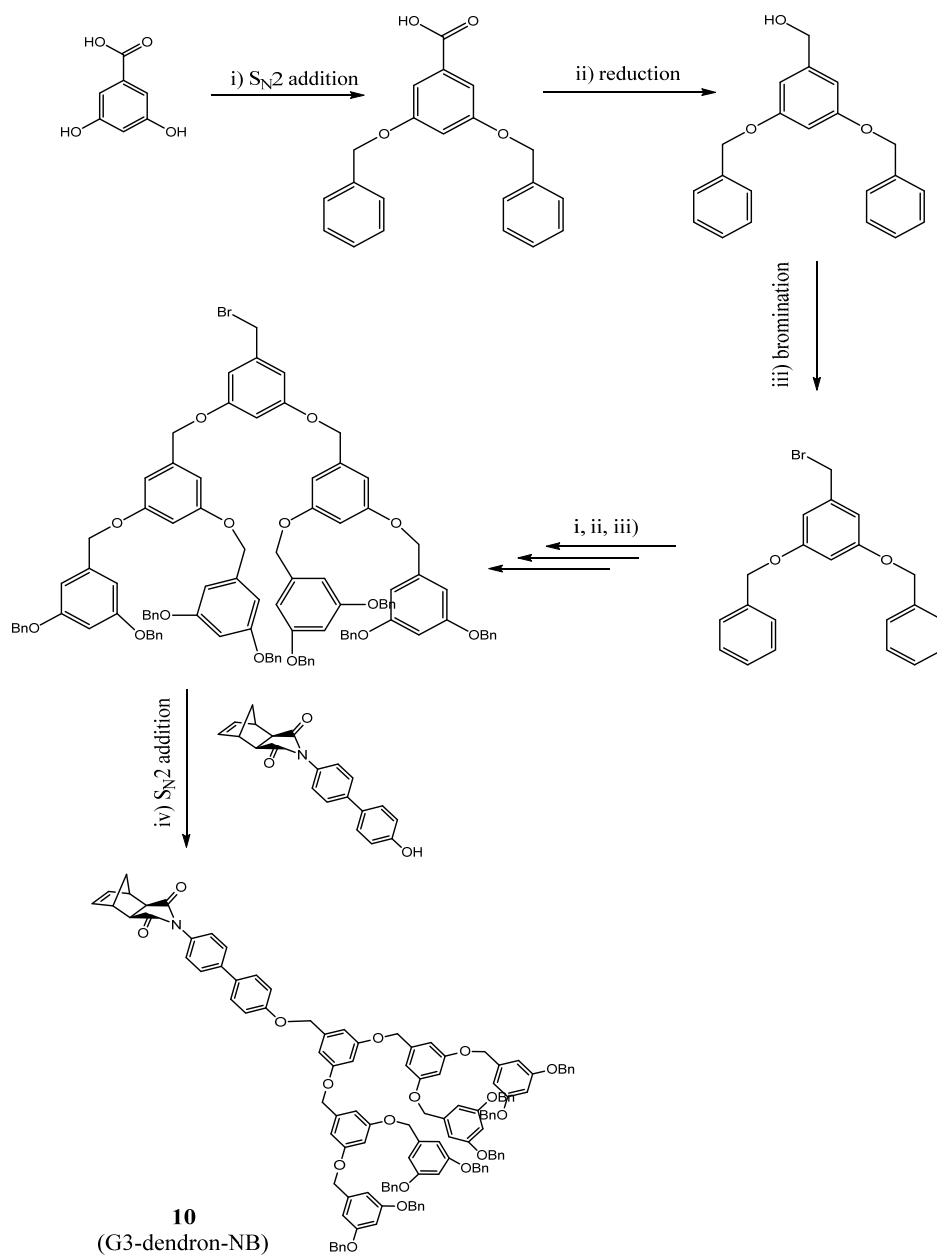
NB macromonomers with fréchet type dendrons were synthesized follow the Scheme 2–3.¹⁶ Only *exo*–isomer was used for the efficient ROMP. The linker moiety was introduced by imidization, and series of dendronized macromonomers were synthesized by repetition of S_N2, reduction, and bromination reaction.



Scheme 2-1. synthesis route for NB macromonomers with ester type dendrons: i) 195 °C, 4 h, recrystallization by EA; ii) 2-aminoethanol, toluene, 120 °C, 20 h; iii) 2-amino-2-methylpropane-1,3-diol, toluene, 120 °C, 20 h; iv) 4-bromoaniline, toluene, 120 °C, 20 h; v) Pd(PPh₃)₄, N₂CO₃, toluene/methanol= 2/1, 95 °C, overnight; vi) Et₃N, DMAP, MC, overnight; vii) TsOH, MeOH, overnight.



Scheme 2-2. synthesis route for TD macromonomers with ester type dendrons: i,ii) chlorobenzene, 165 °C, 1.5 h; iii) 2-aminoethanol, toluene, 120 °C, 20 h; iv) 4-bromoaniline, toluene, 120 °C, 20 h; v) Pd(PPh₃)₄, N₂CO₃, *t*Bu₄NOH toluene/methanol=2/1, 95 °C, overnight; vi) Et₃N, DMAP, MC, overnight; vii) TsOH, MeOH, overnight.



Scheme 2-3. synthesis route for NB macromonomers with Fréchet type dendrons: *i*) benzyl bromide, K_2CO_3 , 18-crown-6-ether, acetone, 60 °C, 3 h; *ii*) $LiAlH_4$, THF, R.T., 1.5 h, quench with NH_4Cl/H_2O ; *iii*) CBr_4 , PPh_3 , THF, R. T., 0.5 h; *iv*) K_2CO_3 , DMF, 60 °C, 5 h.

2.2.3 Polymerization

Synthesis of 3rd generation Grubbs Catalyst (III)

2nd generation Grubbs catalyst (51.8 mg, 0.061 mmol) and pyridine (1 mL) were mixed in 20 mL sized vial for 5 minutes. Cold *n*-pentane was poured to the vial. After storage in freezer a few hours, the 3rd generation Grubbs catalyst was filtered and washed by pentane. The green product (39.3 mg, 0.0542 mmol, 88.7%) was vacuum dried and stored in desiccator.

General procedure for ROMP

Monomer (0.021 mmol) was weighed in a 5 mL sized screw-cap vial with septum and purged with argon. Anhydrous and degassed solvent (0.20 mL) was added to the vial. The solution of initiator (0.05 mL) was added at once under vigorous stirring. After confirming the monomer conversion by TLC, the reaction was quenched by excess ethyl vinyl ether. The concentrated reaction mixture was precipitated by methanol or *iso*-propylalcohol, and the obtained white solid was dried *in vacuo*.

General procedure for ring opening polymerization (ROP)

L-actide was prepared first. *L*-lactic acid in Kugelrohr distillation apparatus was slowly heated from room temperature to 175 °C for 10 minutes with rotation (50 rpm), maintained for 7 hours. Generated water was removed by evaporation from the container during the process. After cooling down to room temperature, 1 mol% of Sn(Oct)₂ relative to the amount of *L*-lactic acid was added to the resulting oligomer. The mixture was distilled at 200 °C under a pressure of 10 – 30 mbar for 1 – 2 hours to obtain the solidified crude lactide mixture (GC-MS: DD,LL/meso=94/6). The crude

mixture was recrystallized three times from ethyl acetate. White solid was obtained in 16 % yield. To a 10 mL Schlenk tube with a magnetic bar, alcohol initiator (51.9 mg, 0.425 mmol), L-lactide (1.225 g, 8.50 mmol), and tin(II) 2-ethyl hexanoate (8.6 mg, 0.0212 mol) were added. The tube was evacuated and backfilled with argon four times, then immersed in 110 °C oil bath. After an hour with stirring, the reaction mixture was cooled down to room temperature, diluted with dichloromethane, and precipitated into methanol. White solid was isolated with filter paper then dried in vacuo (1.152 g, 90.2%).

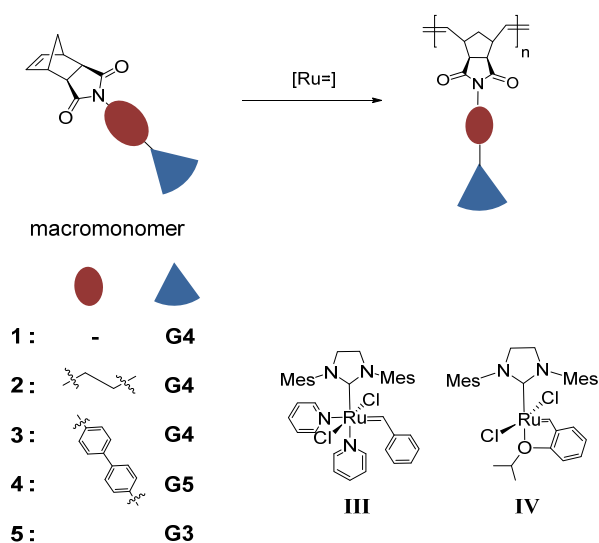
General procedure for Hydrogenation of ROMP polymer

After the ROMP, the olefin backbones are hydrogenated to get single bonded backbone by using *p*-toluenesulfonylhydrazide (*p*-TSH, 2 eq to olefin) and trioctyl amine (1 eq to *p*-TSH) in dichlorobenzene at 140 °C. After 4 hour, the reaction mixture was cooled down to room temperature and precipitated in methanol two times. The precipitated polymers were filtered and dried in vacuo.

2.3 Result and Discussion

2.3.1 Different generation of ester type dendron

The volume of fan-shape dendron increases with generation. It is known that this change in volume of dendron affect to the degree of the polymer chain extension, but there are not much experimental examples. To examine the relationship between generation of dendron and polymer extension, series of polymers with different generation of dendrons and linker groups were prepared.



Scheme 2-4. ROMP of NB macromonomers.

The ROMP of the macromonomer **1**, whose G2 and G3 analogs had undergone the living ROMP in a previous study was examined first.¹⁷ As the dendrons were highly bulky and congested, the ROMP at room temperature was sluggish. Although the complete conversion of **1** occurred at 50 °C (Table 2-1, entry 1), a moderate PDI of 1.35 was measured for poly(**1**) even with the ultrafast-initiating catalyst **III**. This broader PDI than expected, was presumably because of the slow propagation caused by the steric hindrance between the propagating carbene and the bulky monomers. To enhance the ROMP

process, new monomers containing following linkers between NB and the G4 ester dendrons were prepared: a flexible ethylene linker unit and a rigid but linear biphenyl linker unit as in macromonomers **2** and **3**, respectively (Scheme 2-4). The ROMP of **2** still required catalyst activation and the complete conversion of the macromonomer was observed at 40 °C, but without broadening of the PDI this time (1.07, Table 2-1, entry 2). This result suggested that the macromonomer **2** became more reactive to ROMP (due to the higher k_p/k_t) by the introduction of the linker so that the PDI was significantly lower than that of **1**. Further lengthening the linker by increasing the number of the carbon chain would make the side-chain too flexible and such dendronized polymer would not exhibit rod-like conformation.¹⁸ Therefore, we decided to incorporate long but rigid biphenyl group as a new linker. Following this idea, we studied the ROMP of **3** containing the biphenyl linker, and observed very efficient ROMP even at room temperature (Table 2-1, entries 3-7). Moreover, we observed the characteristics of living polymerization, such as narrow PDIs (<1.10) and excellent molecular weight control over a wide range of DP from 50 to 500 (Figure 2-2a). The absolute molecular weight was determined by multi-angle laser light scattering (MALLS) detector and the observed M_n in all cases matched relatively well with the theoretical values within experimental error. The M_n obtained from the MALLS technique was five times higher than that determined by the conventional method using polystyrene (PS) calibration. This implies that the hydrodynamic radius (R_h) of the G4 polymers was greatly underestimated with regard to that of PS standards.¹⁹ This experiment presents the first example of direct synthesis of G4 dendronized polymers by living polymerization.

Table 2–1. ROMP of NB based macromonomers.

entry	monomer	temp (°C)	[M]/[I]	M _n (conv) ^b	PDI (conv) ^b	M _n (Theo) ^c	M _n (MALLS) ^d
1	1	50	300	129 k	1.35	659 k	602 k
2	2	40	300	150 k	1.07	680 k	566 k
3	3	r.t.	50	23 k	1.04	120 k	153 k
4	3	r.t.	100	41 k	1.06	239 k	233 k
5	3	r.t.	200	86 k	1.08	478 k	399 k
6	3	r.t.	300	125 k	1.09	718 k	661 k
7	3	r.t.	500	205 k	1.05	1196 k	1128 k
8	5	r.t.	300	80 k	1.08	391 k	312 k
9 ^e	4	50	300	104 k	1.71	1371 k	1036 k

^a The polymerization was performed by **III** in THF at various temperatures. ^b The numbers were determined by THF–GPC calibrated by PS standards. ^c Theoretical molecular weight. ^d The molecular weight was measured by MALLS–VIS–RI detector. ^e The polymerization was performed by **IV**.

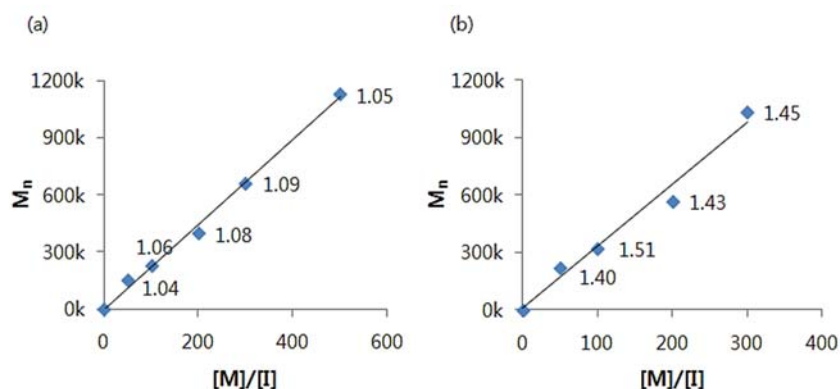


Figure 2–2. The plots for measured M_n vs [M]/[I] to show the controlled polymerization for (a) poly(3) and (b) poly(4). The inset values are PDI.

Based on the results above, the ROMP of G5 macromonomers was attempted. Initially, the macromonomers with and without the ethylene linker were tested for ROMP. However, these attempts did not afford any desired polymers even at high temperature conditions. On the other hand, ROMP of the G5 macromonomer with the biphenyl linker, **4**, resulted in the complete conversion of the monomer using

2nd generation Grubbs catalyst **II** or Hoveyda–Grubbs catalyst **IV** at 50 °C. Poly(**4**) synthesized using the 2nd generation Grubbs catalyst showed a relatively high PDI of 1.7, because of the slow initiation rate (k_i), whereas the PDI decreased to 1.4 when a faster initiating **IV** was used.²⁰ However, the ultra–fast initiating catalyst **III**, which should have resulted in considerably narrower PDI, did not promote an efficient ROMP of **4** because of lower stability of the catalyst. Although the PDI of poly(**4**) was moderate only because of the unsatisfactory k_i/k_p , the molecular weight was remarkably controlled in a linear fashion according to the $[M]/[I]$ ratio (Figure 2–2b) because the bulky dendrons did not allow a chain transfer reaction. In short, ROMP of **4** containing the novel biphenyl linker afforded the largest G5 dendronized polymer obtained by macromonomer approach thus far, with high molecular weight exceeding one million daltons. Again, the molecular weights of poly(**4**) determined by the conventional method were ten times smaller than those obtained by the MALLS detector. This indicates that the R_h of poly(**4**) was underestimated even more than the previous case of poly(**3**).

Table 2–2. Molecular weight control of poly(4).

[M]/[I]	M_n (MALLS) ^b	M_n (Theo) ^c	PDI ^b
50	222k	228k	1.40
100	320k	457k	1.51
200	568k	914k	1.43
300	1036k	1371k	1.45

^a The polymerization was performed by **IV** in THF at 50 °C. ^b The molecular weight was measured by THF–GPC with MALLS–VIS–RI detector. ^c Theoretical molecular weight.

Although many dendronized polymers have been prepared, the relationship between their chemical structure and polymer conformation is rarely investigated in systematic manner.²¹ Hence,

we conducted a detailed investigation of the conformational analysis of various dendronized polymers in THF solution at 35 °C by GPC equipped with MALLS–viscometry (VIS) detectors. From these analysis, shape parameters α and Flory exponent ν were calculated from the slopes of the Mark–Houwink–Sakurada plot ($\log IV$ vs $\log M_w$) and the conformation plot ($\log R_g$ vs $\log M_w$), respectively; these parameters indicate the conformation of the polymer chain in solution. The polymer with a large α and ν resembles more rod–like conformation (for a sphere, $\alpha = 0$, $\nu < 0.3$; for a random coil, $\alpha < 0.8$, $0.3 < \nu < 0.6$; for a rod–like structure, $0.8 < \alpha < 2.0$, $0.6 < \nu < 1.0$ and for a perfect rod $\alpha = 2.0$, $\nu = 1.0$).²² The values measured for the polymers are summarized in Table 2–3; these values showed a definite dependence of the various dendronized polymers on the type of the linkers and the size of the dendrons. We examined the shape parameters for poly(1)–(3), all of which contained the same G4 dendron but different linker units. Among these three polymers, poly(1), which did not contain a linker, showed the largest α and ν values because its dendrons were closest to the polymer backbone and this congestion caused maximum repulsion that stretched the polymer chains further apart. In contrast, poly(2) containing the flexible ethylene linker showed the smallest α and ν values because the randomly rotating dendrons had higher degree of freedom, thus imposing less stress on the polymer conformation. On the other hand, poly(3), which contained the rigid and linear biphenyl linker, showed α and ν values comparable to those of poly(1) because the degree of freedom for the dendrons was limited by the rigid biphenyl linker. As a result, the polymer chain with the restricted motion could retain its rod–like conformation in solution.

Table 2–3. The shape parameter data of poly(1)–(5).

Polymer	Poly(1)	Poly(2)	Poly(3)	Poly(4)	Poly(5)
ν^a	0.78	0.76	0.77	0.87	0.60
α^b	1.08	0.85	1.04	1.20	0.78

^a Calculated from conformation plot measured by MALLS. ^b Calculated from Mark–Houwink plot obtained by VIS detector.

Next, we studied how the generation of the dendrons influenced the solution conformation of the dendronized polymers containing the same biphenyl linker. As anticipated, large α and ν values were obtained for higher generation dendronized polymers (Table 2–3, Figure 2–4, poly(3)–(5)). The increase in α ($0.78 < 1.04 < 1.20$) and ν ($0.60 < 0.77 < 0.87$) from G3 to G5 dendronized polymers verifies that the stiffness of the polymer chain increases with the dendron generation, reaching its maximum value for the G5 polymer. Based on the solution conformation analysis, we successfully conducted systematic studies to investigate the influence of the dendron generation and the structure of linkers on the overall conformation of polymers in solution.

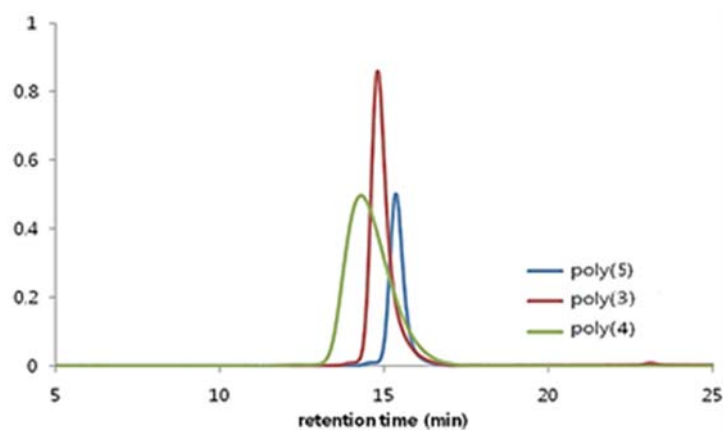


Figure 2–3. GPC trace of poly (3)–(5).

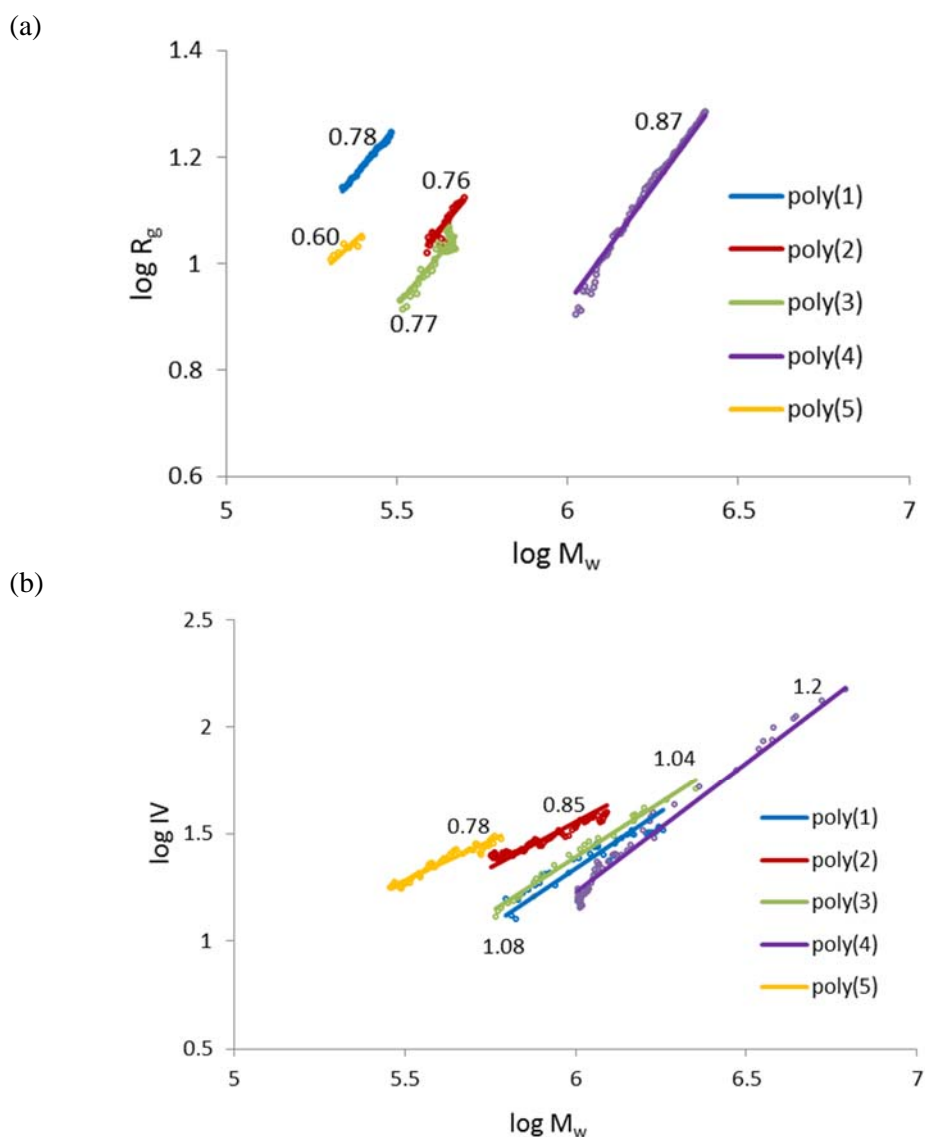


Figure 2-4. (a) conformation plot and (b) Mark-Houwink-Sakurada plot of poly(1)–(5).

The conformational information can be visually interpreted using AFM technique because single polymer chains could be clearly observed deposited on a mica surface by spin coating process (Figure 2-5). The G4 polymers without a linker and with the biphenyl linker, i.e., poly(1) and poly(2), respectively, showed a similar extended conformation (Figure 2-5a and 2-5c), while poly(3), with the

flexible ethylene linker, exhibited more entangled conformation (Figure 2–5b). The largest G5 dendronized polymer, poly(4), also showed the extended rod-like conformation, whereas poly(5) having the smallest G3 dendron showed the most entangled conformation (Figure 2–5d and 2–5e). It is important to note that these images of rigid-rods are not caused by surface because the surface of mica does not show template effect whereas graphite does.²³ From the conformation information for both the solution and solid states, we concluded that the structure of the linker had profound effect on the polymer conformation and introducing the biphenyl linker to the monomers was the excellent strategy to increase the ROMP activity by decreasing the steric hindrance without compromising the rigidity of the polymer chains.

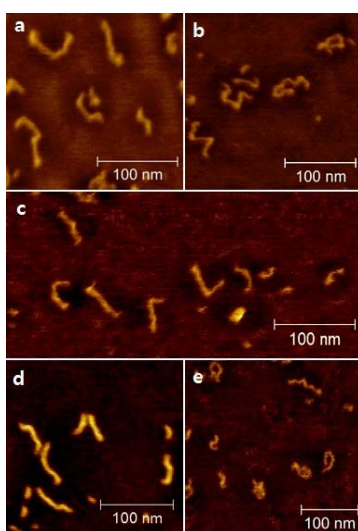


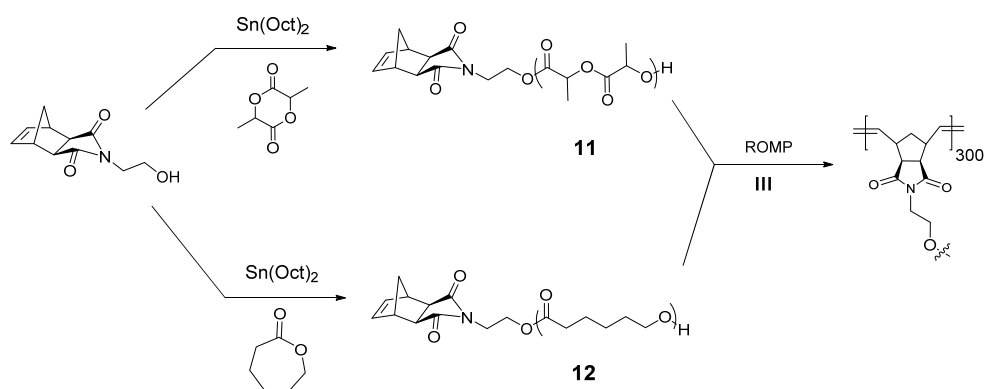
Figure 2–5. AFM images of dendronized poly(1)–(5) on mica surface.

Comparison with brush polymer

The graft or brush polymers are another well-known species for polymer with extended conformation.²⁴ By changing the length of

side chain, the conformation can be controlled to get more extended form. The synthesis of brush polymer by macromonomer approach is relatively easier than dendronized polymer because of less sterically hindered linear shape of its macromonomer. In other hands, this linear shape is unfavourable for conformation control than fan shape dendronized macromonomer. The steric hindrance; one of the main factor for conformation control; of linear shape is smaller than fan shape. As a result, the dendronized polymers have more chance to have extended structure than brush polymers.

To confirm this assumption, we synthesized brush polymers with same NB backbone and ester functionalities (Scheme 2–5). The polylactic acid (PLA, **11**) and polycaprolactone (PCL, **12**) was tethered to the NB with ethylene linker by ROP using tin (II) 2-ethylhexanoate. Those macromonomer **11** and **12** were polymerized again by ROMP to get the brush polymer. The polymerization was done in THF at room temperature and full conversion was obtained after 1 hours. The length of brush part was calculated by ^1H NMR, and absolute molecular weight of whole polymer was measured by THF GPC. The DP of side chain was around 20 and DP of main chain was around 300 for both cases.



Scheme 2–5. Synthesis of brush polymers.

With synthesized brush polymers, MALLS analysis was done to get the shape factor. As demonstrated in Figure 2-7, poly(**11**) and poly(**12**) gave ν value of 0.47 and 0.53, respectively, indicating random coil conformation in conformation plot. Also, α value of 0.13 and 0.15, respectively, were obtained from Mark-Houwink-Sakurada plot indicating sphere shape in solution state. Those values are smaller than poly(**5**) with low generation of dendron (G3) which showed 0.60 and 0.78 for ν and α respectively. Furthermore, more entangled structure was observed from AFM image as we expected. The height of AFM image of brush polymers were also lower than dendronized polymers (around 0.2 nm for brush polymer and 0.4 nm for dendronized polymer) because of smaller volume of side chain in brush polymer. In the case of polymer with PLA side chain showed more aggregated structure than polymer with PCL side chain because of well self-assembling nature of PLA (Figure 2-6). From these results, we can say that dendronized polymer with relatively small G3 dendrons showed more extended conformation than brush polymer with DP of 20 for side chain. This difference came from the different shape between fan-shape dendron having larger volume and linear-shape brush having smaller volume.

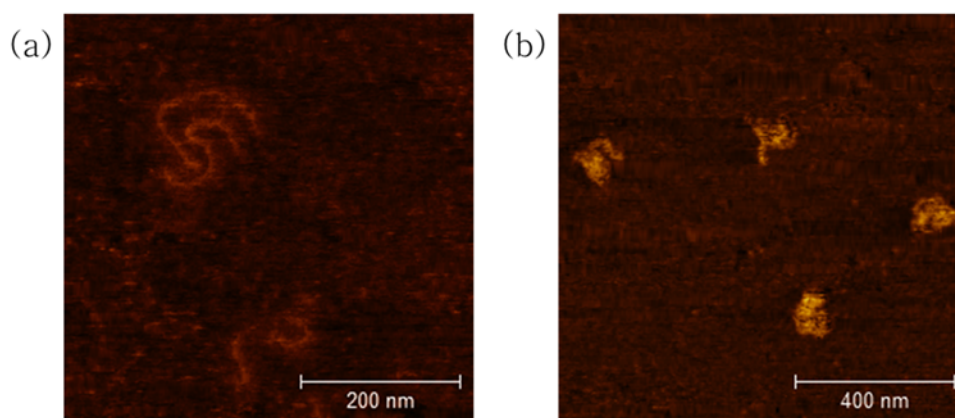


Figure 2-6. AFM image of (a) poly(NBPCL) (b) poly(NBPLA).

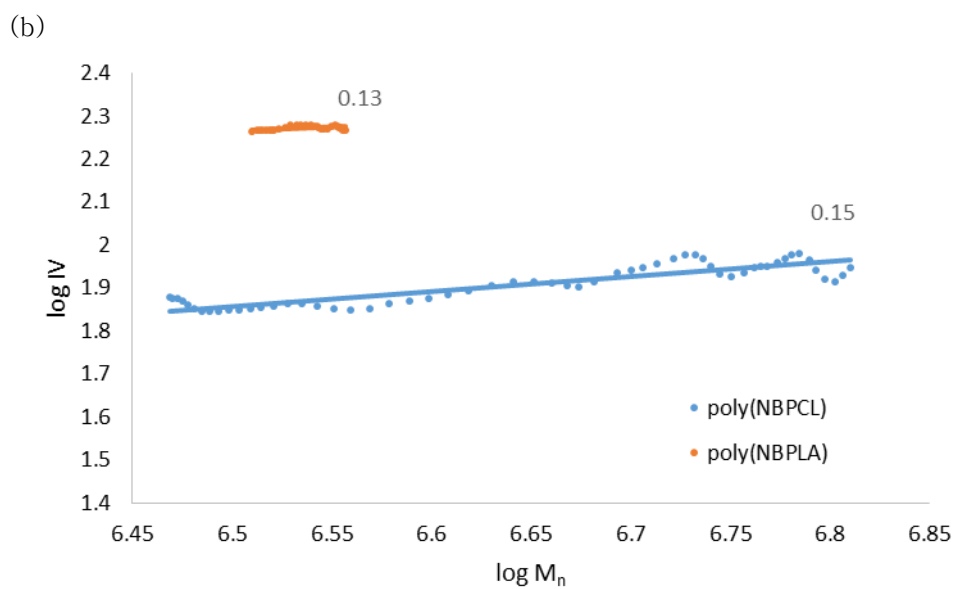
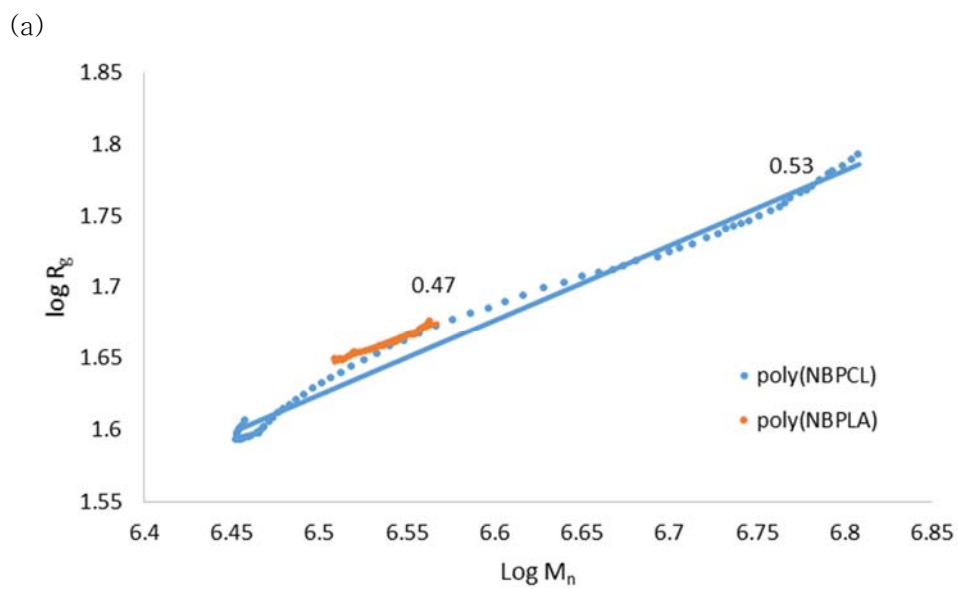


Figure 2-7. (a) conformation plot and (b) Mark-Houwink-Sakurada plot of brush polymers.

2.3.2 Different backbone structure

Polymer chain stiffness can be controlled by not only bulkiness of side chain but also the structure of backbone.¹² If the backbone has more rigidity or less freedom, that polymer would show more stiff and extended conformation. To make clear this point, a series of polymers from same monomer but having different backbone structure were prepared.

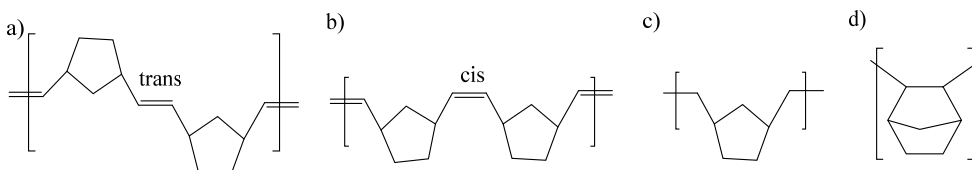
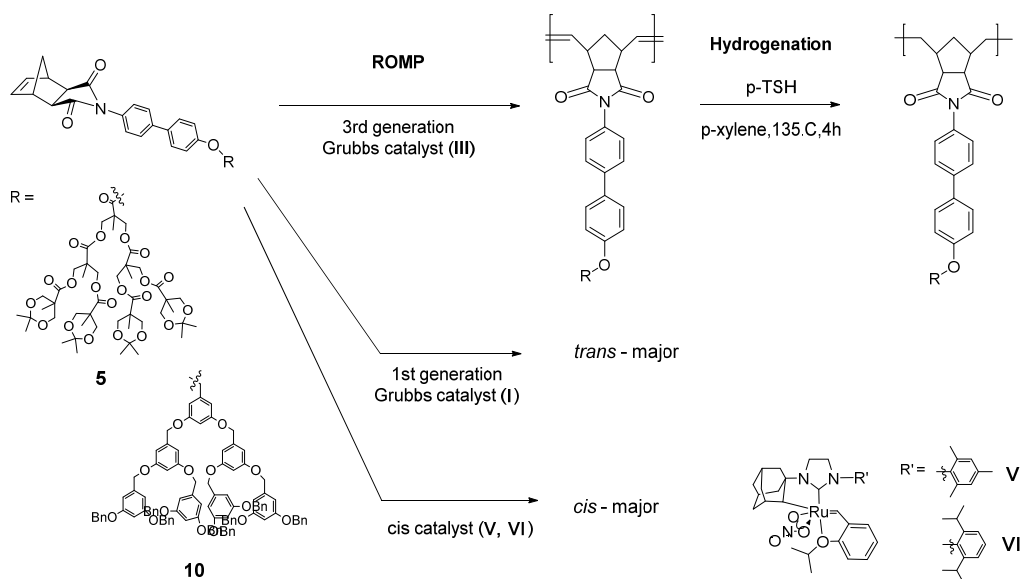


Figure 2–8. Possible backbone structures from NB. (a) *trans*-olefin (b) *cis*-olefin (c) single bond after hydrogenation (d) vinyl type.

The norbornene (NB) is the most popular monomer for ROMP having high ring-strain and living manner with proper design. General structure of polynorbornene from ROMP is *trans/cis* mixture of olefins (Figure 2–8a and b). The ratio between two conformations can be changed relate with catalysts. It is already known that the 1st generation Grubbs catalyst gives *trans* major product, and other Grubbs catalysts give 50:50 mixture of two conformations.²⁵ This difference is coming from the orientation of approaching monomer when they coordinate to the catalyst. Also, *cis* major Grubbs type catalysts possess different direction for coordination of catalyst with monomer which induce the *cis* conformation as a major product.²⁶ Another possible structure is hydrogenated backbone. The olefins on polymer backbone can be hydrogenated after ROMP to produce single bonded structure which has more rotational freedom (Figure 2–8c). In addition, NB can be polymerized by vinyl addition polymerization using palladium catalyst. In this case, only one bond of olefin is

broken and the ring structure is maintained (Figure 2–8d). As a result, resulting polymer has shorter distance between repeating units and stiffer backbone structure than ROMP polymer. Unfortunately, the efficiency of this vinyl addition polymerization was not enough to polymerize macromonomers with high generation dendrons, and we couldn't synthesize the highly dendronized polymer through this vinyl addition polymerization.



Scheme 2–6. Backbone controlled polymerization of NB macromonomers.

NB based macromonomers **5** and **10** having G3 ester and Fréchet type dendrons, respectively, were used for this study (Scheme 2–6). Higher generation of dendrons can give more clear conformation change and AFM image, but ROMP of larger macromonomers with less reactive 1st generation Grubbs catalyst or *cis* catalyst was not possible. Even the ROMP of **5** and **10** with G3 dendrons were hard to achieve with **I** under the mild reaction condition (Table 2–4). The reaction temperature had to be raised up to 70 °C and toluene was used as a solvent instead of THF. Those

harsher condition resulted in broad PDI. The *cis*-major polymerization was sensitive to reaction temperature, and 35 °C for 12 hours was optimized condition. However, only around 80 % conversion was possible. The polymers from table 2–4, entry 2 and 6 were hydrogenated after ROMP to get the single bonded polymer backbone. The 2 w% polymer solution in dichlorobenzene was prepared with *p*-TSH and reflux for 4 hours. Trioctyl amine was added together to protect the ester dendron from deprotection during the hydrogenation induced by *p*-toluenesulfonic acid which is generated from the reaction as a byproduct. We tried to prepare the series of polymers with similar DPs for reliable comparison.

Table 2–4. Result of backbone controlled polymerization.

entry	monomer	catalyst	M _n (MALS) ^a	PDI (MALS) ^a	conv (%)	<i>tr/cis</i> ^b	ν ^c	α ^d
1	5	I	364 k	1.24	>99	95/5	0.73	0.79
2	5	III	381 k	1.03	>99	55/45	0.60	0.68
3	5	V	413 k	1.36	78	20/80	0.71	0.75
4	5	–	419 k	1.02	>99	–	0.30	0.43
5	10	I	548 k	1.13	>99	80/20	0.80	0.85
6	10	III	615 k	1.02	>99	55/45	0.64	0.63
7	10	VI	525 k	1.54	77	29/71	0.66	0.74
8	10	–	628 k	1.02	>99	–	0.57	0.53

^a The molecular weight was measured by THF-GPC with MALLS-VIS-RI detector. ^b Determined by integration of olefin signals in ¹H NMR. ^c Calculated from conformation plot measured by MALLS. ^d Calculated from Mark-Houwink plot obtained by VIS detector.

The *trans* and *cis* major polymers showed most extended and hydrogenated polymers showed most entangled conformation from the MALLS analysis in both dendron cases, as we expected. The dendrons can have free volume as much as they want and fully

stretched in *trans* isomer. In the case of *cis* isomer, the polymer chain can make a kind of helix structure and dendrons will be surrounded this backbone. As a result, polymers can be extended more. On the other hand, hydrogenated polymers having freely rotating single bond have large flexibility and dendrons also can't play a large part in this case. In addition, the polymers with fréchet type dendrons showed more extended conformation compare with ester type dendronized polymers. In opposite, the conformation difference among polymers with different backbone structures was smaller. This is reasonable result because the fréchet type dendron has larger volume than ester type dendron, leading more extended structure.

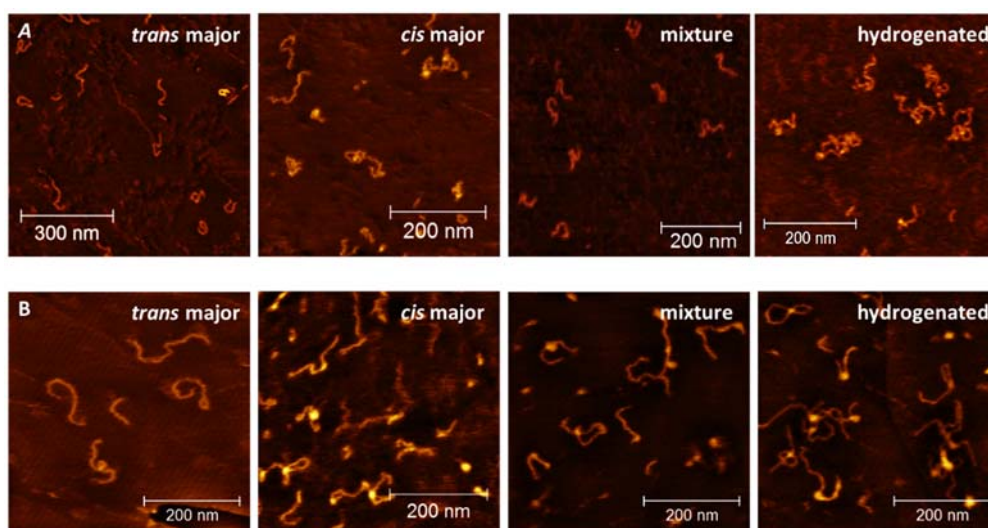
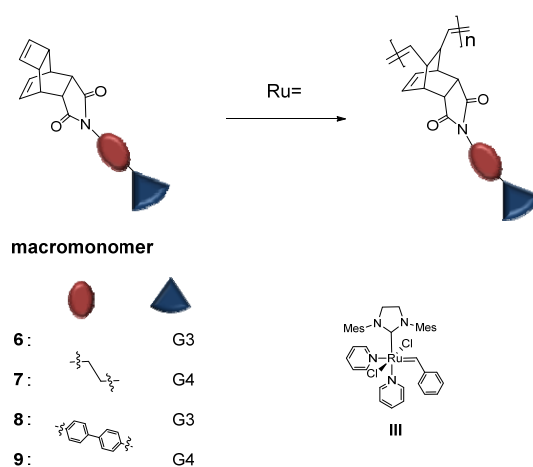


Figure 2-9. AFM image of A) poly(5) and B) poly(10).

We tried to visualize this conformation difference by AFM imaging technique. Unfortunately, the AFM image was not clear to distinguish the conformations. The entangled image of hydrogenated polymers were clearly distinguishable, but images of other three kinds of polymers were hard to distinguish. It probably because the size of G3 dendron was not enough to demonstrate the differences.

2.3.3 *endo*-tricyclo[4.2.2.0^{2,5}]deca-3,9-diene (TD)

The rod-like polymer chain couldn't be obtained from polynorbornenes with one geometric isomer as a major backbone structure. It might be because the ROMP of NB macromonomers with high generation of dendron by less active catalyst is not possible, but both less active catalyst and high generation of dendron are required together for synthesis of rod-like polymer. However, it is clear that the polymer backbone structure is important for conformation control, and the introduction of new monomer with more rigid structure can be a solution.



Scheme 2-7. ROMP of TD macromonomers.

The *endo*-tricyclo[4.2.2.0^{2,5}]deca-3,9-diene (TD) obtained by a series of pericyclic reactions of cyclooctatetraene has an interesting structure that contains two olefins, a cyclobutene fused to a bicyclo[2,2,2]oct-2-ene. This TD derivative was reported to undergo living ROMP with 1st generation Grubbs catalyst (I).²⁷ Of the two olefins, only the cyclobutene moiety, with higher ring strain, underwent ROMP, whereas the sterically hindered bicyclo[2,2,2]oct-2-ene did not react at all. This TD monomer has rarely been

used for ROMP because the reaction is much slower (more than 12 h) than that with NB derivatives, which are the most widely used monomers for ROMP. However, poly(TD) could easily form rod-like polymers because of its rigid backbone. Thus, with a more powerful catalyst, TD derivatives could become more useful monomers for dendronized polymer synthesis.

Table 2–5. ROMP of TD based macromonomers.^a

entry	monomer	[M]/[I]	T (° C)	M _n (Theo) ^c	M _n (Obs) ^d	PDI ^d	ν ^e	L _p (nm) ^f
1	1	300	50	365k	272k	1.06	0.72	16.8
2 ^b	2	300	70	692k	640k	1.22	0.92	27.7
3	3	300	50	402k	300k	1.02	0.87	20.2
4	4	300	50	729k	680k	1.02	0.99	31.2
5	4	200	50	486k	550k	1.04	–	–
6	4	100	50	243k	252k	1.03	–	–
7	4	50	50	122k	119k	1.02	–	–

^a The polymerization was performed in THF at various temperatures and the full conversion was observed within twenty hours. ^b Toluene was used. ^c Theoretical molecular weight. ^d The molecular weight and PDI was measured by MALLS detector. ^e Calculated from conformation plot measured by MALLS. ^f Persistence length calculated by equation 1 using the theoretical unit length, $l_0 = 3.7 \text{ \AA}$.

The syntheses of various TD macromonomers having G3 and G4 ester dendrons and their polymers are summarized in Scheme 2–2 and 2–7. The TD anhydride moiety was generated by electrocyclization of cyclooctatetraene to give a fused bicyclic intermediate, which then underwent a Diels–Alder reaction with maleic anhydride to yield a tetracyclic compound containing a cyclobutene moiety.²⁸ The final product had only one stereoisomer

because of the *endo* rule. To this TD anhydride, two types of linker, a flexible ethylene linker and a rigid biphenyl linker, were attached, and dendrons were incorporated by divergent routes, following previous work. Each macromonomer was purified by flash column chromatography and characterized by NMR spectroscopy and matrix-assisted laser desorption/ionization mass spectrometry.

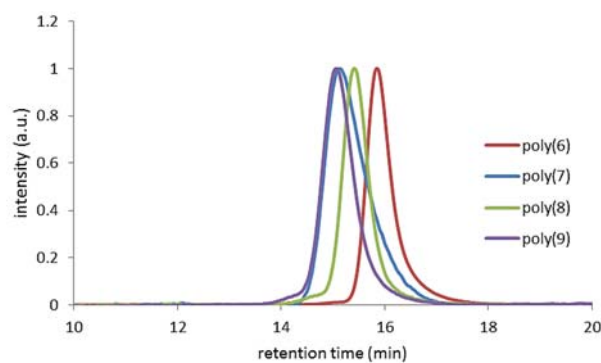


Figure 2–10. GPC traces of poly(6)–(9).

ROMP of these macromonomers was carried out in either tetrahydrofuran or toluene at various temperatures, using 3rd generation Grubbs catalyst **III** to ensure fast initiation, and complete conversion of all the macromonomers (6–9) within 20 h. First, the ROMP of TD macromonomers containing G4 dendrons without any linker was tested, but it did not give any polymer because of the severe steric bulkiness of the large G4 dendron. To enhance the reactivity, two linker moieties were introduced between the TD and the dendrons, similar to work in previous chapter on NB derivatives. A macromonomer (6) containing a flexible ethylene linker and G3 ester dendron with monomer to initiator (M/I) ratio of 300, was polymerized at 50 °C to give complete conversion and a narrow PDI (Table 2–5, entry 1). ROMP was conducted at 70 °C for the analogous macromonomer 7, containing larger G4 dendrons, and

produced poly(**7**) with a slightly broader PDI (Table 2–5, entry 2), presumably due to the reduced stability of the catalyst at 70 °C.²⁹ When a rigid biphenyl linker was incorporated, much better results with narrower PDIs were obtained for macromonomers containing G3 (**8**) and G4 (**9**) dendrons (Table 2–5, entries 3 and 4). Even with large G4 dendrons, **9** could undergo ROMP with complete conversion at 50 °C. To test for living polymerization, we varied the M/I ratio from 50 to 300 and obtained a linear relationship between the DP and the number-average molecular-weight (M_n), and in all cases, the PDIs were well below 1.05 (Table 2–5, entries 4–7, Figure 2–11). It was surprising to observe efficient ROMP of these bulky macromonomers containing the intrinsically less reactive *endo*-TD moiety, because ROMP of NB derivatives containing the *endo*-isomer was highly challenging because of steric hindrance during propagation.³⁰

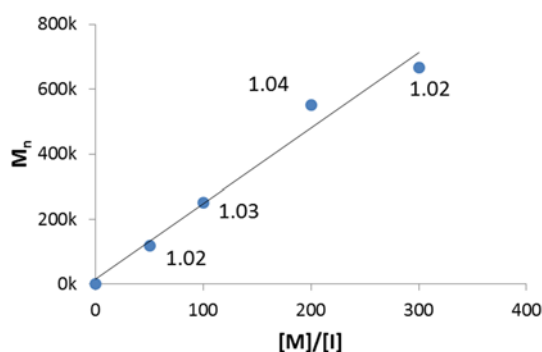


Figure 2–11. The M_n control for poly(**9**). The inset values are PDI.

To examine the conformation of these polymers in solution, MALLS analysis was conducted using GPC. The Flory exponent ν , which is calculated from the slope of the conformation plot ($\log R_g$ vs $\log M_w$) was extracted from this analysis (Table 2–5). This shape parameter predicts the conformation of polymer chains in solution;

ν larger than 0.6 indicates a rod-like conformation and $\nu = 1$ corresponds to a perfect rigid rod. In the previous chapter with NB macromonomers, larger ν values were obtained with polymers containing higher generations of dendrons and also with those containing a rigid biphenyl linker rather than a flexible ethylene linker. Similarly, the new polymers containing higher generation ester dendrons gave larger ν values (**7** > **6** and **9** > **8**), and polymers containing the rigid biphenyl linker [poly(**8**) and poly(**9**)] showed more rod-like conformations than polymers containing the flexible ethylene linker [poly(**6**) and poly(**7**)]. Notably, the ν value of poly(**9**) was 0.99, showing a highly rigid conformation approaching the value for perfect rigid rods ($\nu = 1.0$).²² Furthermore, it is worthwhile to recap that highly rigid polymers with $\nu = 0.87$ were obtained only from polynorbornene containing an extremely large G5 ester dendron whereas in this case, the same shape factor ($\nu = 0.87$) was obtained from the poly(TD) containing only G3 ester dendrons (poly(**8**), Table 2-5, entry 3).

$$F(X) = -\frac{1}{2} \frac{R_g^2}{L^2} X^4 + \frac{1}{6} X^3 - \frac{1}{2} X^2 + X + e^{-X} - 1 \quad (\text{Eq 1})$$

$$X = \frac{L}{L_p}$$

To further support the rigidity of the poly(TD)s, another representative parameter for estimating the polymer chain stiffness, the persistence lengths, was calculated by the following reported method.³¹ Using equation 1, the persistence length (L_p) was calculated from the contour length (L) and the radius of gyration (R_g). L was calculated by multiplying the DP and the unit length (3.7 Å), and R_g was measured by MALLS analysis. As summarized in Table 2-5, the persistence length was larger for polymers containing larger dendrons, and for those containing a rigid biphenyl linker as well.

Poly(9) showed the largest L_p , 31 nm. These results are in excellent agreement with the conformation plot data (ν); the higher the ν values, the higher the persistence lengths of the polymers (Figure 2–13).

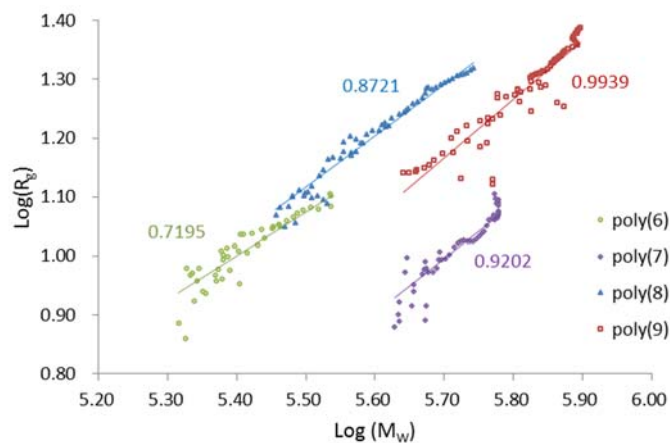


Figure 2–12. Conformation plot of poly(6)–(9).

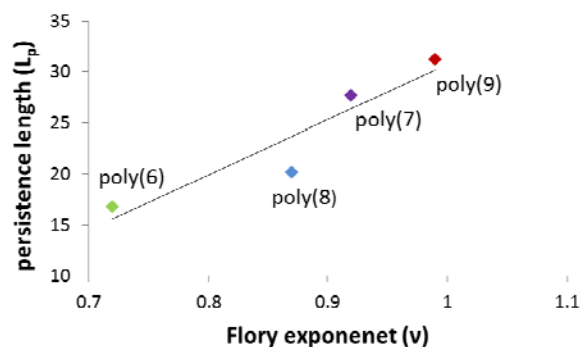


Figure 2–13. The plot of persistence length vs Flory exponent.

Surprisingly, the L_p s of the dendronized polymers prepared from TD macromonomers were larger (16.8–31.2 nm) than those of dendronized polymers prepared from NB containing a G5 ester dendron (8 nm). These results confirm that poly(TD)s are much more rigid than polynorbornenes. Therefore the rigidity of the polymer backbone itself exhibited great influence on the conformation, in a similar way as the size of the dendrons. We

attribute this rigidity to the nature of the polymer repeat unit, which has a bulky bridged tricyclic 3-dimensional structure and more densely grafted dendrons as a result of the fewer carbon atoms between repeat unit (4) than that of NB (5). Consequently, a larger stress was imposed on the polymer backbone, thereby increasing the rigidity and grafting density of the poly(TD)s. Thus, access to the rod-like polymers became much easier with relatively small dendrons. Polymers based on NBs or other vinyl monomers such as styrene require high-generation dendrons to exhibit highly rod-like conformations, because of their flexible backbones.³² However, with the rigid poly(TD), highly rigid rod-like polymers were obtained with much smaller G3 ester dendrons, whose synthesis and purification were much easier and simpler than those containing larger dendrons.

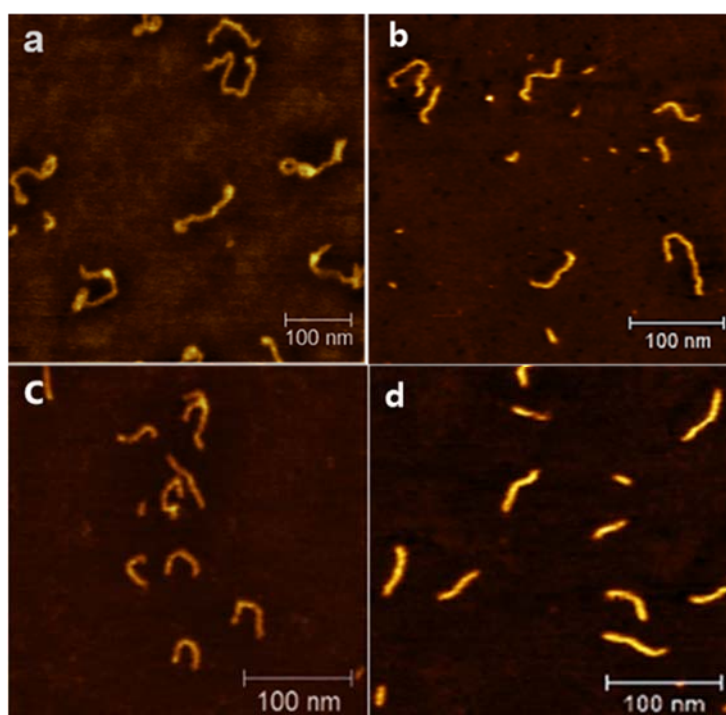


Figure 2-14. AFM images of dendronized homopolymers (a) poly(6), (b) poly(7), (c) poly(8), and (d) poly(9) on mica surface.

The film-state conformation of all polymers was verified using AFM imaging by spin-coating the dilute polymer solution onto a freshly cleaved mica surface, and single chains of the polymers were imaged to reveal rod-like conformations (Figure 2-14). As expected from the shape parameters in solution, polymers containing a biphenyl linker [poly(8) and poly(9)] showed more extended conformations than polymers containing the same dendrons but a flexible ethylene linker [poly(6) and poly(7)]. In particular, among the biphenyl containing polymers, even poly(8) containing G3 dendrons showed a highly extended structure (Figure 2-14c), and poly(9) containing the G4 dendron showed almost rod-like images (Figure 1-14d). The images of the polymers in the film state showed good agreement with the conclusions obtained from the solution state.

2.4 Conclusion

The dendronized polymers with ester type or fr chet type dendrons were synthesized via ROMP by macromonomer approach using NB and TD based monomers. Especially, G5 dendronized polymer is synthesized when the NB and biphenyl linker is used which is the first example of synthesis of G5 dendronized polymer by macromonomer approach. All the polymerization showed controlled manner with controlled molecular weight and narrow to moderate PDIs. The systematic investigation of polymer conformation change with various factors was performed in both solution state and solid state. The conformation of polymers was changed from entangled to extended with increase of generation of dendrons. The backbone structure was another factor for conformation control. Higher ratio of one geometric isomer of olefin; *trans* or *cis*; induced more extended conformation than mixture of those isomers because of the increased chain stiffness. By the same sense, more extended polymer was obtained from the TD based macromonomer even with lower generation of dendrons (G3, G4), owing to the rigid back bone structure of poly(TD) itself. Those conformation change was verified in shape parameters by MALLS analysis and visualized by AFM imaging technique.

2.5 References

- [1] (a) Schlüter, A. D.; Rabe, J. P. *Angew. Chem. Int. Ed.* **2000**, *39*, 864. (b) Frauenrath, H. *Prog. Polym. Sci.* **2005**, *30*, 325.
- [2] (a) Guo, Y.; Beek, J. D.; Zhang, B.; Colussi, M.; Walde, P.; Zhang, A.; Kröger, M.; Halperin, A.; Schlüter, A. D. *J. Am. Chem. Soc.*, **2009**, *131*, 11841. (b) Boydston, A. J.; Holcombe, T. W.; Unruh, D. A.; Fréchet, J. M. J.; Grubbs, R. H. *J. Am. Chem. Soc.*, **2009**, *131*, 5388.
- [3] Li, W.; Wu, D.; Schlüter, A. D.; Zhang, A. *J. Polym. Sci. Polym. Chem.* **2009**, *47*, 6630.
- [4] Deng, J.; Zhou, Y.; Xu, B.; Mai, K.; Deng, Y.; Zhang, L. -M. *Biomacromolecules* **2011**, *12*, 642.
- [5] Kim, J. G.; Yun, M. H.; Lee, J. H.; Kim, J. Y.; Wudl, F.; Yang, C. D. *Chem. Commun.* **2011**, *47*, 3078.
- [6] Chakrabarti, A.; Juilfs, A.; Filler, R.; Mandal, B. K. *Solid State Ionics* **2010**, *181*, 982.
- [7] (a) Karakaya, B.; Claussen, W.; Gessler, K.; Saenger, W.; Schlüter, A. D. *J. Am. Chem. Soc.* **1997**, *119*, 3296. (b) Gao, M.; Jia, S. R.; Kuang, G. C.; Li, Y.; Liang, D. H.; Wei, Y. *Macromolecules*, **2009**, *42*, 4273.
- [8] (a) Shu, L.; Schlüter, A. D.; Ecker, C.; Severin, N.; Rabe, J. P. *Angew. Chem. Int. Ed.* **2001**, *40*, 4666. (b) Lee, C. C.; Fréchet, J. M. J. *Macromolecules* **2006**, *39*, 476.
- [9] (a) Rajaram, S.; Choi, T. -L.; Rolandi, M.; Fréchet, J. M. J. *J. Am. Chem. Soc.* **2007**, *129*, 9619. (b) Hawker, C. J.; Fréchet, J. M. J. *Polymer* **1992**, *33*, 1507. (c) Li, Z.; Ma, J.; Cheng, C.; Zhang, K. Wooley, K. L. *Macromolecules*, **2010**, *43*, 1182. (d) For a review on early reports on the macromonomer approach, see: Schlüter, A. D. *C. R. Chim.* **2003**, *6*, 843.
- [10] Love, J. A.; Morgan, J. P.; Trnka, T. M.; Grubbs, R. H. *Angew. Chem. Int. Ed.* **2002**, *41*, 4035.
- [11] Huang, Y. -L.; Tien, H. -W.; Ma, C. -C. M.; Yang, S. -Y.; Wu, S. -Y.; Liu, H. Y.; Mai, Y. -W. *J. Mater. Chem.*, **2011**, *21*, 18236.
- [12] Nakamura, Y.; Norisuye, T. *Polym. J.*, **2001**, *33*, 874.

- [13] (a) Yoshida, M.; Fresco, Z. M.; Ohnishi, S.; Fréchet, J. M. J. *Macromolecules*, **2005**, *38*, 334. (b) Welch, P. M.; Welch, C. F. *Nano Lett.*, **2006**, *6*, 1922.
- [14] Kim, K. O.; Choi, T. -L. *ACS Macro Lett.*, **2012**, *1*, 445.
- [15] Kim, K. O.; Choi, T. -L. *Macromolecules*, **2013**, *46*, 5905.
- [16] Hawker, C. J.; Fréchet, J. M. J. *J. Am. Chem. Soc.*, **1990**, *112*, 7638.
- [17] Nyström, A.; Malkoch, M.; Furó, I.; Nyström, D.; Unal, K.; Antoni, P.; Vamvounis, G.; Hawker, C.; Wooley, K.; Malmström, E.; Hult, A. *Macromolecules* **2006**, *39*, 7241.
- [18] (a) Carlmark, A.; Malmström, E. E. *Macromolecules* **2004**, *37*, 7491. (b) Jung, H.; Carberry, T. P.; Weck, M. *Macromolecules* **2011**, *44*, 9075.
- [19] Ecker, C.; Severin, N.; Shu, L.; Schlüter, A. D.; Rabe, J. P. *Macromolecules* **2004**, *37*, 2484.
- [20] (a) Trnka, T. M.; Grubbs, R. H. *Acc. Chem. Res.* **2001**, *34*, 18. (b) Sanford, M. S.; Love, J. A.; Grubbs, R. H. *Organometallics* **2001**, *20*, 5314. (c) Garber, S. B.; Kingsbury, J. S.; Gray, B. L.; Hoveyda, A. H. *J. Am. Chem. Soc.* **2000**, *122*, 8168.
- [21] (a) Ouali, N.; Méry, S.; Skoulios, A. *Macromolecules* **2000**, *33*, 6185. (b) Guo, Y. F.; Beek, J. D.; Zhang, B. Z.; Colussi, M.; Walde, P.; Zhang, A.; Kroger, M.; Halperin, A.; Schlüter, A. D. *J. Am. Chem. Soc.* **2009**, *131*, 11841.
- [22] (a) Das, J.; Yoshida, M.; Fresco, Z. M.; Choi, T. -L.; Fréchet, J. M. J.; Chakraborty, A. K. *J. Phys. Chem. B.* **2005**, *109*, 6535. (b) Vanhee, S.; Rulkens, R.; Lehmann, U.; Rosenauer, C.; Schulze, M.; Köhler, W.; Wegner, G. *Macromolecules* **1996**, *29*, 5136.
- [23] (a) Percec, V.; Schlüter, D.; Ronda, J. C.; Johansson, G.; Ungar, G.; Zhou, J. P. *Macromolecules* **1996**, *29*, 1464. (b) Percec, V.; Holerca, M. N. *Biomacromolecules* **2000**, *1*, 6.
- [24] (a) Sheikoa, S. S.; Sumerlin, B. S.; Matyjaszewski, K. *Prog. Polym. Sci.*, **2008**, *33*, 759. (b) Dziezok, P.; Sheiko, S. S.; Fischer, K.; Schmidt, M.; Möller, M. *Angew. Chem. Znr. Ed. Engl.* **1997**, *36*, 2812.
- [25] Grubbs, R. H. *Handbook of metathesis*, Wiley-VCH Verlag GmbH &

Co. KGaA, Weinheim, 2003.

- [26] Keitz, B. K.; Fedorov, F.; Grubbs, R. H. *J. Am. Chem. Soc.*, **2012**, *134*, 2040.
- [27] (a) Charvet, R.; Novak, B. M. *Macromolecules* **2001**, *34*, 7680. (b) Charvet, R.; Novak, B. M. *Macromolecules* **2004**, *37*, 8808. (c) Charvet, R.; Acharya, S.; Hill, J. P.; Akada, M.; Liao, M.; Seki, S.; Honsho, Y.; Saeki, A.; Ariga, K. *J. Am. Chem. Soc.* **2009**, *131*, 18030.
- [28] Reppe, V. W.; Schlichting, O.; Klager, K.; Toepel, T. *Liebigs Ann. Chem.* **1948**, *560*, 1.
- [29] Kim, K. O.; Choi, T. -L. *ACS Macro Lett.* **2012**, *1*, 445.
- [30] (a) Lapinte, V.; Brosse, J. -C.; Fontaine, L. *Macromol. Chem. Phys.* **2004**, *205*, 824. (b) Rule, J. D.; Moore, J. S. *Macromolecules* **2002**, *35*, 7878.
- [31] (a) Das, J.; Yoshida, M.; Fresco, J. M.; Choi, T. -L.; Fréchet, J. M. J.; Chakraborty, A. K. *J. Phys. Chem. B.* **2005**, *109*, 6535. (b) Ouali, N.; Méry, S.; Skoulios, A. *Macromolecules* **2000**, *33*, 6185.
- [32] (a) Nyström, A.; Malkoch, M.; Furó, I.; Nyström, D.; Unal, K.; Antoni, P.; Vamvounis, G.; Hawker, C. J.; Wooley, K.; Malmström, E.; Hult, A. *Macromolecules* **2006**, *39*, 7241. (b) Li, A.; Li, Z.; Zhang, S.; Sun, G.; Policarpio, D. M.; Wooley, K. L. *ACS Macro Lett.* **2012**, *1*, 241.

Chapter 3.

Structural Analysis of Copolymers using 1D Rod-like Dendronized Polymers

3.1 Introduction

Copolymers consist of more than two kinds of monomers. The part from each monomers on one copolymer chain often exhibits the properties of their homopolymer, therefore several desirable properties can be obtained from one polymer. Also, it can improve the weak point of one homopolymer. For this reason, copolymers are getting the limelight, especially in field of material science.¹

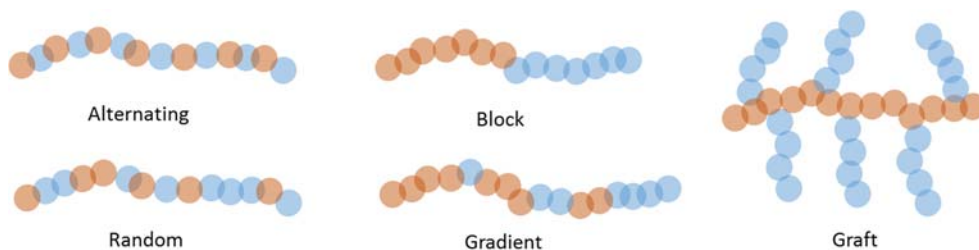


Figure 3–1. Types of various copolymers.

The copolymers are classified based on the arrangement of units along the chain; random, alternating, graft, and so on (Figure 3–1). Among those various types of polymers, block copolymers are one of the most attractive species due to their ability of self-assembly.² The easiest way for synthesis of block copolymer is sequential addition of monomers under the living polymerization

condition. The ROMP of NB derivatives with ultrafast initiating Grubbs catalyst (**III**) is one of the well-known living polymerization.³ Various kinds of block copolymers were already synthesized by this methods. For example, Fréchet's group reported dendronized diblock copolymer and tried to visualize the block structure.⁴ However, the AFM image was not clear because the hydrophilicity of each block was opposite and one block was aggregated on the hydrophilic mica substrate.

Gradient copolymers are a unique class of polymers that have gradual changes in monomer composition along their backbones.⁵ Gradient copolymers are prepared by two approaches: changing the monomer feed rate by continuous addition of co-monomers during polymerization (semi-batch),⁶ or using two monomers having large differences in reactivity in one pot (batch).⁷ Many researchers have synthesized gradient copolymers by powerful controlled radical polymerization. For example, Matyjaszewski's group reported gradient copolymerization under batch conditions via atom transfer radical polymerization (ATRP) exploiting the reactivity differences between methyl methacrylate (MMA) and *n*-butyl acrylate.^{7a} Furthermore, post-functionalization, or another ATRP from this gradient copolymer backbone, produced gradient-brush copolymers and the conformation of the final polymer was observed by AFM imaging. Gradient copolymers were also prepared by ROMP using the semi-batch approach, by controlling the feed rate of the monomers.⁸ Although the batch approach is synthetically much easier, it is hard to find monomer combinations with different reactivities. Also, the single chain imaging analysis of copolymer is rarely studied compared to homopolymer.

3.2 Experimental

3.2.1 Monomer Synthesis

N-hexyl substituted monomers

The *N*-hexyl substituted NB and TD monomers were synthesized simple imidization reaction. The NB(TD) anhydride (1 Eq), hexyl amine (1 Eq), and pyridinium paratoluene sulfonate (0.05 Eq) were dissolved in toluene. Reaction mixture was refluxed for 20 h, and then cool down to the room temperature. The product was purified by column chromatography from crude mixture to get the white solid.

3.2.1 Polymerization

General procedure for block copolymer

Monomer for the 1st block (0.021 mmol) was weighted in a 5 mL vial with septum and purged with argon. Anhydrous and degassed solvent (0.20 mL) was added to the vial and the reaction mixture was stabilized at appropriate temperature. The solution of initiator (0.05 mL) was added at once under vigorous stirring. After the complete consumption of the 1st monomer, the solution of 2nd monomer (0.021 mmol) was added. After complete conversion of monomer, the reaction was quenched by excess ethyl vinyl ether. The concentrated reaction mixture was precipitated into methanol or isopropanol, and the obtained white solid was dried in vacuo.

General procedure for gradient copolymer

Two monomers (0.02 mmol) were added into 5 mL vial and purged with argon gas. Anhydrous and degassed solvent was added and stabilized at appropriate temperature. Then, the solution of initiator (0.00013 mmol) was added. For the experiment of hexyl

monomers 5 times larger amount of reagents were used. After complete conversion of monomer, the reaction was quenched by excess ethyl vinyl ether. The concentrated reaction mixture was precipitated into methanol or isopropanol, and the obtained white solid was dried in vacuo.

***In situ* ¹H NMR kinetics**

Monomer (0.02 mmol) was sealed in screw-cap NMR tube and purged with argon gas. It dissolved in THF-d₈ ampule solvent and stabilized at 50 °C in NMR instrument. Then, the solution of initiator (0.05 mL) was added and the change of olefin signal of each monomers was monitored with time until the complete consumption of both monomers.

Determination of reactivity ratio

The series of monomer mixture with different ratio (70:30, 60:40, 50:50, 40:60, 30:70) was prepared. The reaction was conducted at 0 °C and terminated at early stage of polymerization (<30 sec), and the conversion of each monomer was observed by ¹H NMR.

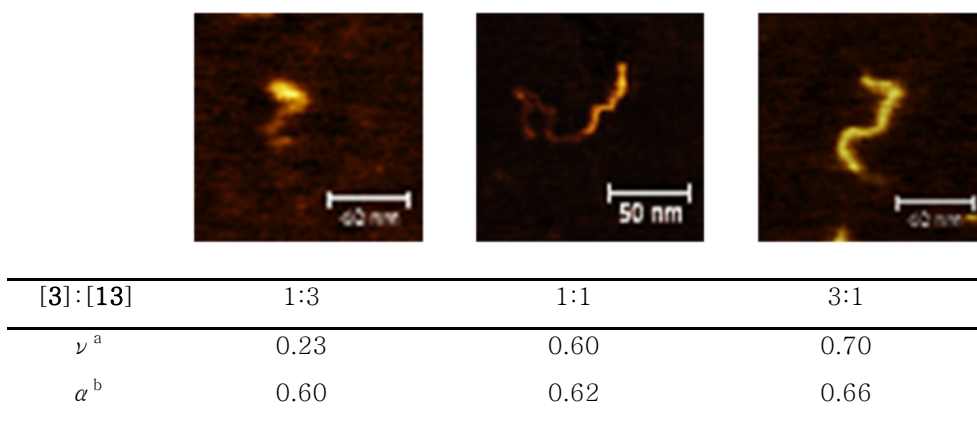
Determination of initiation rate

Monomer (0.02 mmol) was sealed in screw-cap NMR tube and purged with argon gas. It dissolved in THF-d₈ ampule solvent and stabilized at -20 °C in NMR instrument. Then, the solution of initiator (0.05 mL) was added and the change of carbene signal was monitored at an interval of 50 seconds.

3.3 Result and Discussion

3.3.1 Diblock copolymerization

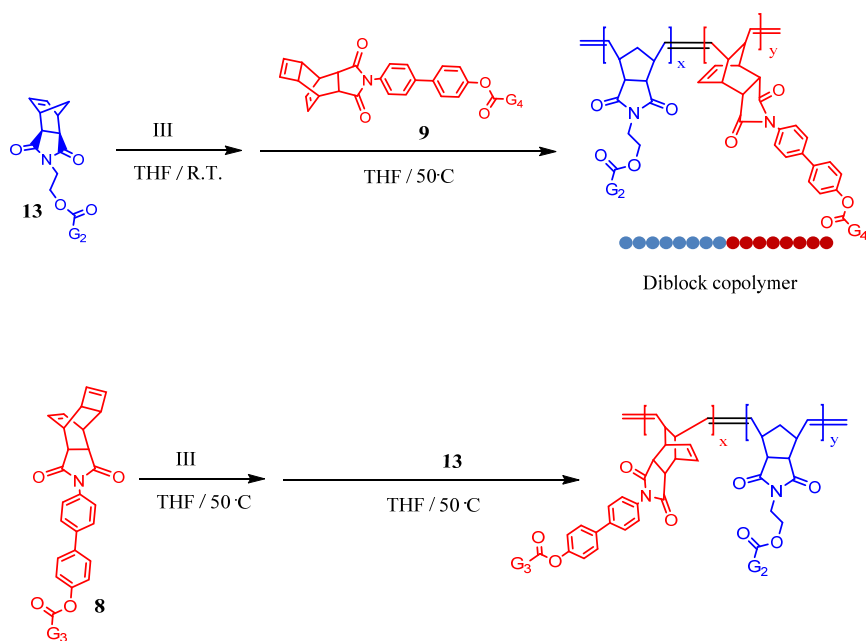
From the previous work on Chapter 2, we confirmed that the ROMPs of our dendronized macromonomers are living polymerization. Encouraged by this result, we polymerized two macromonomers with different size of dendrons (**3** and **13**) by sequential addition, to get the fully dendronized diblock copolymer. The ratio of block was gradually changed from 1:3 to 3:1. With the increase of ratio of bigger macromonomer block (**3**), higher shape factor was obtained from MALLS analysis. AFM image also showed entangled block of **13** and extended block of **3**. Both block have same hydrophilicity because same ester type dendrons are tethered on NB and no severe aggregation of particular block was observed (Figure 3–2).



^a Calculated from conformation plot measured by MALLS. ^b Calculated from Mark-Houwink plot obtained by VIS detector.

Figure 3–2. Conformation comparison of diblock copolymers with different block ratio.

Then we also tried the block copolymerization using both NB and TD macromonomers. The synthesis of dendronized block copolymers with NB and TD derivatives was attempted by sequential addition (Scheme 3–1).



Scheme 3–1. Synthesis of diblock copolymers.

Initially, the NB-based macromonomer containing a G2 ester dendron (**13**) was polymerized in a living manner at room temperature to give the first block. After 30 min, the macromonomer **9** was added as the second block and the reaction temperature was increased to 50 °C to enhance the propagation rate. After 12 h, the ROMP was quenched with ethyl vinyl ether, and poly(**13**)-*b*-poly(**9**) was obtained with an M_n of 663 k and a narrow PDI of 1.10. GPC analysis showed a complete shift of the trace to the higher molecular weight region (Figure 3–3a). Next, by switching the order of the monomer addition, another diblock copolymer having a TD macromonomer containing the same G3 dendron (**8**) as the first block and the same NB macromonomer containing G2 dendron (**13**) as the second block, was attempted. The poly(**8**)-*b*-poly(**13**) was successfully synthesized with a narrow PDI of 1.07, and SEC analysis confirmed the “blocky” microstructure (Figure 3–3b). From the shifts in the GPC traces, a narrow PDI, below 1.10, and an absolute

M_n closely matching the theoretical M_n , we concluded that the living polymerization method for preparing diblock copolymers was indeed successful.

Table 3–1. Results of block copolymerization.^a

entry	monomer	[M]/[I]	time	M_n (Theo) ^b	M_n (Obs) ^c	PDI ^c
1	13	150	0.5h	120k	165k	1.07
	9	200	12h	600k	663k	1.10
2	8	150	4h	201k	210k	1.03
	13	150	1h	296k	267k	1.07

^a The polymerization was performed in THF at various temperatures. ^b Theoretical molecular weight. ^c The values measured by MALLS detector.

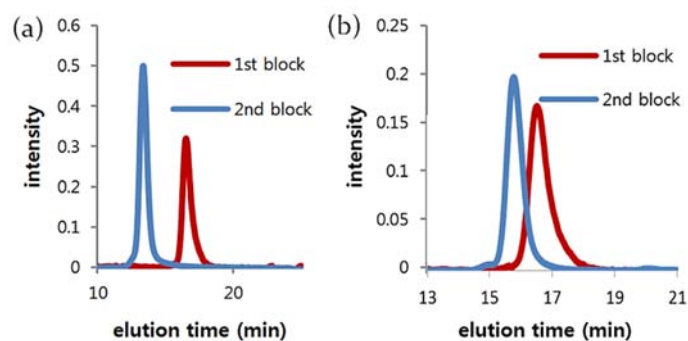


Figure 3–3. GPC traces of (a) poly(13)–*b*–poly(9) and (b) poly(8)–*b*–poly(13).

Because of the bulky side–chains, these fully dendronized diblock copolymers should be easily visualized by AFM imaging. The first AFM imaging of block copolymers was reported by Fréchet’s group,⁴ who prepared diblock copolymers by ROMP of NBs containing G2 ester dendron and G3 Fréchet dendron. Unfortunately, these images had a weakness, as the blocky nature was not clearly revealed, mainly because of the large polarity differences between two

dendrons, polar ester dendrons and nonpolar benzyl ether dendrons. As a result, the block containing hydrophobic Fréchet type dendron aggregated on the polar mica surface, while the other polar block showed extended conformations, thereby leading to tadpole-like nano objects. Also, the size difference between the G2 and G3 dendrons might not be big enough to evidently distinguish each block. Our dendronized diblock copolymers should reveal their true blocky structure with higher resolution because both blocks contained polar ester dendrons and they adsorbed well onto the mica surface, giving a clear image of single chains, without any aggregation. Moreover, each block was differentiated by larger G4 dendron and smaller G2 dendron. Importantly, the height difference was quite large, by a factor of two (1.0 nm vs 0.5 nm), so that clean images of a blocky morphology were visualized (Figure 3–4a). This large difference was a result not only of differences in the generation of the dendrons, but also of the intrinsically bulkier backbones of the TD monomers compared with those of NBs. The other diblock copolymer, poly(8)–*b*–poly(13) was imaged by AFM to reveal a similar blocky morphology with high definition (Figure 3–4b).

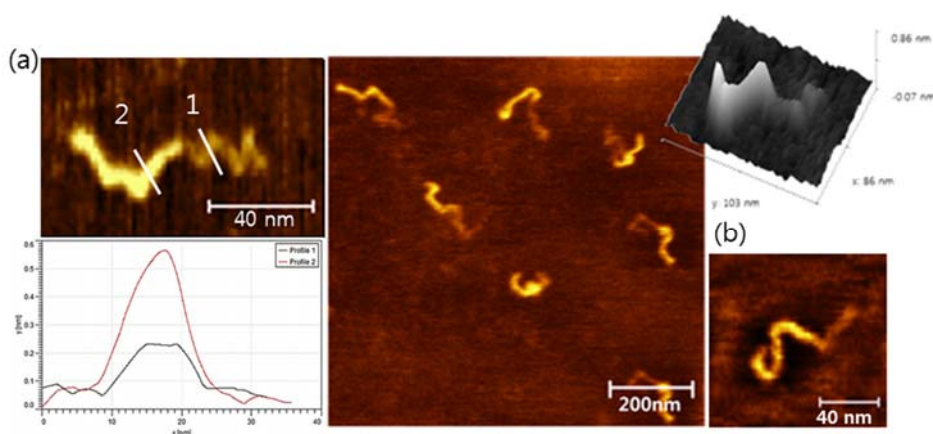
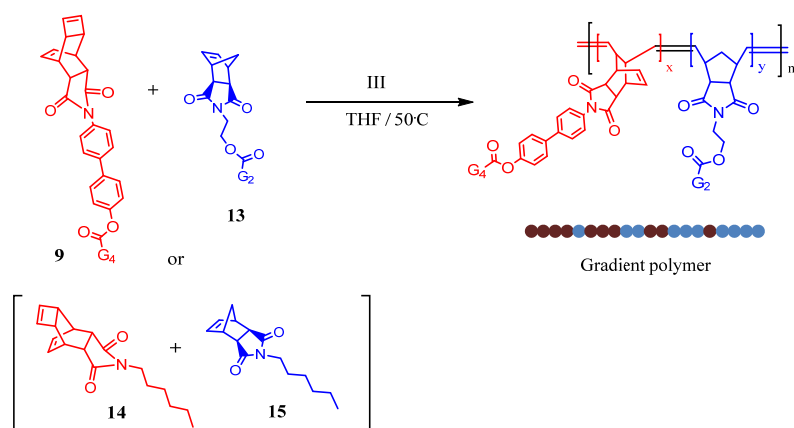


Figure 3–4. AFM image of (a) poly(13)–*b*–poly(9) and (b) poly(8)–*b*–poly(13).

3.3.2 Gradient copolymerization

We then shifted our attention to another type of polymer architecture: gradient copolymers. The simplest method of synthesizing gradient copolymers is that batch copolymerization of two monomers with large difference in reactivities because two monomers are added at the same time for polymerization, whereas the semi-batch method requires a syringe pump technique for continuous addition of co-monomers.



Scheme 3-2. Synthesis of gradient copolymers.

From the observation that the rates of ROMP for TD monomers were much slower than for NB monomers,⁹ gradient copolymerization under batch conditions was tested since both monomers undergo living ROMP. In a model study, two monomers of NB and TD, containing the same *n*-hexyl side chain (**14** and **15** respectively) were simultaneously polymerized at room temperature for 40 min, and the monomer conversions were monitored by ¹H NMR (Figure 3-5a). The copolymers were analyzed by MALLS-GPC, showing M_n close to the theoretical M_n and a fairly narrow PDI. Indeed, the conversion profile showed the expected shape for gradient copolymerization. However, an unexpected result was observed,

when the TD monomer (**14**) was consumed much faster than the NB monomer **15**. To confirm the unexpected kinetics, the reactivity ratios of monomers **14** and **15** were measured using the Finemann–Ross plot method (Figure 3–6).¹⁰ As a result, the reactivity ratios were estimated to be $r_1 = 3.9$ (**14**) and $r_2 = 0.1$ (**15**); these values are in agreement with the commonly accepted values for gradient copolymerization: $r_1 \gg 1$, $r_2 \ll 1$. These results confirmed that the TD monomer was ironically more reactive than the NB monomer, even though it took a much longer time for ROMP.

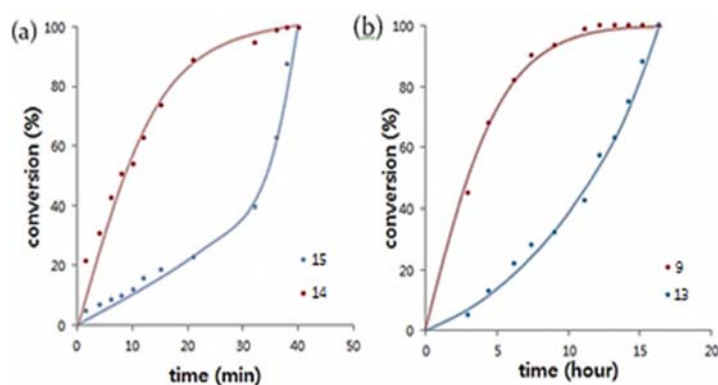


Figure 3–5. Monomer conversion profiles for (a) poly(**14**)–*g*–poly(**15**) and, (b) poly(**9**)–*g*–poly(**13**).

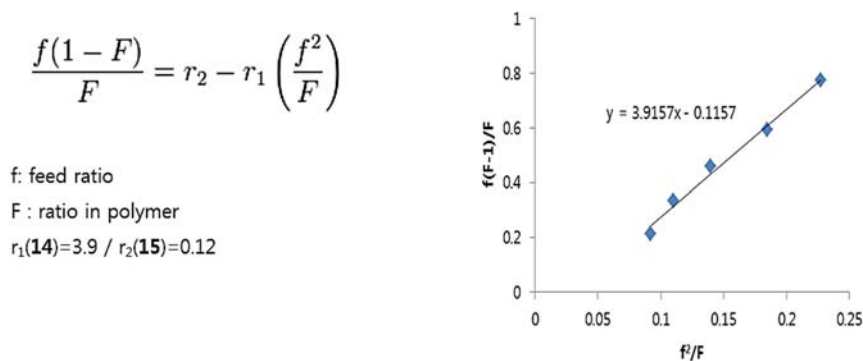
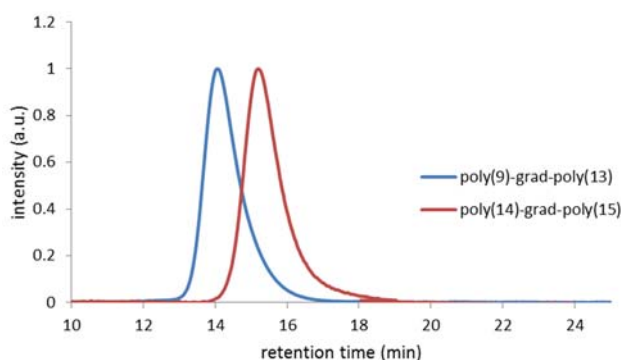


Figure 3–6. Determination of reactivity ratio of monomer **14** and **15** by Fineman–Ross equation.

Table 3–2. Results of gradient copolymerization.^a

entry	monomer	[M]/[I]	time	M _n (Theo) ^b	M _n (obs) ^c	PDI ^c
1 ^d	14	200	1h	106k	101k	1.25
	15	200				
2	9	150	16h	607k	613k	1.35
	13	150				

^a The polymerization was performed in THF at various temperatures in NMR tube. ^b Theoretical molecular weight. ^c The molecular weight and PDI was measured by MALLS detector. ^d The reaction was performed at room temperature.

**Figure 3–7. GPC traces of gradient copolymers.**

From our initial success in synthesizing gradient copolymers, the investigation was further expanded to the copolymerization of dendronized macromonomers **9** and **13**, which were previously used to prepare diblock copolymers. Gradient copolymerization was conducted at 50 °C and the monomer conversion profile for both **9** and **13** was monitored by ¹H NMR. Again, the profiles of gradient microstructures were obtained with the TD macromonomer **9**, which underwent ROMP faster than the NB macromonomer **13**, just as in the previous model study. This was even more surprising because **9** contained much larger *endo*-G4 dendrons than **13**, which contained *exo*-G2 dendron, so **9** should have been much less reactive. The absolute molecular weights of the gradient copolymers, measured by

MALLS, matched the theoretical values well and the PDIs were still relatively narrow (Scheme 3–2, entry 2).

To understand this unexpected reactivity ratio, we measured the initiation rates (k_i) of catalyst **III** for macromonomers **9** and **13** by monitoring the disappearance of the benzylidene signal via ^1H NMR. These experiments were conducted at $-20\text{ }^\circ\text{C}$ to obtain reliable k_i values because of the intrinsically fast k_i of 3rd generation Grubbs catalyst. First-order kinetics obviously showed that the k_i of **9** was five-fold larger than k_i of **13** (0.0035 s^{-1} vs 0.0007 s^{-1}) (Figure 3–8). In other words, surprisingly, the catalyst could approach the seemingly more bulky TD macromonomer **9** faster than the NB macromonomer **13**. This puzzled us at first, but when we considered the local steric hindrance around the active olefins, it became clear that the cyclobutene moiety of the TD monomers was more exposed to coordination by the catalyst than the olefins on the NBs, which contained an extra bridging methylene group, thereby hindering coordination. Hence, more accessible TD monomers could more easily coordinate the active site of the catalyst. Although the steric hindrance about the catalyst became larger after one turnover, the coordination preference for the TD monomer was maintained throughout the whole polymerization (Figure 3–9). From the experimental data, we speculated that the propagation rate of active carbenes containing ring opened TD monomers was slower because of steric congestion around the propagating species, but coordination to the catalysts or propagating species was always favored for TD monomers over the NB derivatives, regardless of the bulkiness of the distal side chains. Thus, the propagating species of TD and NB both preferred to react with TD monomers and, as a result,

gradient copolymers were prepared with faster consumption of TD monomers.

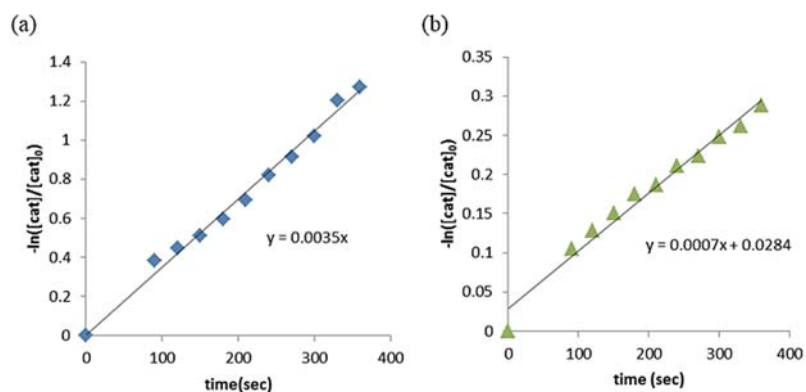


Figure 3-8. Plot for monomer consumption vs time during initiation step for (a) TD macromonomer 9 (b) NB macromonomer 13.

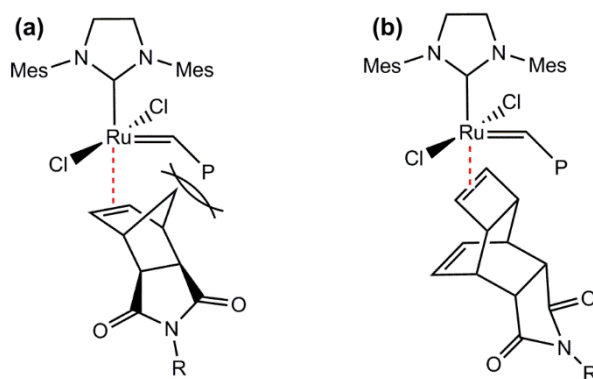


Figure 3-9. Schematic explanation for the steric on (a) NB and (b) TD during initiation.

Prior to this work, there was one report on the visualization of gradient copolymers containing brush type side chains, prepared by post-functionalization or the graft-from method to grow brush side chains.^{7a} Unfortunately, the resolution of the AFM images of those gradient brush copolymers was not high enough because the gradient copolymer comprised mixtures of brush polymer and flexible and small poly(methyl methacrylate) (PMMA). Although

brush polymers showed extended conformations, allowing easy AFM imaging, the flexible PMMA adopted random coil conformations, making it much harder to get clear AFM images. Furthermore, the gradient brush copolymer was prepared by multiple post-functionalization reactions and the inevitable defects, such as incomplete deprotection or initiation of ATRP, would prevent clear visualization. Here, we report AFM imaging of more well-defined dendronized gradient copolymers, prepared directly in a single step from larger G4 and smaller G2 dendronized macromonomers. Figure 3-10 shows one-dimensional nanostructures exhibiting a gradual decrease in not only the heights, from 1 nm to 0.4 nm, but also a gradual decrease in the thickness, from 5.5 nm to 2.8 nm. This fully dendronized gradient copolymer adopted highly extended conformations, making AFM imaging easier. Also, it was prepared from two monomers containing dendrons of vastly different sizes by the macromonomer approach, and defect-free and linear gradient copolymers were visualized by AFM with high resolution.

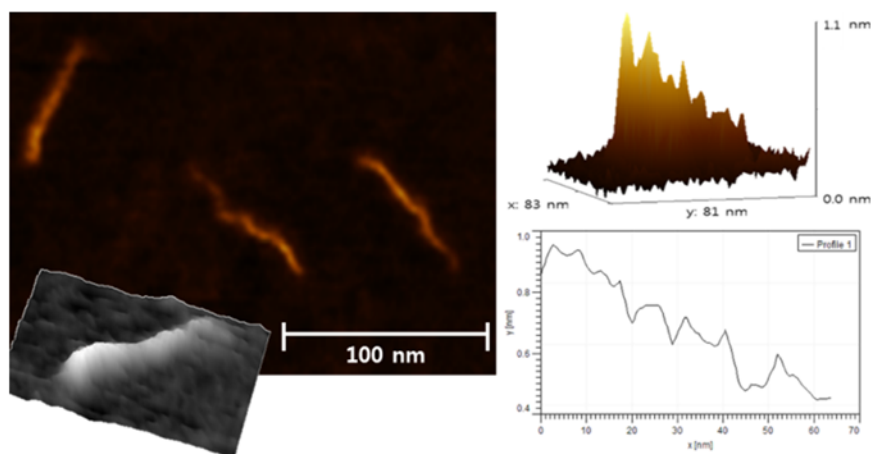


Figure 3-10. AFM images of gradient copolymers.

3.3.3 Comparison the structure of two copolymers

With these high resolution images of diblock and gradient copolymers prepared from the same two macromonomers (**9** and **13**), the structural differences between these two copolymers was compared in detail by AFM. The gradient copolymer showed smooth and gradual changes in both height and thickness, without any interfacial boundary, whereas the diblock copolymer contained a clear junction, showing abrupt changes in both height and thickness (Figure 3–11). In addition, the chains of the gradient copolymer exhibited highly extended conformations without local regions of entangled random coil conformations. However, two distinct conformations were observed for the diblock copolymer because the block composed of small dendron (**13**) showed more entangled conformation, whereas the other block, composed of large dendron (**9**), showed extended conformations.

With these different conformations of two types of copolymers, observed by AFM, we investigated their behaviour in solution by conducting MALLS analysis to obtain the shape factor, ν . The ν value for the gradient copolymer was much greater than that for the diblock copolymer (0.82 vs 0.60, Figure 3–11) but these values were obviously much lower than the value for the homopolymer (**9**), 0.99. This confirmed that the dendronized gradient copolymer was much stiffer than the dendronized diblock copolymer in solution as well as in the solid state, because the highly rigid macromonomer **9** was incorporated throughout the whole copolymer, thereby stretching the chains, whereas half of the polymer was relatively flexible for the diblock copolymer, thereby lowering the rigidity of the whole copolymer. This was a noteworthy observation because even though these diblock and gradient copolymers were

prepared from the same monomers, their conformations and rigidities were very different as a result of different monomer sequences.

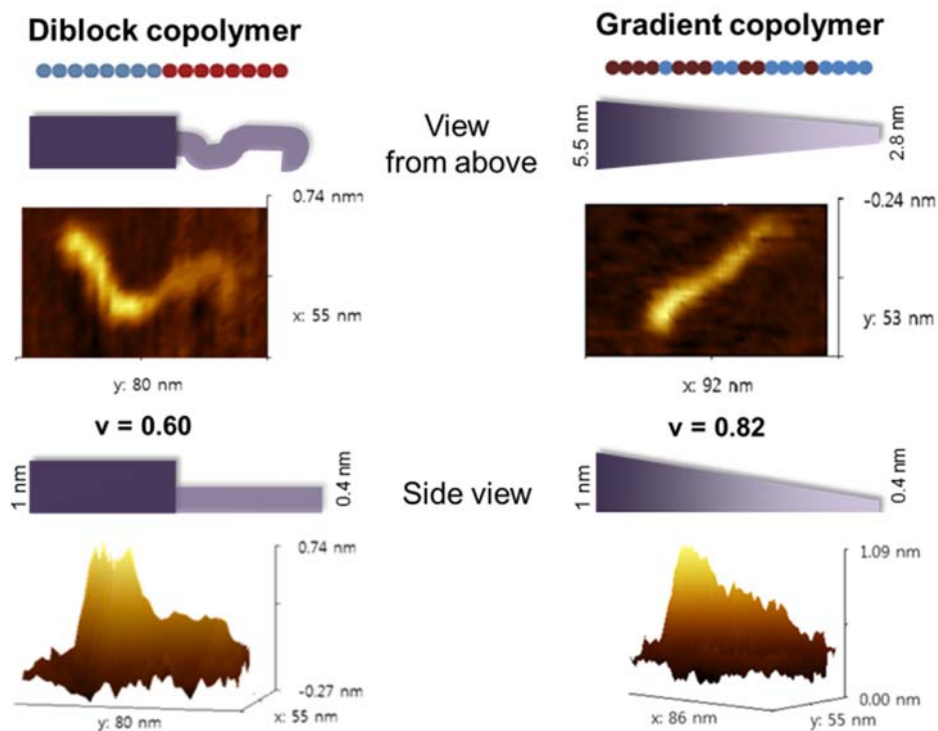


Figure 3-11. Structural difference between single chains of block copolymer and gradient copolymer.

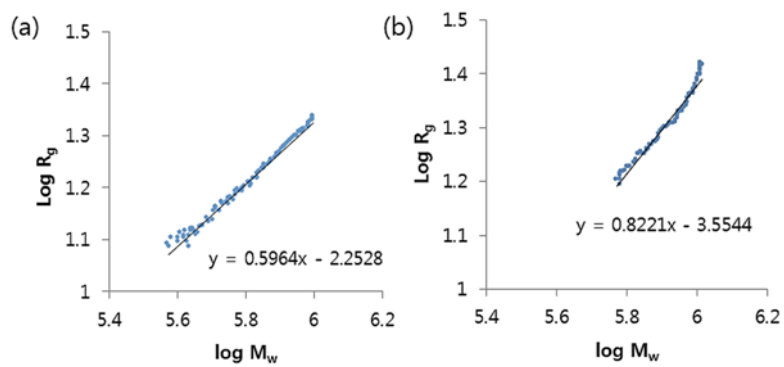


Figure 3-12. Conformation plot of (a) diblock copolymer and (b) gradient copolymer.

3.4 Conclusion

The diblock copolymers and gradient copolymers were easily synthesized from dendronized macromonomers based on NB and TD moieties. The sequential addition of the two monomers produced diblock copolymers whereas the simultaneous reaction of NB and TD monomers produced gradient copolymers as a result of the large differences in reactivity. TD monomers were consumed faster because of the more reactive cyclobutene moiety. Detailed microstructures of copolymers were visualized by high resolution AFM. Accurate imaging was possible because both dendronized polymers were large enough to show clear AFM images, and the size differences between the two dendrons was also large enough to differentiate their microstructures. The change of each block length with different monomer feeding ratio was clearly defined. Furthermore, an interesting contrast between the structures of diblock and gradient copolymers was observed, as the high resolution images distinguished both types of polymers from the presence of a boundary for each block or gradual changes in height and thickness. Lastly, conformational analysis in solution indicated that the gradient copolymers were stiffer than the corresponding diblock copolymers.

3.5 References

- [1] (a) Harper, C.A. *Handbook of plastic and elastomers*, McGraw–Hill, New York, **1975** (b) Couchman, P. R. *Macromolecules*, **1982**, *15*, 770.
- [2] (a) Mai, Y. Y.; Eisenberg, A. *Chem. Soc. Rev.*, **2012**, *41*, 5969. (b) Darling, S. B. *Prog. Polym. Sci.*, **2007**, *32*, 1152. (c) Bates, C. M.; Maher, M. J.; Janes, D. W.; Ellison, C. J.; Willson, C. G. *Macromolecules*, **2014**, *47*, 2.
- [3] (a) Choi, T. –L.; Grubbs, R. H. *Angew. Chem. Int. Ed.* **2003**, *42*, 1743. (b) Love, J. A.; Morgan, J. P.; Trnka, T. M.; Grubbs, R. H. *Angew. Chem. Int. Ed.* **2002**, *41*, 4035.
- [4] Rajaram, S.; Choi, T. –L.; Rolandi, M.; Fréchet, J. M. J. *J. Am. Chem. Soc.* **2007**, *129*, 9619.
- [5] (a) Beginn, U. *Colloid. Polym. Sci.* **2008**, *286*, 1465. (b) Steinhauer, W.; Hoogenboom, R.; Keul, H.; Moeller, M. *Macromolecules* **2013**, *46*, 1447. (c) Matyjaszewski, K.; Xia, J. *J. Chem. Rev.* **2001**, *101*, 2921.
- [6] (a) Gray, M. K.; Zhou, H.; Nguyen, S. T.; Torkelson, J. M. *Macromolecules* **2004**, *37*, 5586. (b) Matyjaszewski, K.; Ziegler, M. J.; Arehart, S. V.; Greszta, D.; Pakula, T. J. *Phys. Org. Chem.* **2000**, *13*, 775.
- [7] (a) Lee, H. –I.; Matyjaszewski, K.; Yu, W.; Sheiko, S. S. *Macromolecules* **2005**, *38*, 8264. (b) Hu, Z.; Zhang, Z. *Macromolecules* **2006**, *39*, 1384. (c) Mignard, E.; Leblanc, T.; Bertin, E.; Guerret, O.; Reed, W. F. *Macromolecules* **2004**, *37*, 966.
- [8] Dettmer, C. M.; Gray, M. K.; Torkelson, J. M.; Nguyen, S. T. *Macromolecules* **2004**, *37*, 5504.
- [9] Charvet, R.; Novak, B. M. *Macromolecules* **2001**, *34*, 7680.
- [10] (a) Kelen, T.; Tüdös, F. J.; *Macromol. Sci. Chem. A.* **1975**, *9*, 1. (b) Tidwell, P. W.; Mortimer, G. A. *J. Polym. Sci. Part A.* **1965**, *3*, 369.

Chapter 4.

Controlled ROMP of TD Based Monomers

4.1 Introduction

Living polymerization is a very attractive tool not only for controlling the molecular weights of polymers with excellent predictability and narrow PDIs, but also to prepare more complex structure such like block copolymers or star polymers.¹ To obtain polymers with precise control, side reactions, such as chain termination or chain transfer, should be eliminated and the initiation/propagation rate ratio (k_i/k_p) should be sufficiently high. The most popular examples of living polymerization by olefin metathesis mechanism are ROMP of NB derivatives,² and, more recently, cyclopolymerization of 1,6-heptadiynes using 3rd generation Grubbs or Schrock catalysts.³

Various ruthenium catalysts have been developed for efficient ROMP;⁴ among them, the ultra-fast initiating 3rd generation Grubbs catalyst is the best catalyst for living polymerization due to its high activity and large k_i/k_p . On the other hand, 2nd generation Hoveyda-Grubbs catalyst is generally not suitable for living polymerization because of slow initiation and small k_i/k_p .^{4a} In 2004, Slugovc reported controlled ROMP of a NB derivative containing an *endo,exo*-bis-ketone group using 2nd generation Hoveyda-Grubbs catalyst.⁵ Coordination of the *endo*-carbonyl group to the catalyst significantly decreased the propagation rate, thereby increasing the k_i/k_p .

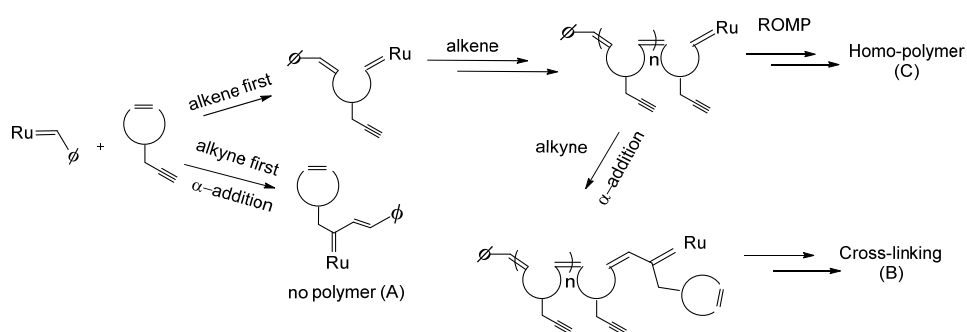
However, the monomer scope was limited to *endo,exo*-diketone or -diester functionalities and block copolymers could not be synthesized using this method, as evidenced by the bimodal traces in the GPC analysis. For the same reaction, 2nd generation Grubbs catalyst exhibited an extremely small k_i/k_p owing to even slower initiation and extremely fast propagation:^{4b} accordingly, polymers with broad PDIs and much higher molecular weights than the theoretical values were obtained. Therefore, to the best of our knowledge, no report on controlled ROMP using 2nd generation Grubbs catalyst has been published. Nevertheless, 2nd generation Grubbs and Hoveyda-Grubbs catalysts are still very useful due to their superior catalytic activity, thermal stability, and long-term stability in storage than 1st and 3rd generation Grubbs catalysts.⁶ As a result, some monomers only undergo ROMP with these active catalysts.⁷ TD has an interesting structure comprising two olefins with ROMP-active cyclobutene fused to ROMP-inactive bicyclo[2,2,2]oct-2-ene; its derivatives undergo living ROMP in the presence of 1st generation Grubbs catalyst.⁸ These TD monomers are rarely used for ROMP because their propagation rate (they typically require 24 h for complete conversion) is much slower than those of NB derivatives, which are the most widely used monomers. Fortunately, we observed much faster initiation or faster coordination of the Grubbs catalyst to TD derivatives than to NB derivatives from the previous chapter, implying that a much larger k_i/k_p may be possible for TD derivatives.

Multi-arm star polymers are specific class of polymers that have star-like shape consisted of more than three polymer arms from a focal point. These polymers have attracted much attention because based on their unique topologies, they promote unique self-

assemblies which can't be realized from conventional linear polymers.⁹ Synthetic strategies for the star polymers include core-first and arm-first approaches.¹⁰ Between two methods, core-first method is more effective to produce star polymers with well-defined number of arms. Many examples have been reported especially using the core-first method by controlled radical polymerization (CRP) such as ATRP with multi-arm initiators.^{10a} Still the synthesis of star polymers is challenging, especially via ROMP. Several attempts were made, but low conversion and broad PDI was observed because of either low activity of stable catalyst or non-living system with highly active catalyst.¹¹ If ROMP can provide more reliable synthetic pathway for the star polymers, this method would be very powerful because potentially, dendronized or graft star polymers can be directly prepared by the macromonomer approach.

The controlled ROMP of olefin monomers containing alkyne is another challenge for polymer synthesis. Several research groups have already investigated on this field. In 2004, Binder et al. attempted ROMP of an oxonorbornene derivative containing a terminal alkyne substituent by using 1st generation Grubbs catalyst.¹² However, this direct polymerization produced oligomers having broad polydispersity indices (PDIs of 1.8), and it was proposed that the alkyne and alkene moieties competed for reaction in the presence of this catalyst, resulting in side reactions (Scheme 4-1). Nevertheless, this group could install the alkyne moiety after ROMP of the oxonorbornene derivative, by post-functionalization via an S_N2 reaction, enabling subsequent click reaction with an azide. Other research groups have also carried out ROMP of NB monomers containing cobalt- or silyl-protected alkynes and executed the click reaction following deprotection of the polymer.¹³ However, protecting

and deprotecting the alkyne moiety requires an additional post-functionalization step, increasing the likelihood of introducing defects into the polymer architecture due to the intrinsic challenges associated with such modifications. It is therefore desirable to perform direct ROMP of monomers containing active alkyne moieties in order to prepare polymers with better-defined functionality and microstructure in fewer synthetic steps. In order to achieve this goal, the chemoselectivity issue needs to be resolved by increasing the reactivity of the cycloalkene toward ROMP while simultaneously decreasing the reactivity of the alkyne.



Scheme 4-1. Competition between alkenes and alkynes for reaction with a metathesis catalyst.

4.2 Experimental

4.2.1 Monomer synthesis

7,8-dimethylene benzyloxy-*endo*-tricyclo[4.2.2.0^{2,5}]deca-3,9-diene (17)

The 25 mL RBF with dialcohol (0.10 g, 0.52 mmol) solution in THF (1.8 mL) was prepared. Then sodium hydride (60 %, 62.4 mg, 1.6 mmol) was added at room temperature and the reaction mixture was stirred for 30 min, then benzyl bromide (99 %, 0.16 mL, 1.3 mmol) was added and the mixture was stirred for 3 h. After completion of the reaction, the mixture was washed with saturated NH₄Cl solution and NaHCO₃ solution then organic layer was extracted with ethyl acetate 3 times. The organic layer was dried with MgSO₄ anhydrous and the solvent was removed on a rotary evaporator. The product was purified by column chromatography with ethyl acetate-hexane mixture (1:30 in volumetric ratio). The separated product solutions were collected and concentrated to yield 0.18 g of final product.

7,8-bis(((*tert*-butyldimethylsilyl)oxy)methyl)-*endo*-tricyclo[4.2.2.0^{2,5}]deca-3,9-diene (18)

The 25 mL RBF with dialcohol (0.10 g, 0.5 mmol) solution in dichloromethane (1.8 mL) and triethylamine (0.22 mL, 1.6 mmol) was prepared. Then *t*-butyldimethylsilane chloride (0.24 g, 1.6 mmol) and 4-dimethylaminopyridine (DMAP) (3.2 mg, 0.027 mmol) were added at room temperature, and the reaction mixture was stirred for 4 h. After completion of the reaction, saturated NaHCO₃ aqueous solution was added and stirred for 1 h. The mixture was washed with saturated NH₄Cl solution and NaHCO₃ solution then organic layer was

extracted with ethyl acetate 3 times. The organic layer was dried with MgSO₄ anhydrous and the solvent was removed on a rotary evaporator. The product was purified by column chromatography with ethyl acetate–hexane mixture (1:90 in volumetric ratio). The separated product solutions were collected and concentrated to yield 0.16 g of final product.

7,8–dimethylene acetate–*endo*–tricyclo[4.2.2.0^{2,5}]deca–3,9–diene (19)

The 25 mL RBF with dialcohol (0.10 g, 0.52 mmol) solution in dichloromethane (1.8 mL) and triethylamine (0.43 mL, 3.2 mmol) was prepared. Then acetic anhydride (0.16 mL, 1.6 mmol) and 4–dimethylaminopyridine (DMAP) (3.2 mg, 0.027 mmol) were added at room temperature, and the reaction mixture was stirred for 6 h. After completion of the reaction, the mixture was washed with saturated NH₄Cl solution and NaHCO₃ solution then organic layer was extracted with ethyl acetate 3 times. The organic layer was dried with MgSO₄ anhydrous and the solvent was removed on a rotary evaporator. The product was purified by column chromatography with ethyl acetate–hexane mixture (1:10 in volumetric ratio). The separated product solutions were collected and concentrated to yield 0.14 g of final product.

7,8–*N*–methyleneferrocenylsuccimide–*endo*–tricyclo[4.2.2.0^{2,5}]deca–3,9–diene (20)

Anhydride *endo*–Tricyclo–[4.2.2.0^{2,5}]deca–3,9–diene (0.22 g, 1.2 mmol) and ferrocenyl methylamine (0.27 g, 1.3 mmol) were dissolved in toluene (10 mL). The reaction mixture was stirred at 40 °C about 30 min and then refluxed overnight. After completion of

the reaction, the reaction mixture was cooled down to room temperature and the solvent was removed on a rotary evaporator. The product was purified by column chromatography with dichloromethane–hexane mixture (2:1 volumetric ratio). The separated product solutions were collected and concentrated to yield 0.37 g of final product.

[7,8-*N*-methylenealkyenesuccimide-*endo*-tricyclo[4.2.2.0^{2,5}]deca-3,9-diene] [dicobalt hexacarbonyl] complex(21)

7,8-*N*-propargyl *endo*-Tricyclo-[4.2.2.0^{2,5}]deca-3,9-diene (0.10 g, 0.42 mmol) was dissolved in dichloromethane (4 mL) and the solution temperature was decreased to 0 °C. Then dicobalt octacarbonyl (0.29 g, 0.84 mmol) was added and the reaction mixture was stirred for 2 hours at 0 °C and then was stirred 2 hours at room temperature. After completion of the reaction, the solvent was removed on a rotary evaporator. The product was purified by column chromatography with dichloromethane. The separated product solutions were collected and concentrated to yield 0.14 g of final product.

NB containing alkyne moieties

The *exo*-NB anhydride (1 Eq) was purged with argon gas. Then 10mL of anhydrous toluene was added and the flask was fitted with a Dean–Stark trap and a condenser. Subsequently alkyne amine (1.2 Eq) was added at room temperature. The reaction mixture was refluxed with oil bath at 120 °C for 15 h. After reaction, the solvent was removed on a rotary evaporator. The product was purified by column chromatography (EA:Hex=1:3). The separated product solutions were collected and concentrated to yield final product.

TD containing alkyne moieties

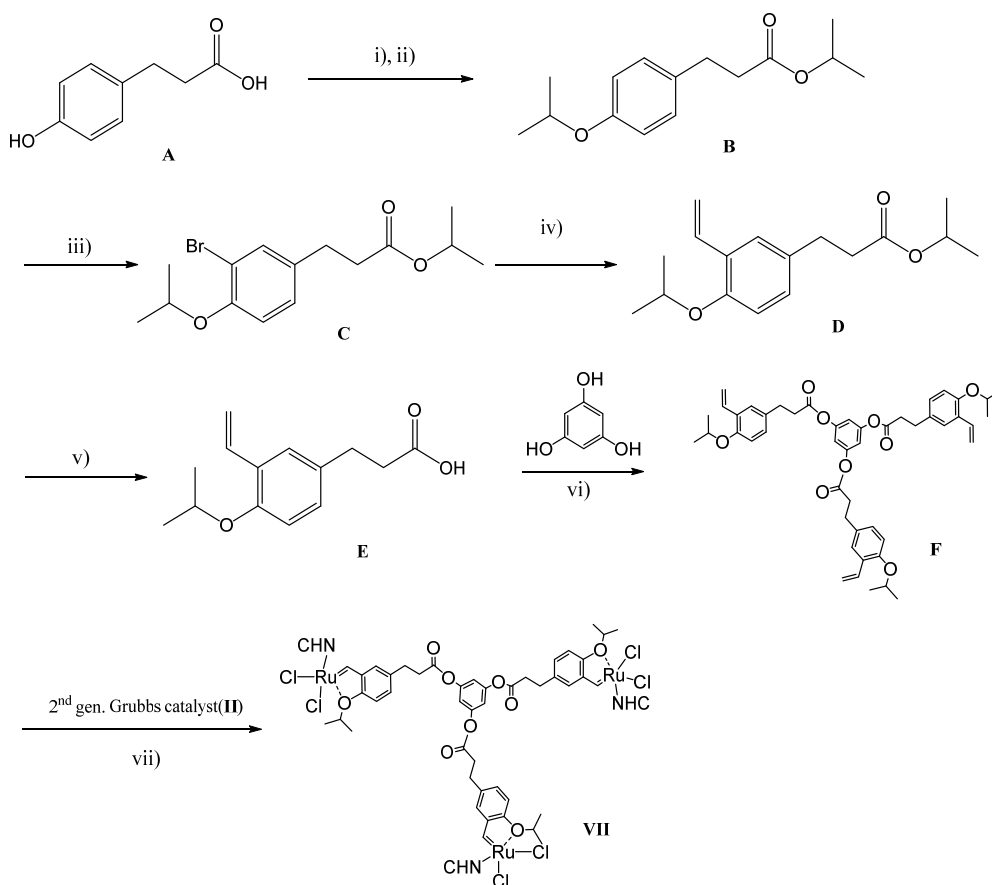
The anhydride *endo*-Tricyclo-[4.2.2.0^{2.5}]deca-3,9-diene (1 Eq) was purged with argon gas. Then 15 mL of anhydrous toluene was added and the flask was fitted with a Dean-Stark trap and a condenser. Then alkyne amine (1.2 Eq) was added at room temperature. The reaction mixture was refluxed with oil bath at 120 °C for 15 h. After the reaction, the solvent was removed on a rotary evaporator. The product was purified by column chromatography (EA:Hex=1:3). The separated product solutions were collected and concentrated to yield final product.

General procedure for synthesis of azide compounds

The bromide complex (1 Eq) and sodium azide (1.5 Eq) were equipped in RBF and dissolved in acetone/water = 5/1 mixture. The reaction mixture was stirred at room temperature for overnight. After finish the reaction, acetone is evaporated and product was extracted from aqueous layer by dichloromethane. The organic layer was collected and dried by MgSO₄ and concentrated.

4.2.2 Tri-functionalized catalyst synthesis

Tri-functionalized catalyst based on 2nd generation Hoveyda-Grubbs catalyst was synthesized follow the Scheme 4-2. The compound **A** - **E** was synthesized by minor modification of previous paper.¹⁴



Scheme 4-2. Synthesis of tri-functionalized catalyst.

i) K_2CO_3 , DMF, IPA, 60 °C, 3 h; ii) NaH, DMF, IPA, room temperature, 5 h; iii) Br_2 , Acetic acid, dichloromethane, room temperature, 1 h; iv) $\text{Pd}(\text{PPh}_3)_4$, tributyl(vinyl)Tin, toluene, 110 °C, 12 h; v) KOH, 100 °C, overnight; vi) EDA, DMAP, Et_3N , dichloromethane, room temperature, overnight; vii) dichloromethane, room temperature, 12 h.

Benzene-1,3,5-triyl tris(3-(4-isopropoxy-3-vinyl) propanoate (F)

1-(*p*-isopropoxy-*m*-vinylphenyl)propionic acid (0.21 g, 0.90 mmol) and phlorogluciol (0.028 g, 0.22 mmol) was dissolved in triethylamine (0.13 mL) and dichloromethane (3 mL). Then 4-dimethylaminopyridine (1.34 mg, 0.011 mmol) and 1-Ethyl-3-(3-dimethylaminopropyl)carbodiimide (0.19 g, 1.0 mmol) was added and

the reaction mixture was stirred for 5 hours at room temperature. After completion of the reaction, the reaction mixture was washed with saturated ammonium chloride aqueous solution and brine. The organic layer was collected and dried with MgSO₄ and rotary evaporator. The product was purified by column chromatography with hexane/ethyl acetate = 5/3. The separated product solutions were collected and concentrated to yield 104 mg of final product.

Benzene-1,3,5-*tris*[(4,5-DihydroIMES)Cl₂Ru=CH-*o*-O*Pr*C₆H₃(CH₂)₂COO] (VII)

Benzene-1,3,5-triyl tris(3-(4-isopropoxy-3-vinyl)propanoate (25.00 mg, 0.03 mmol) and CuCl (12.50 mg, 0.12 mmol) and 2nd generation Grubbs catalyst (104.00 mg, 0.12 mmol) was purged with Ar gas for three times, then dissolved in degassed anhydrous dichloromethane (3 mL). The reaction mixture was stirred for 2 hours at room temperature. As the reaction goes, the color of reaction mixture was changed to dark green. After completion of the reaction, the solvent was removed on a rotary evaporator. The product was purified by flash column chromatography with dichloromethane to remove remained 2nd generation Grubbs catalyst. Then eluent was changed to hexane/ether = 5/3 and gradually increase the amount of ether till ether only. The separated product solutions were collected and concentrated to yield 50.77 mg of final product. Yield : 78%; light green solid; ¹H-NMR (500 MHz, CDCl₃): δ 1.28 (d, 18 H), 2.42-2.49 (m, 54 H), 2.81 (m, 6 H), 3.03 (m, 6 H), 4.19 (s, 12 H), 4.88 (m, 3 H), 6.74-6.84 (m, 9 H), 7.09 (s, 12 H), 7.39 (m, 3 H) ; ¹³C-NMR (125 MHz, CDCl₃): δ 21.06, 21.11, 29.17, 29.29, 36.05, 68.36, 75.02, 112.98, 122.43, 129.38, 129.40, 129.41, 133.76, 138.89, 145.33, 150.99, 151.06, 166.18, 167.19,

170.49, 171.72, 211.28, (LRMS): $[M+3H]^+$: calcd. for $C_{108}H_{133}Cl_6N_6O_9Ru_3$, 2173.5, found, 2173.5.

4.2.3 Polymerization

General procedure for click reaction (CuAAC)

To the solution of Poly (**28**) (conv: 71%, DP ~ 70) (35 mg, 0.13 mmol) and CuI (2.47 mg, 1.3 μ mol) in DMF (0.40 mL) each azide (0.19 mmol, 1.5 eq) and *N,N'*-diisopropylethylamine (8.4 mg, 0.07 mmol) were added sequentially at room temperature. Then the reaction mixture was heated by oil bath to 50 °C for 20 h. After reaction, the DMF was evaporated a bit and polymer was precipitated in methanol from DMF.

Determination of initiation and propagation rate by 1H NMR

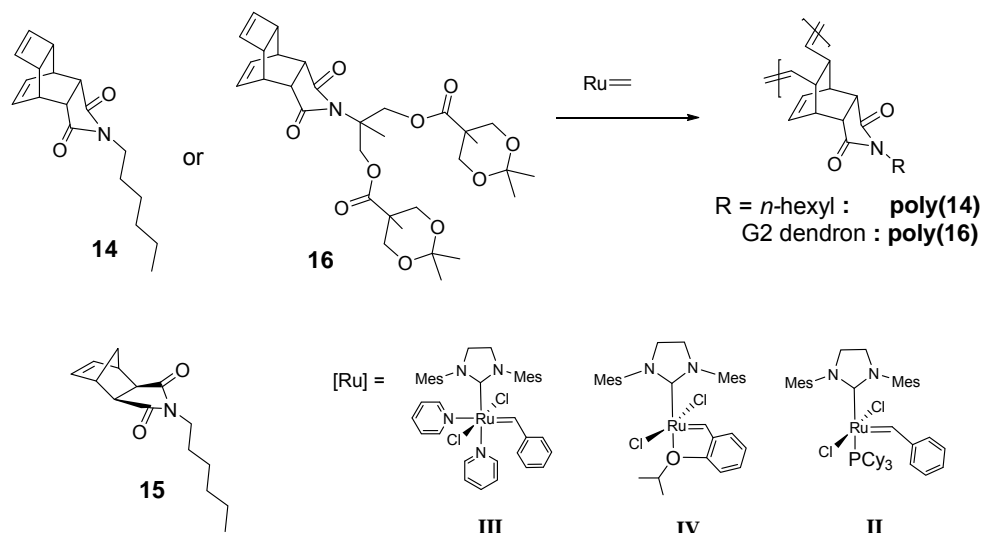
Monomer (1 eq) was sealed in screw-cap NMR tube and purged with argon gas. It dissolved in 0.6 mL THF- d_8 ampule solvent and stabilized at proper temperature in NMR instrument. Then, the solution of initiator (0.05 mL, 0.05 Eq) was added and the change of carbene signal (19.13 ppm for cat **III**, 16.31 ppm for cat **IV**, 19.27 ppm for cat **II**) and olefin signal (5.86 ppm and 5.80 ppm for monomer **14**, 6.28 ppm for monomer **16**) was monitored at an interval of 30 – 150 seconds, respectively.

Condition $[M] \sim 0.22M$ and $[I] \sim 0.011M$ and $[M]/[I] = 20$ for **III** and **IV**
 $[M] \sim 0.1M$ and $[I] \sim 0.004M$ and $[M]/[I] = 25$ for **II**

4.3 Result and Discussion

4.3.1 Living ROMP using 2nd generation Grubbs and 2nd generation Hoveyda–Grubbs catalysts

From the kinetic study for initiation rate of TD based monomer in Chapter 3, we concluded that the initiation rate of TD monomers are much faster than conventional NB monomers. The fast initiation increase the k_i/k_p ratio which is one of the required condition for living polymerization. This is important point for the living ROMP with thermally stable Hoveyda type catalyst, because the slow initiation rate of this catalyst inhibits the living polymerization whereas high reactivity and stability enables the polymerization of less reactive or sterically hindered monomers.^{4,7}



Scheme 4-3. ROMP of TD monomers 14–16.

The TD moiety was prepared by initial electrocyclization of cyclooctatetraene followed by a stereo-specific Diels–Alder reaction with maleic anhydride to give the *endo* product. From this basic unit, various TD monomers (14–21) were easily prepared by following previous methods. To generate a monomer with a bulky

side-chain, a macromonomer containing a G2 ester dendron was synthesized via a divergent route. Each monomer was purified by flash column chromatography and characterized by NMR spectroscopy and high-resolution mass spectroscopy (HRMS) or matrix-assisted laser desorption/ionization mass spectrometry (MALDI-MS). ROMP of these monomers was carried out using catalysts **II**, **III**, and **IV** in THF at room temperature, and was completed within 2 h even for [M]/[I] = 500 (less than 30 min for lower [M]/[I]), which is much faster than the previously reported ROMP using 1st generation Grubbs catalyst.⁸

Table 4-1. ROMP of monomers 14-16 using catalyst II-IV.^a

entry	monomer	cat	[M]/[I]	M _n (Theo) ^b	M _n (MALS) ^c	PDI(MALS) ^c
1	14	III	300	86 k	80k	1.02
2	14	IV	50	14 k	15 k	1.02
3	14	IV	100	29 k	27 k	1.02
4	14	IV	200	57 k	47 k	1.02
5	14	IV	300	86 k	77 k	1.03
6	14	IV	500	143 k	120 k	1.03
7	14	II	300	86 k	296 k	1.35
8	16	II	50	30 k	27 k	1.15
9	16	II	100	60 k	76 k	1.19
10	16	II	200	120 k	118 k	1.20
11	16	II	300	180 k	165 k	1.28
12	15	III	300	74 k	81 k	1.03
13	15	IV	300	74 k	309 k	1.59
14	15	II	300	74 k	564 k	1.72

^a Polymerization was performed in THF at room temperature for 2 h using various catalysts. ^b Theoretical molecular weight. ^c Absolute molecular weights were measured using a MALLS-RI detector.

First, ROMP of **14** using ultra-fast initiating catalyst **III** was investigated. As expected, living polymerization was achieved; the absolute molecular weight (measured by MALLS) of the polymer was close to the theoretical molecular weight and a narrow PDI of 1.02 was obtained (Table 4-1, entry 1). Next, ROMP of **14** using the more thermally stable 2nd generation Hoveyda-Grubbs catalyst (**IV**) was studied, and surprisingly, the result obtained was almost the same as that observed with **III** (Table 4-1, entries 1 and 5), i.e., the molecular weight was close to the theoretical value and the PDI was narrow (1.03). This is in significant contrast with the results of the ROMP of an analogous NB monomer, **15**, which produces poly(**15**) with a molecular weight four times greater than the theoretical value and a broad PDI of 1.59 (Table 4-1, entry 13). Furthermore, to control the molecular weight using **IV**, monomer to initiator ratio ([M]/[I]) was varied from 50 to 500:1 and a linear increase in the molecular weight with the slope corresponding to the molecular weight of **14** was observed (Table 4-1, entries 2-6). In all cases, narrow PDIs (below 1.03) were observed (Figure 4-1). It is worth noting that a previous study reported that the controlled ROMP of NB containing bis-ketone by **IV** resulted in slightly broader PDIs (1.1-1.2).⁵ The precise control of both the molecular weight and PDI indicates that living ROMP was successfully achieved using the TD monomer (**14**) and 2nd generation Hoveyda-Grubbs catalyst (**IV**).

We then focused on the ROMP of TD monomer **14** using the slowest initiating catalyst, i.e., 2nd generation Grubbs catalyst (**II**). Poly(**14**) with 3.4 times higher molecular weight than the theoretical value and a broader PDI of 1.35 was obtained (Table 4-1, entry 7). Although this result was not satisfactory, the difference between the theoretical and observed values was much smaller, and the PDI was

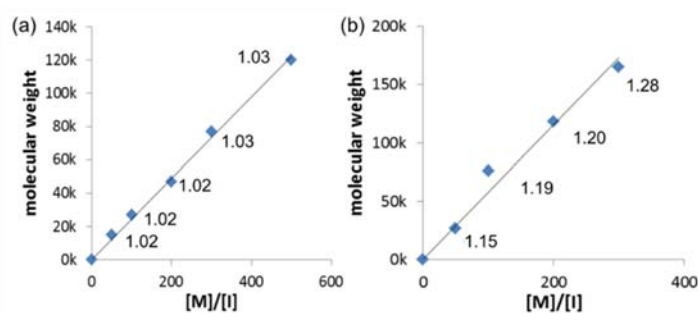


Figure 4–1. Plots of molecular weight versus $[M]/[I]$ for (a) monomer 14 & catalyst IV and (b) monomer 16 & catalyst II . Inset values indicate PDI.

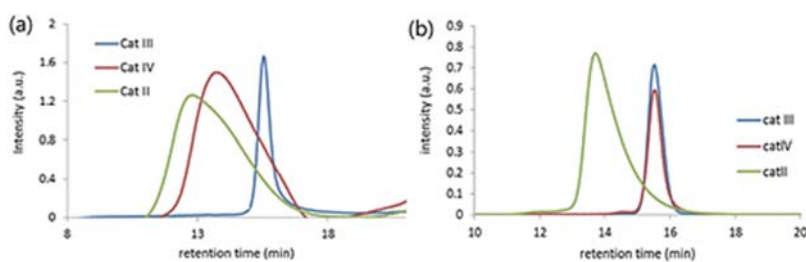


Figure 4–2. GPC traces of (a) poly(15) and (b) poly(14) polymerized by three catalysts.

much narrower than those obtained from conventional ROMP of the NB analog **15** (7.6 times higher molecular weight and a PDI of 1.72 (entry 14)). This suggests that the ROMP of **14** using **II** enables better control than the corresponding ROMP of **15** and that even better controlled ROMP could be achieved using a modified monomer that would attenuate propagation to increase k_i/k_p . To test this idea, monomer **16**, which contained a bulky G2 ester dendron instead of an *n*-hexyl chain, was subjected to ROMP using catalyst **II**, and successfully produced poly(**16**) with a molecular weight close to the theoretical molecular weight and a narrow PDI of 1.15 (Table 4–1, entry 8). Furthermore, the molecular weight control experiment was performed by varying the $[M]/[I]$ from 50 to 300:1 and a linear increase in the molecular weights according to the $[M]/[I]$ was observed (Figure 4–1b, 4–3). In all cases, relatively narrow PDIs

(<1.3) were obtained (Table 4–1, entries 8–11). Based on these observations, controlled ROMP was achieved even using the slow–initiating 2nd generation Grubbs catalyst (**II**).

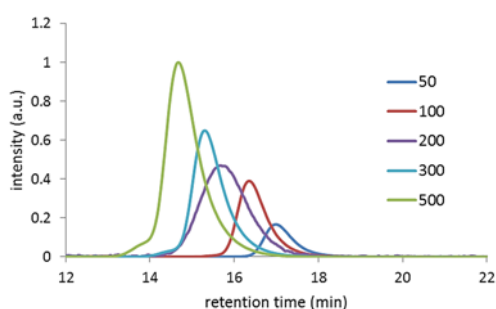


Figure 4–3. GPC traces of poly(16) .

Table 4–2. Kinetic parameters for monomers 14–16 by three catalysts.^a

entry	monomer	cat	temp (°C)	k_i ($M^{-1} \text{min}^{-1}$)	k_p ($M^{-1} \text{min}^{-1}$)	k_i/k_p
1	1	I	–10	0.68	0.15	4.5
2	1	II	0	0.11	0.30	0.37
3	1	III	25	0.021	11	0.0019
4	3	I	–10	0.57	0.18	3.2
5	3	II	0	0.068	1.5	0.045
6	3	III	25	0.0081	85	0.000095
7	2	III	25	0.023	1.2	0.019

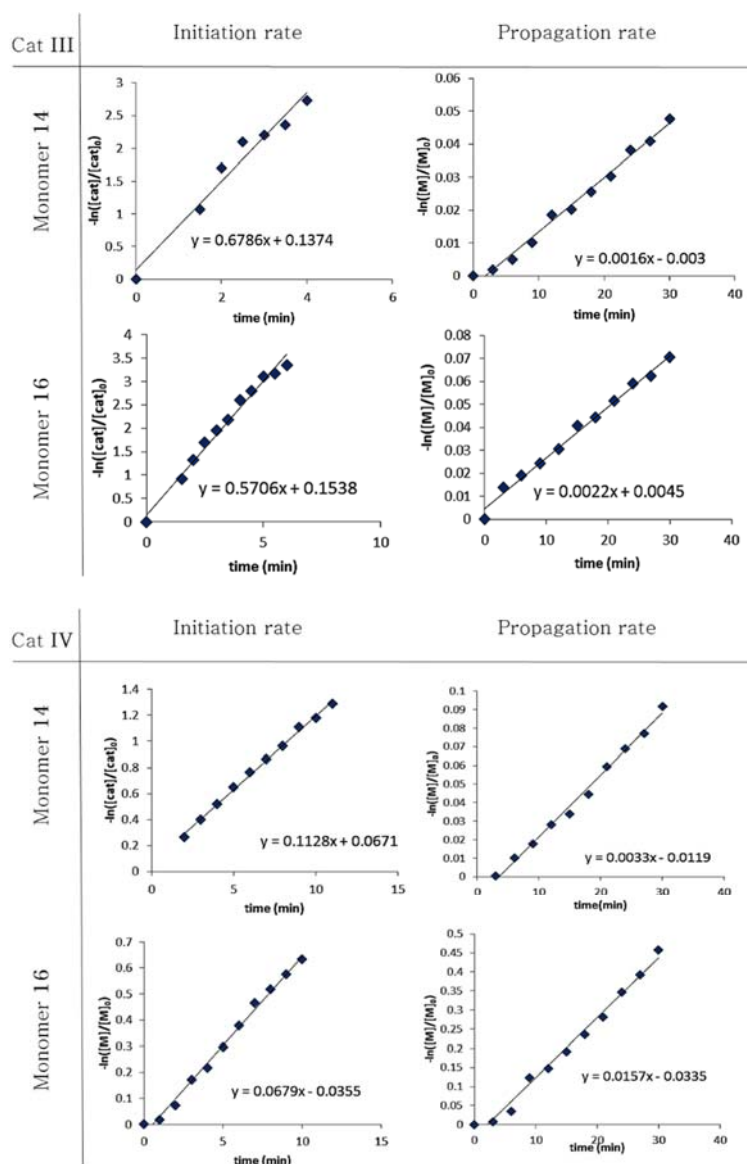
^a Experiments were performed in THF-*d*₈ using *in situ* ¹H NMR analysis. [M] = 0.22 M and [catalyst] = 0.011 M (20 equiv).

To understand the origin of the living nature of this polymerization, kinetic analysis was attempted to measure the rates of both initiation and propagation using *in situ* NMR to determine k_i/k_p for each case (Table 4–2).¹⁵ The kinetic measurements were performed at room temperature for catalyst **II**, and at 0 °C and –10 °C for catalysts **IV** and **III**, respectively, because the initiation of these two catalysts at room temperature occurred too quickly for kinetic

studies. Although the direct comparison of the rate constants for the different catalysts is not valid due to the different reaction temperatures, direct comparisons between the reactivity of the monomers with the same catalyst and k_i/k_p are possible. According to the kinetic data obtained from ROMP of **14**, a higher k_i and lower k_p than those from ROMP of **15** was evident for all three catalysts (Table 4–2). Consequently, the k_i/k_p values for ROMP of **14** were larger than those for ROMP of **15** (catalyst **III**: 1.5 x, catalyst **IV**: 8 x, catalyst **II**: 20 x); this increase for **IV** could explain successful living polymerization with a narrow PDI (Table 4–2, entry 2), whereas the k_i/k_p for ROMP of analogous NB monomer **15** was still low (0.045) for living polymerization (Table 4–2, entry 5). On the other hand, the k_i/k_p for ROMP of **14** using 2nd generation Grubbs catalyst (**II**) was still too low for living polymerization even though it was 20 times higher than that of the NB monomer (Table 4–2, entries 3 and 6). However, catalyst **II** promoted living polymerization of monomer **16** containing G2 ester dendron because k_p was nine times slower than the k_p of **14**, which is due to the bulky side chain, while k_i remained similar. As a result, the k_i/k_p for ROMP of **16** using **II** was 10 times larger than that for **14** and 200 times larger than that for **15**, thereby, leading to the controlled polymerization (Table 4–2, entries 3, 6, and 7).

To elucidate the origin of the intrinsically larger k_i/k_p value for TD monomers than for NB monomers, the structures of the two monomers were compared. Firstly, the steric bulk around the cyclobutene moiety on the TD olefin is much smaller than that of NB containing a methylene bridge, which hinders the coordination of the catalyst; therefore, the k_i of the TD monomers was faster. However, after ring–opening, the newly generated propagation species of the

TD derivatives are much bulkier than those of the NB derivatives (i.e., a tricyclic versus bicyclic moiety). Furthermore, the *endo*-imide on the TD moiety hinders the approach of the next TD monomer, which attenuates propagation with respect to that of the NB containing an *exo*-imide (Figure 2).¹⁶ Overall, the faster k_i and slower k_p for the ROMP of TD derivatives leads to a much larger k_i/k_p , thereby enabling living ROMP.



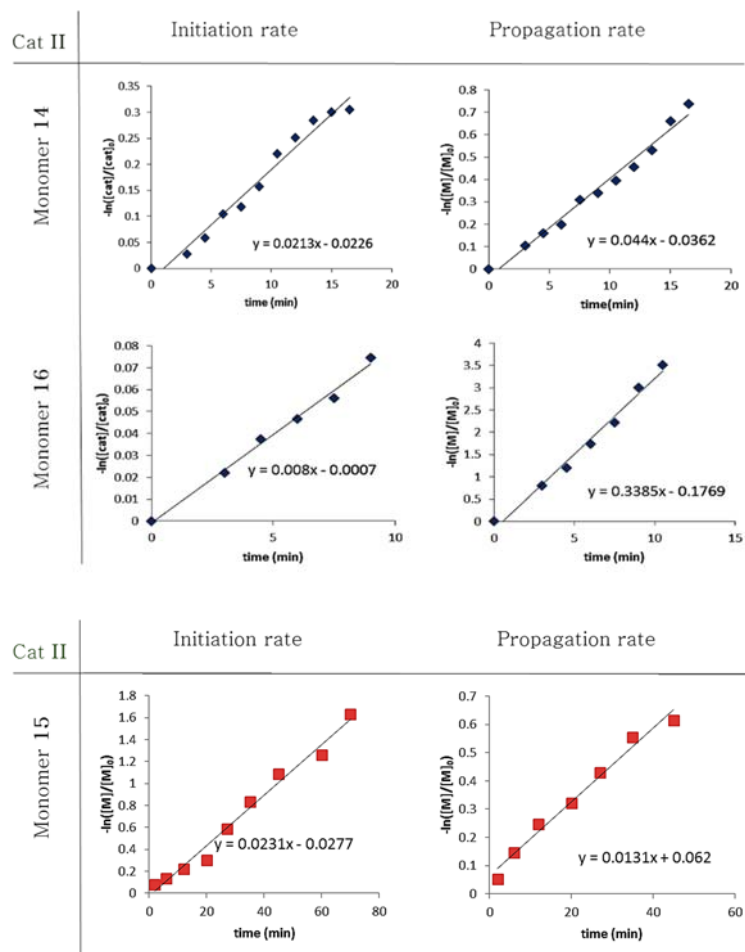


Figure 4–4. Determination of the rate constant for monomers 14–16 by three catalysts.

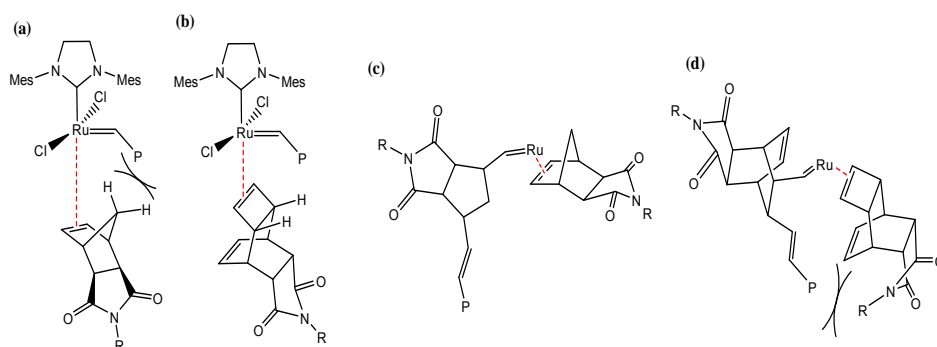
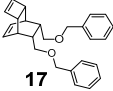
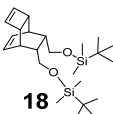
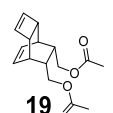
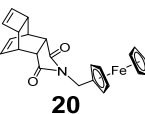
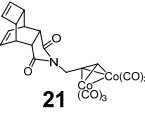


Figure 4–5. Schematic explanation for the steric on NB and TD during initiation and propagation.

Table 4–3. ROMP of various TD monomers using catalyst IV.^a

entry	monomer	solvent	[M]/[I]	M _n (Theo) ^b	M _n ^c	PDI ^c
1	 17	THF	300	112 k	104 k	1.04
2	 18	THF	300	126 k	119 k	1.02
3	 19	THF	300	74 k	80 k	1.01
4	 20	DCM	50	20 k	19 k	1.07
5	 21	DCM	75	39 k	35 k	1.06

^a Polymerization was performed at room temperature for 2 h. ^b Theoretical molecular weight. ^c Absolute molecular weight was measured using a MALLS–RI detector.

To examine the monomer scope of living ROMP using **IV**, ROMP of various monomers containing different functionalities on the 7 and 8 positions were attempted (Table 4–3). Instead of the *N*-succinyl imide moiety, *endo*-dimethylene alkoxy moieties with various functional groups were introduced to monomers **17–19** (Table 4–3, entries 1–3). As expected, living polymerization with controlled molecular weights and narrow PDIs (≤ 1.04) was achieved in all cases. From these results, a clear contrast to the previous report on the ROMP of the *endo,exo*-NB monomers is evident:⁵ since the bulky *tert*-butyldimethylsilyl ether (OTBS) groups in **18** are unable to chelate to the catalyst, the anchoring effect of the *endo*-carbonyl groups is not necessary for living polymerization. In addition, monomers **20** and **21**, which contain complexes of iron and cobalt,

respectively, also showed controlled ROMP (Table 4–3, entries 4 and 5). These successful examples demonstrate that living ROMP of TD monomers is versatile with a broad monomer scope. As expected, all these monomers didn't undergo controlled polymerization with slow-initiating **II**, resulting in 3–4 times higher molecular weights and broader PDIs (≥ 1.54) than those of ROMP using catalyst **IV**.

ROMP of the TD monomer resulted in better living polymerization than the previously reported ROMP of the NB containing *endo,exo*-diketone because k_i increased in addition to the suppression of k_p for the TD monomer, whereas only the suppressed k_p by chelation of the carbonyl group for the ROMP of the NB might be insufficient for ideal living polymerization. Also, the chelation of the carbonyl group might also increase the rate of termination by poisoning the catalyst.

Table 4–4. Results of diblock copolymerizations.^a

entry	polymer	time	$M_n(\text{Theo})^b$	$M_n(\text{MALS})^c$	$\text{PDI}(\text{MALS})^c$
1	Poly(17) ₁₀₀	0.25 h	37 k	32 k	1.02
	Poly[(17) ₁₀₀ - <i>b</i> -(18) ₂₀₀]	1 h	121 k	127 k	1.02
2	Poly(14) ₁₀₀	0.25 h	29k	28k	1.03
	Poly[(14) ₁₀₀ - <i>b</i> -(15) ₃₀₀]	1 h	103k	101k	1.20

^a Polymerization was performed in THF at room temperature using catalyst **IV**. ^b Theoretical molecular weight. ^c Absolute molecular weights were measured using a MALLS-RI detector.

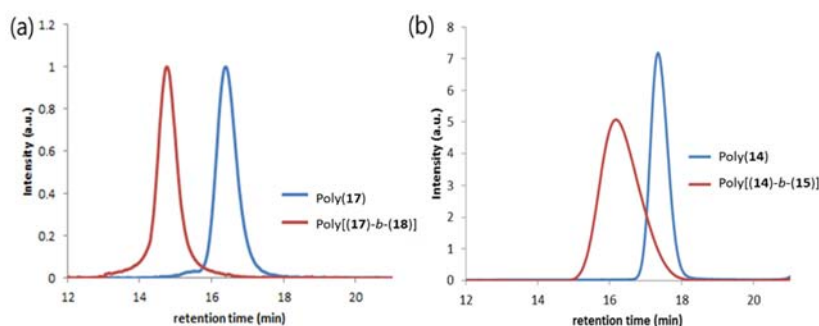


Figure 4–6. GPC traces of (a) poly(**17**)–*b*–poly(**18**) and (b) poly(**14**)–*b*–poly(**15**).

To further exploit the living polymerization, block copolymerization with TD monomers **17** and **18** as the first and second blocks, respectively, was performed via sequential addition of the monomers (Table 4-4, entry 1). A clear shift from the trace of the first block to a higher molecular weight region upon the addition of the second monomer was observed by GPC analysis (Figure 4-6a). The molecular weight of the diblock copolymer also matched well with the theoretical value and a narrow PDI of 1.02 was obtained. Block copolymerization of TD monomer **14** and a NB monomer **15** as the first and second blocks, respectively, was performed similarly (Table 4-4, entry 2). Again, the diblock copolymer was successfully produced with a clear shift of the GPC trace (Figure 4-6b). The molecular weight was close to the theoretical value and the PDI was still narrow (1.20). It is remarkable that monomer **15**, whose ROMP was completely uncontrolled by **IV**, produced block copolymer with excellent control. The slight PDI broadening compared to entry 1 was caused by the relatively slower insertion of the NB monomer **15** into the sterically congested propagating species. In this example, the order of the monomer addition is important because switching the order (**15** as the first block) would result in uncontrolled polymerization. These successful diblock copolymerizations are in sharp contrast to previous unsuccessful attempts, which showed bimodal GPC traces.^{5a}

4.3.2 Three-arm star polymer

With the living polymerization condition of TD based monomers and stable Hoveyda-Grubbs catalyst, we shifted our attention to synthesis of more complex structure, multi-arm star polymer by ROMP.

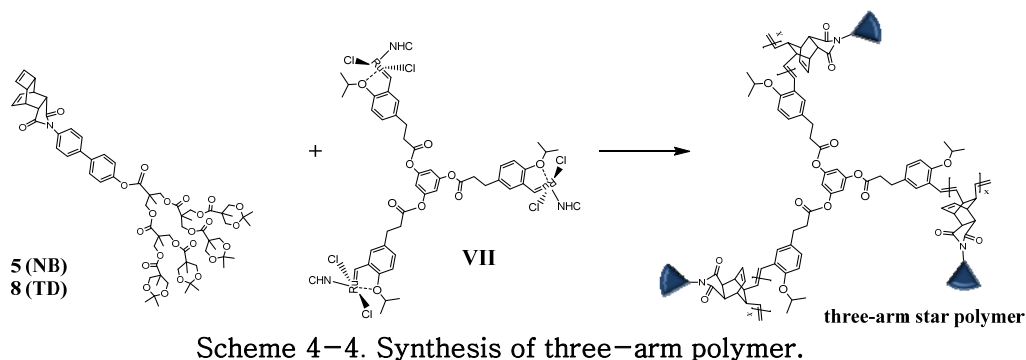


Table 4-5. Results of three-arm polymerization.^a

entry	monomer	[M]/[I]	$M_{n(\text{Theo})}^b$	$M_{n(\text{MALS})}^c$	$\text{PDI}_{(\text{MALS})}^c$
1	5	100	391 k	747 k	1.29
2	8	50	201 k	146 k	1.04
3	8	100	402 k	357 k	1.04
4	8	200	805 k	720 k	1.06
5	8	300	1207 k	1117 k	1.04

^a Polymerization was performed in THF at 50 °C for 12 h using tri-functionalized catalyst **VII**.
^b Theoretical molecular weight. ^c Absolute molecular weights were measured using a MALLS-RI detector.

In 2003, J. L. Hedrick and R. D. Miller group successfully synthesized multi-arm star polymer by the arm-first approach via ROMP using the tri-functional norbornene cross-linker. However, the number of arms in the star polymer could not be controlled with this method.¹⁷ In another report, D. Astruc group synthesized star polymer from dendritic multi-arm ruthenium catalysts using NB as a monomer. However, broad PDI (≥ 2.2) and incomplete conversion

was observed because of slowly initiating catalyst.¹⁸ In all cases, no structural information to confirm the star–shape topology was provided. Just as ATRP provided a reliable route for the synthesis of star polymers with well–defined arms,¹⁹ if a stable multi–arm initiator promoting living ROMP could be prepared easily, ROMP could become another powerful tool for the synthesis of the well–defined star polymers. At this point, encouraged by the living ROMP of TD with stable 2nd generation Hoveyda–Grubbs catalyst (**IV**), we envisioned that even dendronized star polymers could be prepared for the first time by using powerful ROMP of macromonomers. For the synthesis of three–arm star polymers, the stable tri–functionalized catalyst **VII** with chelating benzylidene was easily synthesized by following the previous work with a minor modification and purified by flash column chromatography.¹⁴ The ROMP was conducted with macromonomers containing a G3–ester dendron to confirm the topology of star structure by AFM (Scheme 4–4). First, homopolymerization of **8** was conducted with various [M]/[I] ratios (from 50:1 to 300:1). As a result, the molecular weights were well controlled and matched well with the theoretical values and narrow PDI (≤ 1.06) was obtained in all cases (Table 4–5, entries 2–5). From the AFM imaging of TD star polymers, three–arm star shape was clearly observed with regular length of each arm (Figure 4–7). Also the length of arm gradually increased with the increase in [M]/[I] ratio; from 18 nm for [M]/[I] ratio of 50 to 120 nm for [M]/[I] ratio of 300 (Figure 4–7). This result was in sharp contrast with star ROMP of another G3 macromonomer of NB analog **5**, whose k_i/k_p was much smaller with 2nd generation Hoveyda–Grubbs catalyst (Table 4–2, entries 2 and 5). Inevitably, twice higher molecular weight than the theoretical value and broader PDI (1.29) was obtained (Table 4–

5, entry 1). AFM analysis revealed more drastic difference between star ROMP of the NB and the TD macromonomers, as only linear polymers were observed from the ROMP of the NB macromonomer without any star-shaped topology.

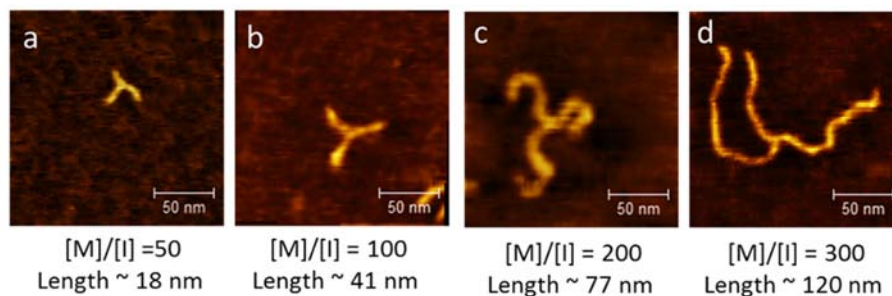
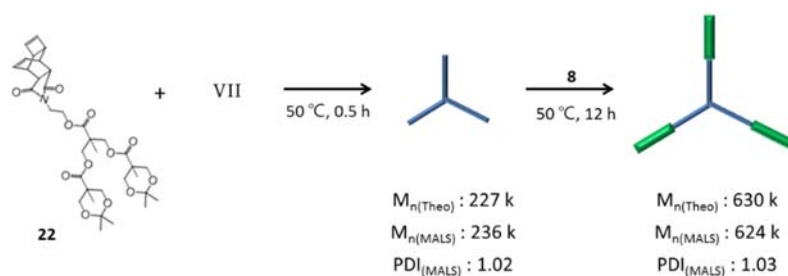


Figure 4-7. AFM image of star polymers with various $[M]/[I]$ ratio (a) 50, (b) 100, (c) 200, (d) 300 and average length of arm .



Scheme 4-5. Result of three-arm diblock copolymerization.^a

With this success in the synthesis of the three-arm star polymer, the investigation was further expanded to the one-pot synthesis of star diblock copolymer from dendronized macromonomers **8** (G3) and **22** (G2). The block copolymerization was conducted by adding the three-arm initiator (**VII**) to a smaller macromonomer **22** as the first block, and then the larger macromonomer **8** was injected after the complete consumption of **11** (Scheme 4-5). This successfully produced poly[(**22**)₁₀₀-*b*-(**8**)₁₀₀] star diblock copolymers with molecular weight close to the theoretical molecular weight and narrow PDI of 1.03 and the GPC traces showed a clear shift to the left (Figure 4-8). More definitively,

the microstructure of the block copolymer was confirmed by AFM imaging, showing the three-arm having two different sizes on each arm. Figure 4-9 shows clear three-arm star structure comprised of shorter inner arm (0.4 nm in height) and taller outer arm (0.6 nm in height) because the smaller **22** was polymerized first.

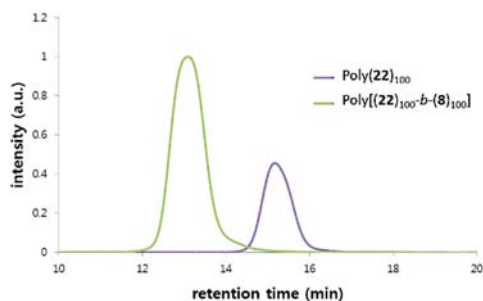


Figure 4-8. GPC traces of three-arm diblock poly[(22)₁₀₀-*b*-(8)₁₀₀].

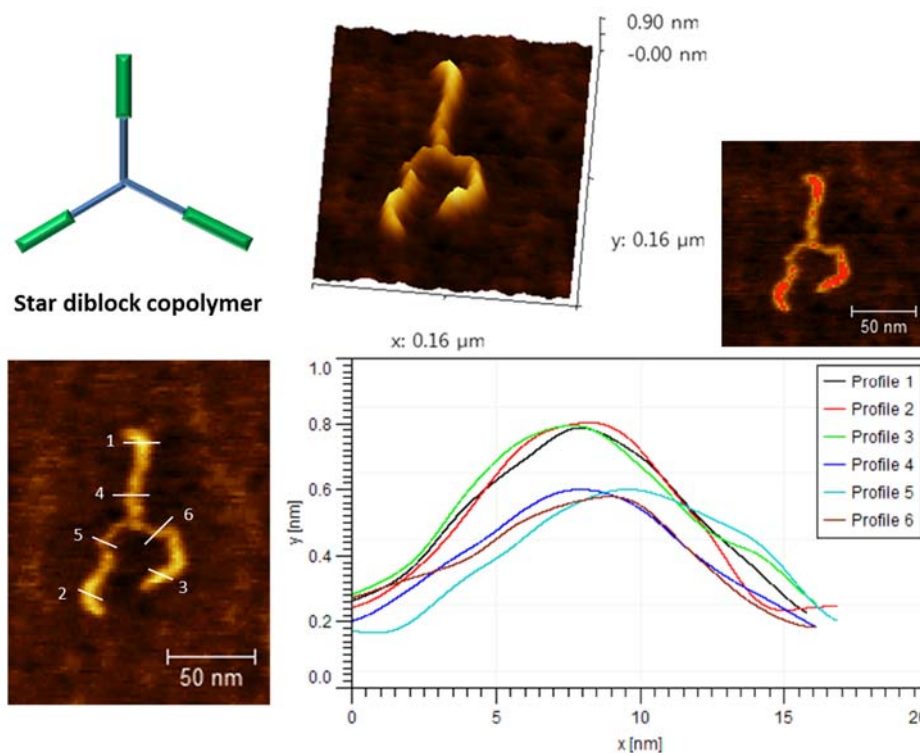
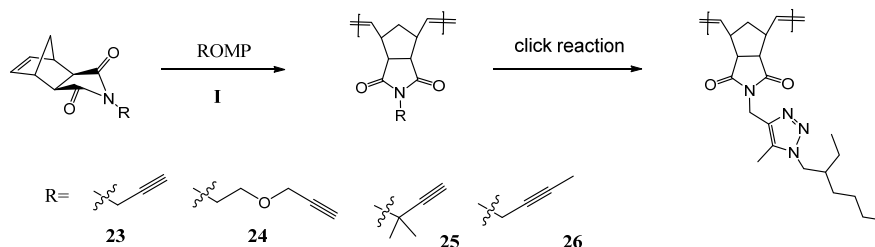


Figure 4-9. AFM image of three-arm diblock copolymer, Poly[(22)₁₀₀-*b*-(8)₁₀₀] and its height profile. The red part indicates the region having higher height than 0.55 nm.

4.3.3 Controlled ROMP of monomer containing alkyne moiety

The ROMP of cycloolefin containing alkyne moiety is still challenge because of competition between two functional groups (Scheme 4-1). However, there are possibilities, if we can activate the olefin or deactivate the alkyne moiety by shielding.



Scheme 4-6. Structure of NB monomers containing alkyne moiety and scheme for polymerization and post-functionalization.

The study was started from NB based monomers (Scheme 4-6) and 1st generation Grubbs catalyst (**I**) which have preference to the alkene over the alkyne moiety. For the first trial, ROMP of **23** with terminal alkyne was done at the 0 °C in THF, because lower temperature decrease the reactivity of catalyst which can increase the chemoselectivity toward to the cycloalkene and ROMP in THF showed more controlled manner compare with polymerization in DCM. However, this reaction didn't generate any polymer species. According to the stoichiometric reaction of **23** and **I**, almost all the catalysts are react with the alkyne first and the reaction is stopped (Scheme 4-1, A). In the case of **24**, it was worse because oxygen act as a directing group and catalyst react with alkyne faster. To disrupt the reaction between alkyne and catalyst, dimethyl group was introduced to the next of alkyne moiety (**25**), but this was not enough to block the reaction of alkyne. It was thought that di-substituted cycloalkene can't have advantage over the mono-substituted alkyne.

Based on this assumption, the monomer **26** with internal alkyne was introduced. The ROMP was worked now in THF, but the resulting polymer was gel-like and not completely soluble in THF. This problem was overcome when the solvent is changed to DCM with lowered conversion. To increase the conversion, the reaction was conducted in higher concentration or for longer reaction time. However, cross-linking was more severe in high concentration. We could find optimized condition with longer reaction time (Table 4–6, entry 8), but still full conversion couldn't be achieved and cross-link couldn't be completely blocked.

Table 4–6. ROMP result of NB monomers containing alkyne moiety.^a

entry	monomer	solvent	temp	time	conc ^b	M _{n(conv)} ^c	PDI _(conv) ^c	conv ^d
1	23	THF	0 °C	3 h	10mL/1g	–	–	–
2	24	THF	0 °C	3 h	10mL/1g	–	–	–
3	25	THF	0 °C	3 h	10mL/1g	–	–	–
4	26	THF	R.T.	1 h	10mL/1g	24 k	1.84	75%
5	26	DCM	R.T.	1 h	10mL/1g	47 k	1.21	60%
6	26	DCM	0 °C	1 h	30mL/1g	26 k	1.12	60%
7	26	DCM	0 °C	1 h	20mL/1g	36 k	1.16	66%
8	26	DCM	0 °C	3 h	10mL/1g	52 k	1.13	85%

^a The polymerization was done by catalyst **I** and [M]/[I]=150. ^b Concentration of monomer solution. ^c M_n and PDI were calculated by THF GPC using PS standards. ^d Conversion was calculated from ratio of the remaining alkene to polymeric alkene by ¹H-NMR.

With poly(**26**) (Table 4–6, entry 8), post-functionalization was tried by click reaction using ruthenium based catalyst (Table 4–7). The copper catalyzed click reaction is more common, but copper catalyst is not reactive with internal alkyne. Also the reactivity of CpRu(PPh₃)₂Cl was not enough, only Cp*Ru(PPh₃)₂Cl was possible to

do click reaction. Various reaction conditions were tried with different solvent, temperature, and reaction time. However, 45 % was highest conversion we can achieve in this system, and solubility of the resulting polymer in common organic solvent was bad. The reason of unsuccessful result would be caused from the uncontrolled ROMP of **26** and undefined (cross-linked) chemical structure.

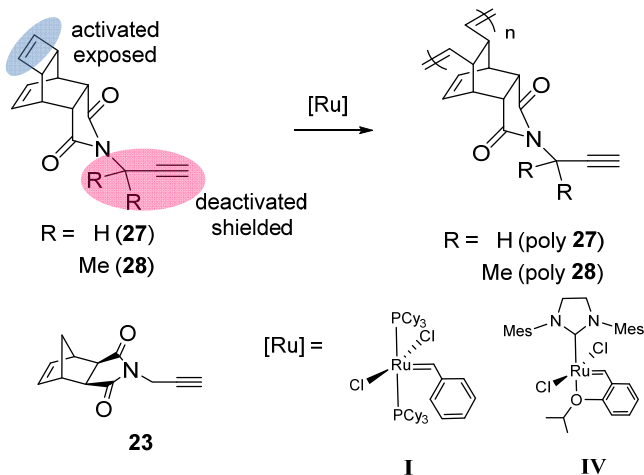
Table 4–7. Result of post-functionalization of poly(26) by click reaction.^a

entry	catalyst	solvent	temp	time	$M_n(\text{conv})^b$	$PDI(\text{conv})^b$	conv ^c
1	CpRu(PPh ₃) ₂ Cl	dioxane	60 °C	6 d	30k	1.13	–
2	Cp*Ru(PPh ₃) ₂ Cl	dioxane	60 °C	4 d	27k	1.23	12%
3	Cp*Ru(PPh ₃) ₂ Cl	DMF	75 °C	4 d	9k	1.49	35%
4	Cp*Ru(PPh ₃) ₂ Cl	DMF	75 °C	1 d	36 k	1.33	45%
5	Cp*Ru(PPh ₃) ₂ Cl	Tol	75 °C	1 d			–
6	Cp*Ru(PPh ₃) ₂ Cl	DCE	75 °C	1 d	47 k	1.34	35%
7	Cp*Ru(PPh ₃) ₂ Cl	DMF	R.T	1 d			0%

^a Prepolymer with M_n : 36 k and PDI: 1.16 was used. ^b M_n and PDI were calculated by THF GPC using PS standards. ^c Conversion was calculated by ¹H NMR.

From the studies on previous chapter, we found that ROMP of monomers containing the TD unit using 2nd and 3rd generation Grubbs catalysts, proceeded much faster initiation than the ROMP of conventional NB monomers. This is because the reactivity of cyclobutene on TD-derived monomers is much higher than that with NB analogs, resulting in faster coordination of TD-derived monomers to the catalyst, and thereby increasing the k_i/k_p ratio. Furthermore, living polymerization of the TD-derived monomers became possible even with the slow-initiating (but thermally stable) 2nd generation Hoveyda–Grubbs catalyst. This result led us to propose the use of TD monomers might improve the catalyst

preference for the alkene (cyclobutene) over the alkyne, thereby allowing for the direct ROMP of monomers containing the unprotected terminal alkyne moiety.



Scheme 4–7. ROMP of TD monomers containing alkyne moiety.

Alkyne-containing monomers (**23**, **27–28**) were synthesized by the reported procedures.²⁰ Each monomer was purified by flash column chromatography and characterized by NMR spectroscopy and HRMS. The polymerization was carried out using 1st generation Grubbs catalyst **I** or 2nd generation Hoveyda–Grubbs catalyst **IV** in THF or DCM at various temperatures (Scheme 4–7).

First, the ROMP of a TD monomer with non-substituted alkyne **27** was tested in THF at room temperature using Grubbs catalyst **I**, which is reported to exhibit some preference for alkenes over alkynes²¹ (Table 4–8, entry 1). However, after 3 h, an insoluble cross-linked gel started to form, and the soluble portion was isolated for characterization. When the same reaction was carried out in DCM for 3 h, the resulting polymer was completely soluble (Table 4–8, entry 2). However, these results were markedly different from those obtained in the ROMP of a NB analog **23**, which failed to provide any evidence of polymerization; almost no monomer was consumed when

analyzed by ^1H NMR (Table 4–8, entry 10). From this result, one could conclude that the higher reactivity of the catalysts toward the cyclobutene on TD resulted in ROMP, while the catalyst seemed to preferentially react with the alkyne over the alkene on the NB moiety, and this produced no polymer (Scheme 4–1, A). Although the TD-containing monomer was reactive, the resulting poly(**27**) showed a rather large PDI, implying that lack of selectivity for alkene over alkyne resulted in side reactions and eventually cross-linking (Scheme 4–1, B).

Table 4–8. ROMP of TD monomers containing alkyne moiety.^a

entry	monomer	cat	solvent	temp(°C)	time(h)	M_n (kDa) ^c	PDI ^c	conv ^d
1	27	I	THF	RT	3	23	1.96	64%
2	27	I	DCM	RT	3	16	1.84	46%
3	28	I	DCM	RT	3	–	–	–
4	28	IV	DCM	RT	1	27	1.17	>99%
5	28	IV	DCM	0°C	2	27	1.07	>99%
6	28	IV	DCM	–15	12	26	1.13	>99%
7 ^b	28	IV	DCM	0	0.6	21	1.06	81%
8 ^b	28	IV	DCM	0	0.4	18	1.07	71%
9 ^b	28	IV	DCM	0	0.25	14	1.06	53%
10	23	I	THF	RT	3	–	–	–

^a $[\text{M}]/[\text{I}]=100$. ^b The polymerization was terminated intentionally at certain conversion. ^c M_n and PDI were calculated by THF GPC using PS standards. ^d Conversion was calculated from ratio of the remaining alkene to internal standard by ^1H -NMR.

To overcome this problem, we intentionally deactivated the alkyne on the TD monomer by introducing dimethyl groups at the carbon adjacent the alkyne moiety (monomer **28**). This substitution caused steric hindrance to inhibit coordination of the alkyne functionality to the catalyst, thereby further increasing the catalyst's preference for the alkene over the alkyne. Unfortunately, catalyst I

could not polymerize monomer **28** (Table 4–8, entry 3), presumably because of the low reactivity of **I** toward the sterically bulky monomer. To our delight, switching to the more active 2nd generation Hoveyda–Grubbs catalyst (**IV**) led to successful ROMP, producing poly(**28**) with full conversion in 1 h. Moreover, the PDI of the resulting polymer was narrow (1.17), implying that controlled polymerization of **28** should be possible (Table 4–8, entry 4). However, a closer look at the GPC trace of poly(**28**) revealed a small shoulder peak in the high molecular weight region, which might indicate the occurrence of some side reaction involving the alkyne (Figure 4–10a). To further inhibit reactivity of the alkyne, kinetic control was exerted by cooling the reaction to 0 °C. After 2 h at this temperature, full conversion was achieved, and the PDI of the resulting polymer had decreased to 1.07 (Table 4–8, entry 5). Although the shoulder present in the GPC trace became much smaller at the reduced temperature, implying that the side reaction had been suppressed, we could not completely eliminate this undesired pathway (Figure 4–10a). Lowering the temperature further to –15 °C slowed down the reaction substantially (Table 4–8, entry 6) and did not result in any improvement in selectivity, since a very small shoulder was again observed in the GPC trace.

The relative concentration of two species is one of the most important determinants of selectivity in this competition reaction.²² As the cycloalkene monomer is selectively consumed, the relative concentration of the alkyne increases, as does the likelihood of competing side reactions involving the increasingly dominant alkyne. In order to obtain a pure homopolymer of **28** (Scheme 4–1, C), its polymerization was intentionally terminated before full conversion (Table 4–8, entries 7–9), and as expected, the shoulder peak in GPC

trace completely disappeared, with up to 81% conversion (DP = 81) of monomer **28** (Figure 4–10a). To further support this assumption, polymerization of **28**, with [M]/[I] ratios of 50 and 70, was conducted, resulting in full conversion. The resulting polymer samples again showed small shoulder peaks in the GPC traces in each case, whereas in the cases where polymerization was terminated early, clear monomodal traces with narrower PDI (<1.07) were observed for the poly(**28**) with similar DPs. To confirm that **28** was polymerized in a controlled manner by catalyst **IV**, monomer consumption was monitored by *in situ* NMR analysis as the reaction progressed. A linear relationship between $-\ln([M]/[M]_0)$ and time was confirmed (Figure 4–10b). From the results, we could conclude that the controlled ROMP of the monomer containing alkyne was achieved without any defects, owing to proper application of a monomer containing an activated olefin within the TD subunit, and a sterically shielded alkyne.

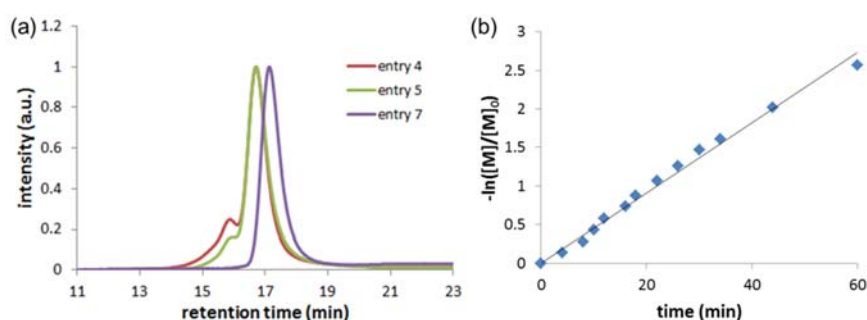


Figure 4–10. (a) GPC traces and (b) plot of reaction time vs $-\ln([M]/[M]_0)$ of poly(**28**).

With polymer samples in hand, we shifted our focus to the post-functionalization of poly(**28**) by employing the click reaction. In an initial trial, poly(**28**), 3 equiv of *n*-heptyl azide, and a catalytic quantity of $\text{CuBr}(\text{PPh}_3)_3$ were heated to 50 °C in DMF for 20 h.

Unfortunately, the reaction was not complete after this time (Table 4–9, entry 1), and it appeared that a more reactive catalytic system was required for this post–functionalization, because the sterically hindered alkyne moiety was resistant to the CuBr(PPh₃)₃–catalyzed click reaction. Encouraged by the work of Fukuzawa’s group,²³ which reported that the bulkiness of ligands affect the rate of the click reaction, we sought a catalyst containing a smaller ligand in order to improve the post–functionalization. By simply changing catalyst to CuI, the reaction was complete in 20 h, with only 1.5 equiv of azide (Table 4–9, entry 2). Complete conversion was verified by ¹H NMR spectroscopy, revealing that the alkyne signal ($\delta = 2.4$ ppm) had completely disappeared and a broad triazole signal ($\delta = 7.5$ ppm) had appeared (Figure 4–11a). The NMR spectrum was same with poly(**28a'**), polymerized from the monomer **28a'** which derived from the click reaction before ROMP. Complete conversion of the alkyne was also confirmed by the disappearance of the signal at 3300 cm⁻¹ corresponding to C≡C–H stretching frequency in the IR spectrum (Figure 4–11b). The molecular weight of the polymer increased from 14 kDa to 22 kDa following post–functionalization, and the PDI remained narrow (1.10) with a clean shift of the GPC trace (Figure 4–11c). To demonstrate the applicability of this methodology to a wider range of substrates, CuAAC was attempted using a series of azides (Table 4–9, entries 3–6). Click reactions employing the polar ethylene glycol azide and aromatic 3,5–dimethylbenzyl azide also showed full conversion to give polymers with narrow PDI of 1.1. Notably, excellent post–functionalization was achieved even with much bulkier azides containing both polar and non–polar dendrons (Table 4–9, entries 5–6). These results indicate that ROMP, followed by the direct click reaction, is a suitable method for the preparation

of dendronized polymers via a graft-to approach.²⁴ These examples demonstrate a method that provides a useful strategy for the facile synthesis of various functional polymers with a uniform structure and narrow PDI.

Table 4-9. Post-functionalization of poly(28) via Cu-Catalyzed Azide-Alkyne Cycloaddition.^a

Poly(28) + N₃-R (1.5 eq) $\xrightarrow[\text{DMF, 50 } ^\circ\text{C, 20 h}]{\text{Catalyst (0.1 eq), DIPEA (0.5 eq)}}$ Poly(28a-e)

entry	R	cat	M _n (kDa) ^b	PDI ^b	conv ^c	Yield ^d
1		CuBr(PPh ₃) ₃ ^e	20	1.09	90%	70%
2	a	CuI	22	1.10	>99%	75%
3		CuI	20	1.09	>99%	82%
4		CuI	17	1.12	>99%	83%
5		CuI	20	1.11	>99%	93%
6		CuI	27	1.11	>99%	69%

^a Prepolymer with M_n: 14 k and PDI: 1.09 was used. ^b M_n and PDI were calculated by THF GPC using PS standards. ^c Conversion was calculated by ¹H NMR. ^d Isolated yield after precipitation in MeOH. ^e 3 equiv of azide was used for CuAAC and reaction time was 1 d.

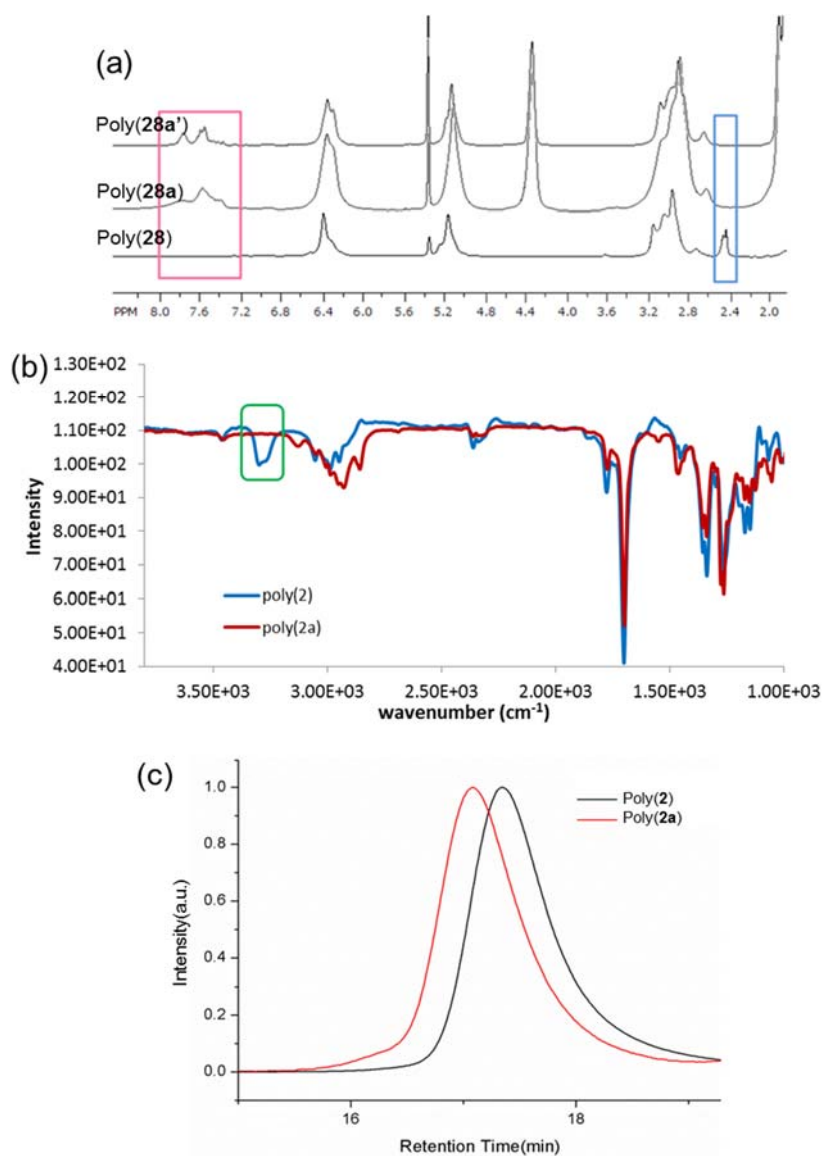


Figure 4–11. (a) ^1H NMR spectra and (b) IR spectra and (c) GPC traces of poly(28) and poly(28a) after the post-functionalization. For the poly(28a'), click reaction was done with monomer 28 and ROMP was performed with this monomer. The signal outlined in a blue square corresponds to the terminal alkyne C–H, and the signal outlined in a pink square corresponds to the triazole.

4.4 Conclusion

We performed the controlled ROMP of various TD monomers with a broad monomer scope using slow initiating but thermally more stable 2nd generation Grubbs and Hoveyda–Grubbs catalysts to produce polymers with controlled molecular weights and narrow PDIs. Under this controlled polymerization condition, clean block copolymers were prepared for the first time using 2nd generation Hoveyda–Grubbs catalyst. In addition, star polymer was synthesized by the core–first approach using Hoveyda–Grubbs type three–arm initiator. Also, star diblock copolymer was prepared by sequential addition of macromonomers. Moreover, controlled ROMP was achieved even with the monomer containing alkyne moiety by optimizing the reaction conditions, which do competition with cycloalkene and exhibit polymerization. Lastly, the resulting polymer underwent successful post–functionalization via click reactions with various azides. All the results were clearly contrast to the results from NB monomers because controlled ROMP with Hoveyda–Grubbs catalyst or alkyne moiety was not possible in NB case. In–depth kinetic analysis proved the reason; ROMP of the TD monomers showed faster initiation but slower propagation compare with NB monomers, which increased k_i/k_p and promoted living ROMP. This controlled ROMP of a TD based monomer provides a good synthetic strategy for the convenient preparation of a broad range of functional polymers.

4.5 References

- [1] (a) Matyjaszewski, K., Müller, A. H. E. *Controlled and Living Polymerization : From Mechanisms to Applications*; Wiley–VCH: Weinheim, 2009. (b) Baskaran, D. *Prog. Polym. Sci.* **2003**, *28*, 521. (c) Aoshima, S.; Kanaoka, S. *Chem. Rev.* **2009**, *109*, 5245. (d) Greszta, D.; Mardare, D.; Matyjaszewski, K. *Macromolecules* **1994**, *27*, 638. (e) Schrock, R. R.; Feldman, J.; Cannizzo, L. F.; Grubbs, R. H. *Macromolecules* **1987**, *20*, 1169.
- [2] (a) Walker, R.; Conrad, R. M.; Grubbs, R. H. *Macromolecules* **2009**, *42*, 599. (b) Bielawska, C. W.; Grubbs, R. H. *Prog. Polym. Sci.* **2007**, *32*, 1. (c) Choi, T. -L.; Grubbs, R. H. *Angew. Chem. Int. Ed.* **2003**, *42*, 1743. (d) Lynn, D. M.; Kanaoka, S.; Grubbs, R. H. *J. Am. Chem. Soc.*, **1996**, *118*, 784.
- [3] (a) Kang, E. -H.; Lee, I. S.; Choi, T. -L. *J. Am. Chem. Soc.*, **2011**, *133*, 11904. (b) Fox, H. H.; Wolf, M. O.; O'Dell, R.; Lin, B. L.; Schrock, R. R.; Wrighton, M. S. *J. Am. Chem. Soc.*, **1994**, *116*, 2827. (c) Fox, H. H.; Schrock, R. R. *Organometallics*, **1992**, *11*, 2763.
- [4] (a) Garber, S. B.; Kingsbury, J. S.; Gray, B. L.; Hoveyda, A. H. *J. Am. Chem. Soc.* **2000**, *122*, 8168. (b) Scholl, M.; Ding, S.; Lee, C. W.; Grubbs, R. H. *Org. Lett.* **1999**, *1*, 953. (c) Sanford, M. S.; Love, J. A.; Grubbs, R. H. *Organometallics* **2001**, *20*, 5314. (d) Trnka, T. M.; Grubbs, R. H. *Acc. Chem. Res.* **2001**, *34*, 18. (e) Mohr, B.; Lynn, D. M.; Grubbs, R. H. *Organometallics* **1996**, *15*, 4317. (f) Nguyen, S. T.; Johnson, L. K.; Grubbs, R. H.; Ziller, J. W. *J. Am. Chem. Soc.* **1992**, *114*, 3974.
- [5] (a) Leitgeb, A.; Szadkowska, A.; Michalak, M.; Barbasiewicz, M.; Grela, K.; Slugovc, C. *J. Polym. Sci. Part A. Polym. Chem.* **2011**, *49*, 3448. (b) Wappel, J.; Urbina-Blanco, C. A.; Abbas, M.; Albering, J. H.; Saf, R.; Nolan, S. P.; Slugovc, C. *Beilstein J. Org. Chem.* **2010**, *6*, 1091. (c) Slugovc, C.; Demel, S.; Riegler, S.; Hobisch, J.; Stelzer, F. *Macromol. Rapid Commun.* **2004**, *25*, 475.
- [6] Hong, S. H.; Wenzel, A. G.; Salguero, T. T.; Day, M. W.; Grubbs, R. H. *J. Am. Chem. Soc.* **2007**, *129*, 7961.
- [7] (a) Wilson, G. O.; Caruso, M. M.; Reimer, N. T.; White, S. R.; Sottos, N. R.; Moore, J. S. *Chem. Mater.* **2008**, *20*, 328. (b) Kim, K. O.; Choi, T. -L. *ACS Macro Lett.* **2012**, *1*, 445.

- [8] (a) Charvet, R.; Novak, B. M. *Macromolecules* **2001**, *34*, 7680. (b) Charvet, R.; Novak, B. M. *Macromolecules* **2004**, *37*, 8808. (c) Charvet, R.; Acharya, S.; Hill, J. P.; Akada, M.; Liao, M.; Seki, S.; Honsho, Y.; Saeki, A.; Ariga, K. *J. Am. Chem. Soc.* **2009**, *131*, 18030.
- [9] (a) Khanna, K.; Varshney, S.; Kakkar, A. *Polym. Chem.* **2010**, *1*, 1171. (b) Liu, C.; Hillmyer, M. A.; Lodge, T. P. *Langmuir* **2008**, *24*, 12001. (c) Nederberg, F.; Appel, E.; Tan, J. P. K.; Kim, S. H.; Fukushima, K.; Sly, J.; Miller, R. D.; Waymouth, R. M.; Yang, Y. Y.; Hedrick, J. L. *Biomacromolecules* **2009**, *10*, 1460.
- [10] (a) Gao, H.; Matyjaszewski, K. *Macromolecules* **2008**, *41*, 1118. (b) Matyjaszewski, K.; Xia, J. *Chem. Rev.* **2001**, *101*, 2921. (c) Hawker, C. J.; Bosman, A. W.; Harth, E. *Chem. Rev.* **2001**, *101*, 3661. (d) Kade, M. J.; Burke, D. J.; Hawker, C. J. *J. Polym. Sci., Part A: Polym. Chem.* **2010**, *48*, 743.
- [11] (a) Gatard, S.; Nlate, S.; Cloutet, E.; Bravic, G.; Blais, J. -C.; Astruc, D. *Angew. Chem. Int. Ed.* **2003**, *42*, 452 (b) Beerens, H.; Verpoort, F.; Verdonck, L. *J. Mol. Cat. A.Chem.* **2000**, *151*, 279.
- [12] Binder, W. H.; Kluger, C. *Macromolecules* **2004**, *37*, 9321.
- [13] (a) Yang, S. K.; Weck, M. *Soft Matter.* **2009**, *5*, 582. (b) Shaefer, M.; Hanik, N.; Kilbinger, A. F. M. *Macromolecule* **2012**, *45*, 6807. (c) AL-Badri, Z. M.; N. Tew, G. *Macromolecules* **2008**, *41*, 4173.
- [14] Garber, S. B.; Kingsbury, J. S.; Gray, B. L.; Hoveyda, A. H. *J. Am. Chem. Soc.* **2000**, *122*, 8168.
- [15] (a) Love, J. A.; Morgan, J. P.; Trnka, T. M.; Grubbs, R. H. *Angew. Chem. Int. Ed.* **2002**, *41*, 4035. (b) Sanford, M. A.; Love, J. A.; Grubbs, R. H. *J. Am. Chem. Soc.* **2001**, *123*, 6543. (c) Love, J. A.; Sanford, M. S.; Day, M. W.; Grubbs, R. H. *J. Am. Chem. Soc.* **2003**, *125*, 10103. (d) Holland, M. G.; Griffith, V. E.; France, M. B.; Desjardins, S. G. *J. Polym. Sci. Part A. Polym. Chem.* **2003**, *41*, 2125. (e) Demel, S.; Schoefberger, W.; Slugovc, C.; Stelzer, F. *J. Mole. Cat. A. Chemical.* **2003**, *200*, 11.
- [16] Lapinte, V.; Brosse, J. -C.; Fontaine, L. *Macromol. Chem. Phys.* **2004**, *205*, 824.
- [17] Connor, E. F.; Sundberg, L. K.; Kim, H. -C.; Cornelissen, J. J.; Magbitang, T.; Rice, P. M.; Lee, V. Y.; Hawker, C. J.; Volksen, W.;

- Hedrick, J. L.; Miller, R. D. *Angew. Chem. Int. Ed.* **2003**, *42*, 3785.
- [18] Gatard, S.; Kahlal, S.; Méry, D.; Nlate, S.; Cloutet, E.; Saillard, J. -Y.; Astruc, D. *Organometallics* **2004**, *23*, 1313.
- [19] (b) Cho, H. Y.; Averick, S. E.; Paredes, E.; Wegner, K.; Averick, A.; Jurga, S.; Das, S. R.; Matyjaszewski, K. *Biomacromolecules* **2013**, *14*, 1262. (c) Matyjaszewski, K.; Qin, S.; Boyce, J. R.; Shirvanyants, D.; Sheiko, S. S. *Macromolecules* **2003**, *36*, 1843. (d) Huang, J.; Jia, S.; Siegwart, D. J.; Kowalewski, T.; Matyjaszewski, K. *Macromol. Chem. Phys.* **2006**, *207*, 801.
- [20] Kim, K. O.; Choi, T. -L. *Macromolecules* **2013**, *46*, 5905.
- [21] (a) Sanford, M. S.; Ulman, M.; Grubbs, R. H. *J. Am. Chem. Soc.* **2001**, *123*, 749. (b) Kim, K. H.; Ok, T.; Lee, K.; Lee, H. S.; Chang, K. T.; Ihee, H.; Sohn, J. H. *J. Am. Chem. Soc.* **2010**, *132*, 12027.
- [22] Chen, G.; Ma, X. S.; Guan, Z. *J. Am. Chem. Soc.* **2003**, *125*, 6697.
- [23] Nakamura, T.; Terashima, T.; Kenichi, O.; Fukuzawa, S. *Org. Lett.* **2011**, *13*, 620.
- [24] (a) Karakaya, B.; Claussen, W.; Gessler, K.; Saenger, W.; Schlüter, A. D. *J. Am. Chem. Soc.* **1997**, *119*, 3296. (b) Mynar, J. L.; Choi, T.-L.; Yoshida, M.; Victor, K.; Hawker, C. J.; Fréchet, J. M. J. *Chem. Commun.* **2005**, *41*, 5169.

Chapter 5.

Fabrication of Polymer Nanostructure using ROMP polymer

5.1 Introduction

The self-assembly of block copolymers (BCPs) with two immiscible block can be occurred in selective solvent, which is a good solvent for one block but a poor solvent for the other block, to produce various intriguing nanostructures, such as spheres, cylinders, and crystallizationdriven self-assemblies.¹ These well-defined nanostructures are attractive for the use in broad applications, like drug delivery, nanolithography, molecular nanowire because of structural and chemical diversity.²

There are various kinds of factors which affect to the assembly. Among them, extended conformation or reduced entanglement is a particular factor to overcome the kinetic barrier of self-assembly, especially for high molecular weight polymer like brush or dendronized polymers.³ In these polymers, the densely grafted side chains enables to have stiffness or limited flexibility compare to their linear analogs. Recently, Grubbs group reported that the self-assembly of brush block copolymer, PLA-*b*-PnBA, can be achieved efficiently with large domain structure and controlled intermaterial dividing surfaces.⁴ This large domain structures are one of the attractive character because of potential to control the light,

but challenge to achieve with linear block copolymers. However, the self-assembly of dendronized polymers having more extended conformation than brush polymer has been less explored.

All of these BCP self-assemblies mentioned above inevitably require various additional post-synthetic processes such as redissolution in selective solvents, dialysis, change in temperature, aging, chemical modification, or introduction of glue molecules,⁵ whereas nature provides more complex nanostructures in much simpler manners. These time consuming post-synthetic treatments are necessary because the synthesis of the polymers does not guarantee a sufficiently strong driving force for their self-assembly. This problem was partially resolved by *in situ* self-assembly of amphiphilic BCPs, termed polymerization induced self-assembly.⁶ Nevertheless, these supramolecules are not thermodynamically stable adducts because the driving force holding the unimers of BCPs together is not strong enough. For this reason, small changes in solvent, temperature, or concentration would easily alter the nanostructures or even break the self-assembly. Therefore, another chemical post-functionalization process to produce further cross-linking of either the core or the shell is required to obtain stable adducts.⁷ If stable supramolecules could be prepared directly by means of a simple one-pot procedure under mild conditions without any postsynthesis modification, even the large scale production of nanostructured polymers would be possible.

5.2 Experimental

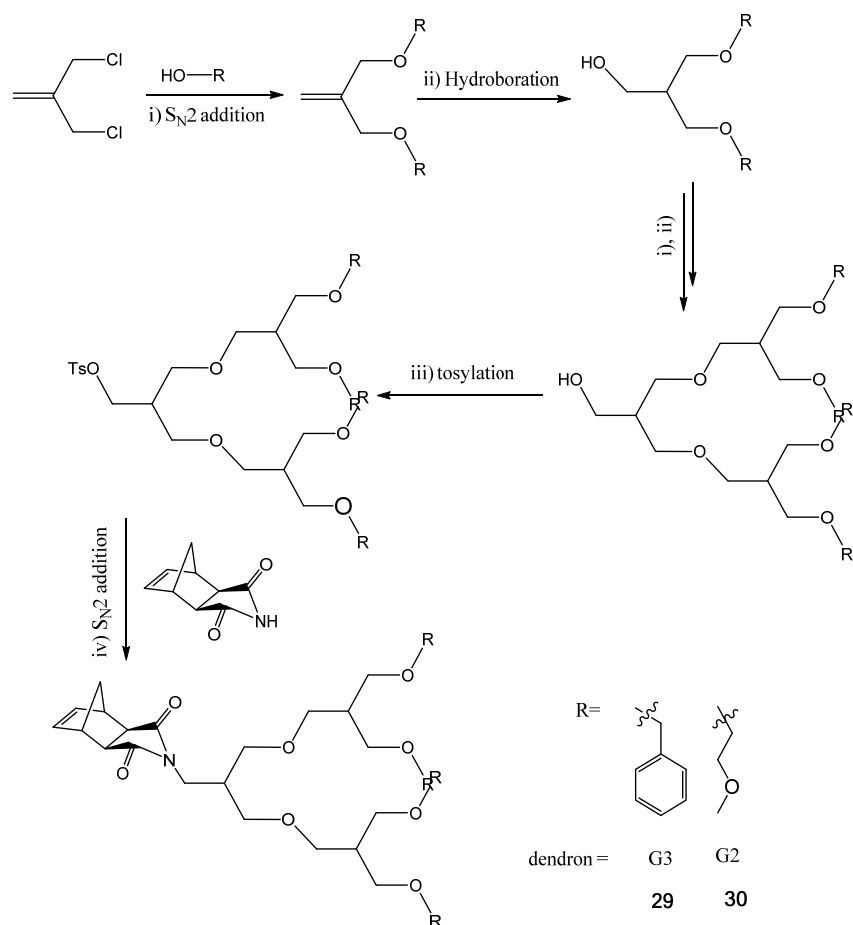
5.2.1 General considerations

All the reagents were commercially available from Alfa Aesar or Sigma–Aldrich® and was used without further purification. UV/Vis spectra were obtained by Jasco Inc. UV/vis–Spectrometer V–550. Cyclic voltammetry (CV) measurements were carried out on a CHI 660 Electrochemical Analyzer (CH Instruments, Insc., Texas, USA). The polymer molecular weight analysis was carried out by chloroform GPC with Waters system (515 HPLC pump and 2410 refractive refractive index detector), Acme 9000 UV/Vis detector, and THF GPC with Waters system (1515 pump) and Shodex GPC LF–804 column eluted chloroform or THF (HPLC grade, J. T. Baker). Flow rate was 0.8 mL/min and temperature of column was maintained at 35 °C. Samples in 0.5–1.0 mg/mL solvent were filtered by 0.45– μ m PTFE filter before injection. X–ray diffraction was also performed by National Center for Inter–University Research Facilities at SNU using Bruker D8 DISCOVER (Germany). Multimode 8 and Nanoscope V controller (Veeco Instrument) were used for AFM imaging. JEM–2100 (JEOL) was used for transmission electron microscopy analysis. Cryo–TEM analysis was carried out by using JEM–3010. Dynamic Light Scattering (DLS) data were obtained by Malvern Zetasizer Nano ZS.

5.2.2 Synthesis of monomer

NB macromonomers with ether type dendrons

NB macromonomers with ether type dendrons were synthesized follow the scheme 5-1.⁸ Only *exo*-isomer was used for the efficient ROMP. The series of dendronized macromonomers with two kinds of terminal groups were synthesized by repetition of S_N2 addition and hydroboration reaction.



Scheme 5-1. synthesis route for TD macromonomers with ether type dendrons: i) NaH, DMF, 0 °C to room temperature, 14 h; ii) BH₃ · THF, THF, Ar atm, 0 °C, 3 h, quench with NaOH and H₂O₂, K₂CO₃ work up; iii) tosyl chloride, DCM, pyridine, Ar atm, room temperature, 5 h, 10 % HCl work up; iv) NaH, DMF, Ar atm, 3 h.

5.2.3 Polymerization

¹H NMR analysis for COT conversion and benzene formation

Monomer **31** (101.3 mg, 0.4134 mmol) was weighed in a 4-mL sized screw-cap vial with septum and purged with argon. A degassed anhydrous deuterium solvent was added (0.1 mL) to the vial. The solution of initiator **III** (6.0 mg) was added (0.1 mL) to the monomer solution at once under vigorous stirring. Within 20 mins, cyclooctatetraene (COT) (28 μ L) and hexamethyldisilane (\sim 15 μ L, an internal standard) was added, and a tiny amount of the COT solution (\sim 5 μ L) was sampled out and diluted with 0.5 mL CD₂Cl₂ to ascertain the initial ratio between COT and the internal standard by ¹H-NMR analysis. After that, the solution was added to the reaction vial, and the vial was tightly sealed by using parafilm and Teflon tape. The mixture was stirred for 12–16 h at the room temperature. The reaction was quenched by excess ethyl vinyl ether at 0 °C, and then a tiny amount of the crude mixture (\sim 5 μ L) was sampled out and diluted with 0.5 mL CD₂Cl₂ to know the final ratio between COT and the internal standard. COT conversion was calculated from the final COT/(internal standard) ratio divided by initial COT/(internal standard) ratio. Also, benzene formation (%) was calculated from the number of double bonds to form benzene divided by the number of total double bonds theoretically attached to the polymer. We used deuterium solvents that had no TMS because the signal of TMS overlapped that of hexamethyldisilane. This overlapping interfered the COT/(internal standard) ratio (Chemical shift – CH₃ of Hexamethyldisilane : δ 0.05 , CH of COT : δ 5.76, CH of Benzene : δ 7.36)

5.2.4 Sample preparations

Thin film morphology study with dendronized BCPs

The 1 w% polymer solutions in chloroform (CF), THF, methanol were prepared by direct dissolution method. No other further process was done for micelle formation. Each solutions were spin-coated on mica and HOPG for AFM imaging, and drop casted on the carbon coated copper grid and stained by RuO_4 or OsO_4 for TEM imaging. The RuO_4 prefer to stain benzene group and OsO_4 prefer to stain alcohol group. For the thermal annealing, spin-coated or drop casted samples were kept in oven under the air.

Redox reaction with BCPs containing ferrocene

The polymer solutions in chloroform (CF), THF at desired temperature for several hours (1 mg/0.2 L concentration for AFM, and 1 mg/2 L concentration for TEM) were prepared by direct dissolution method. 1.5 Eq of FeCl_3 and 2Eq of NaBH_4 was added to the polymer solution for oxidation and reduction, respectively. Each solutions were spin-coated on mica and HOPG for AFM imaging, and drop casted on the carbon coated copper grid for TEM imaging.

5.3 Result and Discussion

5.3.1 BCP with two kinds of dendrons

Various kinds of dendronized block copolymers were prepared by combination of polar ester, ether, and nonpolar fréchet type dendrons with different generations to get the efficient self-assembly (Figure 5-1). The BCPs were synthesized easily by sequential addition of monomers with high molecular weight and moderate PDIs (<1.15) (Table 5-1).

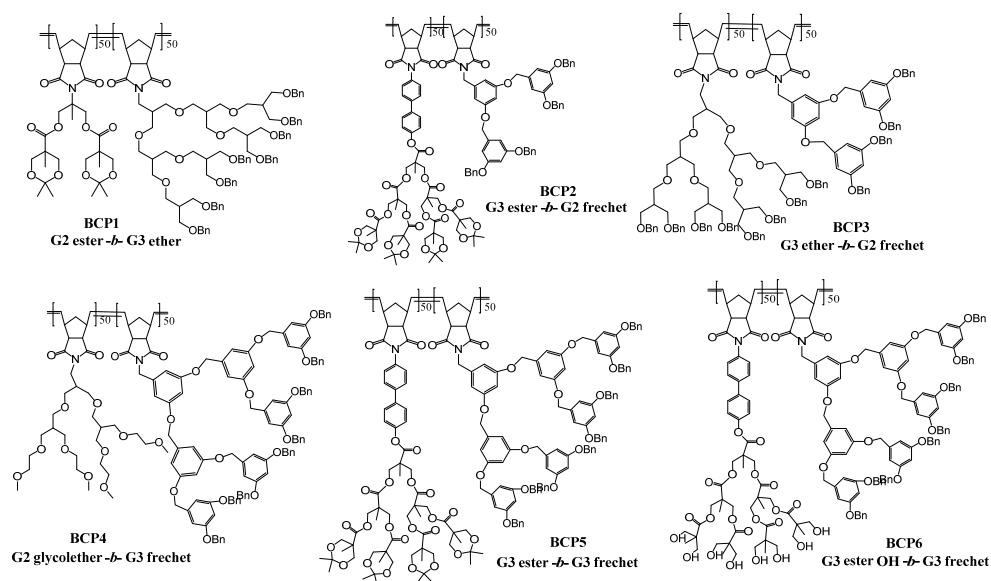


Figure 5-1. Structure of fully dendronized BCPs.

The synthesized BCPs(1-3) were dissolved in toluene (2 w%) and spin-coated on the graphite at room temperature with 2000 rpm. The thickness of prepared thin film was around 70 nm which is determined by ellipsometer. For all the cases, no microstructures were observed right after spin-coating, but BPC(3) showed sphere shape aggregation after thermal annealing at 70°C which is higher temperature than the T_g of three kinds of dendrons ($T_{g,ester} \sim 50$ °C, $T_{g,ether} \sim 40$ °C, $T_{g,fréchet} \sim 70$ °C) (Figure 5-2). The size of sphere

grows to 2 μm with the longer time for annealing. Longer time than 12 hours or higher temperature such like 90 $^{\circ}\text{C}$ was also tried to observe the structural change of assemblies, but only burned results were obtained. Also, BCP(1–2) didn't show any assemblies because the polarity difference between two blocks was not enough.

Table 5–1. Molecular weight information of dendronized BCPs.^a

entry	BCP	$M_{n(\text{Theo})}^{\text{b}}$	$M_{n(\text{MALS})}^{\text{c}}$	$M_{n(\text{conv})}^{\text{d}}$	$\text{PDI}_{(\text{conv})}^{\text{d}}$
1	BCP(1)	103 k	101 k	60 k	1.06
2	BCP(2)	111 k	109 k	73 k	1.06
3	BCP(3)	120 k	116 k	81 k	1.08
4	BCP(4)	120 k	110 k	57 k	1.14
5	BCP(5)	152 k	171 k	71 k	1.15
6	BCP(6)	135 k	2770 k ^e (43730 k)	46 k	1.07

^a The ROMP was done in THF at room temperature for 15 min and 1h for each block. [M1]/[M2]/[I]=50/50/1. ^b Theoretical molecular weight. ^c The molecular weight was measured by MALLS–VIS–RI detector. ^d The numbers were determined by THF–GPC calibrated by PS standards. ^e Two signal was measured which indicate single molecule and self–assembled species, respectively.

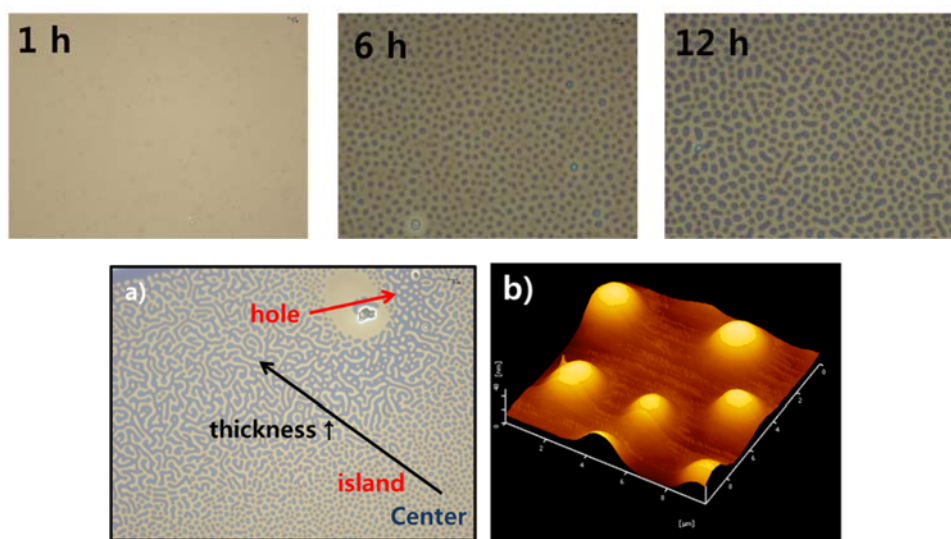


Figure 5–2. Morphology change of BCP(3) after thermal annealing at 70 $^{\circ}\text{C}$ for 12h. a) Photomicrograph and b) AFM topography.

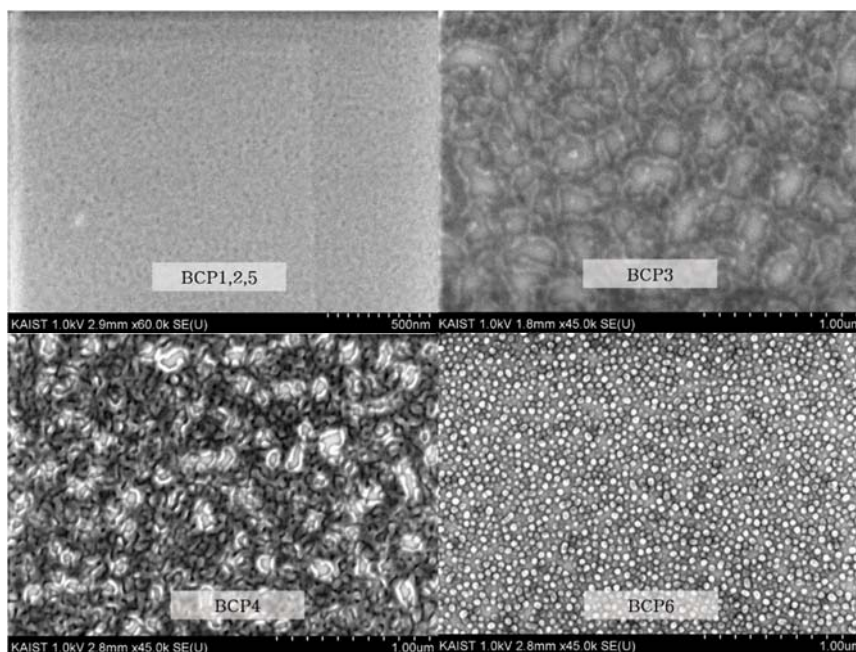


Figure 5–3. Photomicrograph of dendronized BCPs after spin coating.

The BCP(4) with more polar ethylene oxide terminal group on ether dendron showed irregular self-assemblies right after spin-coating, but this structures were collapsed easily under the heating condition. We thought that larger polarity difference is required to get the clear self-assembly and structure change after annealing. BCP(6) with large number of alcohol groups on ester dendron and nonpolar fréchet dendron was synthesized for this purpose. As we expected, clear micelle formation was observed from the photomicrograph (Figure 5–3). Also, it showed huge solubility difference with solvent polarity (Figure 5–4). The polymer solution in good solvent for both block like THF was completely clear, but colloid type turbid solution was observed from moderate solvent like chloroform, and completely insoluble in bad solvent like methanol or toluene. The size of micelles were determined using dynamic light scattering (DLS). Large sized micelles having around 130 nm diameter was formed in moderate solvent but also around 30 nm sized

micelles were formed from the good solvent (Figure 5–4). In the ^1H NMR spectrum, the signal from both block was observed in THF but only fr chet dendron signal was observed in chloroform. According to these results, we concluded that BCP (6) formed perfect micelle in chloroform with ester dendron core and fr chet dendron shell, but imperfect micelles with ambiguous boundary were formed in THF because both block can be dissolved in this solvent. The ester dendron might be positioned more to shell part owing to the polar–polar interaction between alcohol group on ester dendron and THF.

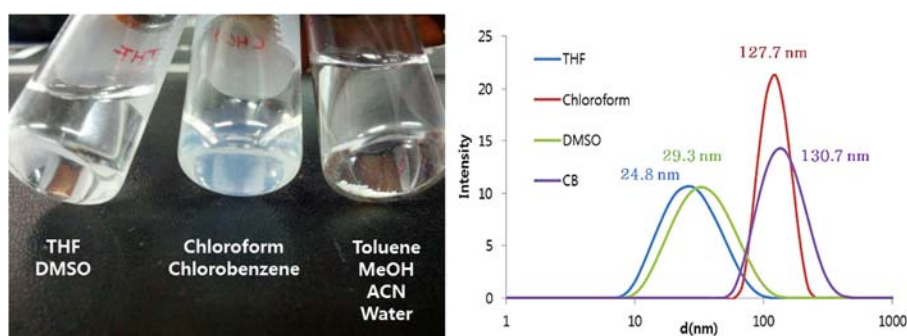


Figure 5–4. Solvent dependent solubility and micellization of BCP (6).

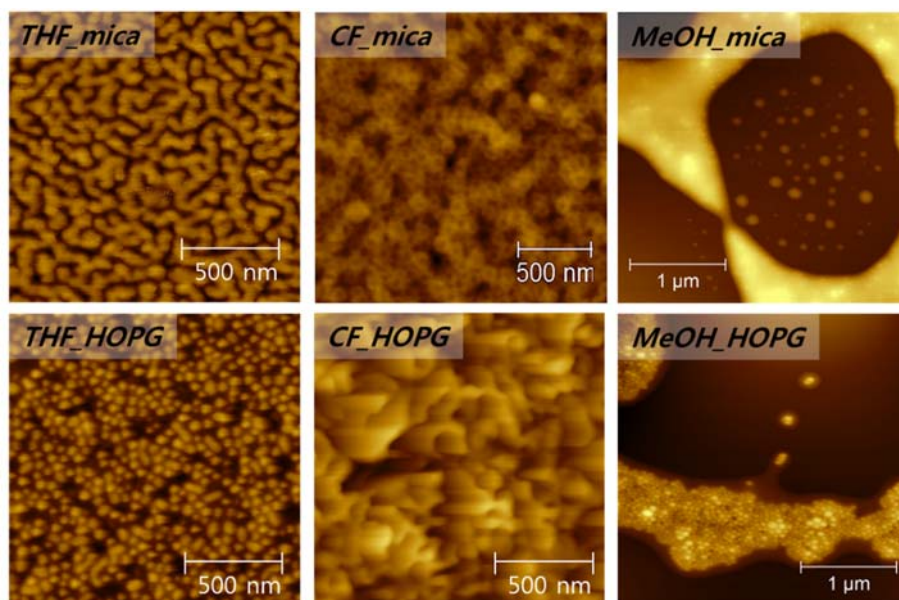


Figure 5–5. AFM topography of BCP (6) from the various solvents.

The structural information of micelles were obtained by AFM imaging technique (Figure 5–5). BPC (6) was dissolved in three kinds of solvents in 1 w% concentration and spin-coated on two kinds of substrates, which are mica with polar surface and HOPG with nonpolar surface, to see the effect of surface and solvent dependency. First, THF solution showed cylindrical micelle on mica and spherical micelle on HOPG. On the contrary, cylindrical micelle was observed on HOPG and vesicular micelle was observed on mica in the case of chloroform solution. The cylindrical micelle is formed when the polarity of shell part and surface of substrate is well matched. However, BCP forms spherical micelle when the polarity is not matched, to decrease the surface energy. A noteworthy feature in here is that polymer solution in chloroform formed vesicular micelles on the mica because ester dendron part can be swelled due to the ester groups on the inner part of dendrons even with large amount of alcohol groups as an end group. The methanol solution didn't show any substrate dependency because firmly aggregated spherical micelles are already formed due to the bad solubility of both blocks in BCP(6). The same structure was observed from transmission electron microscopy (TEM) using nonpolar carbon coated copper grid (Figure 5–6). The densely packed spherical micelle, cylindrical micelle, and spherical micelle were observed from THF, chloroform, and methanol, respectively.

Then we tried to check the possibility of structure change in film state by thermal annealing. The cylindrical micelle from chloroform solution and spherical micelle from methanol didn't show any structural change at 70 °C, but all the structures were collapsed after 1 h. The densely packed spherical micelle from THF solution showed capability for structure change to cylindrical micelle and

toroidal shape when it is annealed at 70 °C for 6 hours, and at 90 °C for 30 hours, respectively (Figure 5–7). Using this solvent, substrate and thermal annealing condition dependent morphology change, BCP(6) would be applied for the further material science such like nano–patterning or photonic crystal.

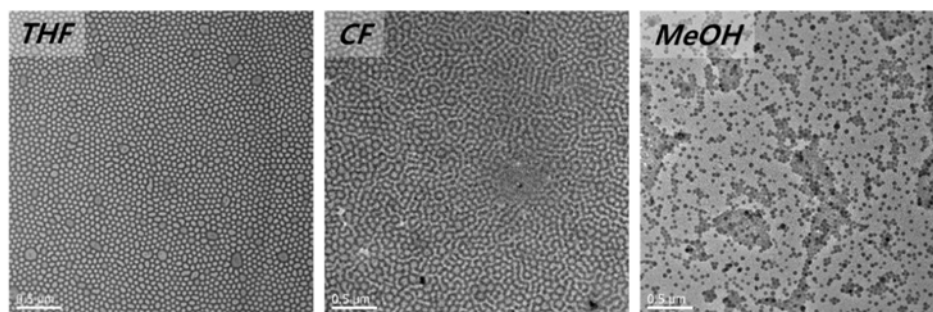


Figure 5–6. TEM image of BCP(6) from the various solvents.

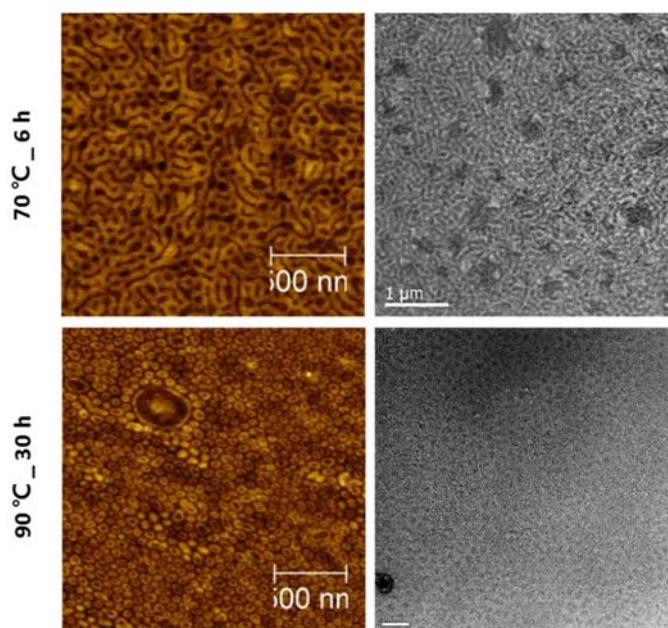
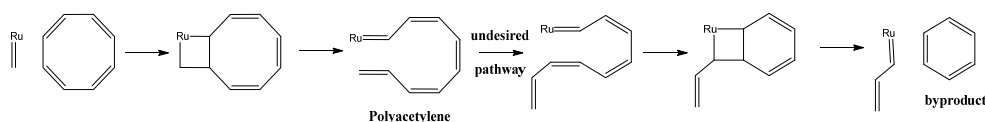


Figure 5–7. Thin film morphology of BCP(6) from THF solution on C–grid by AFM (brown) and TEM (grey) after thermal annealing.

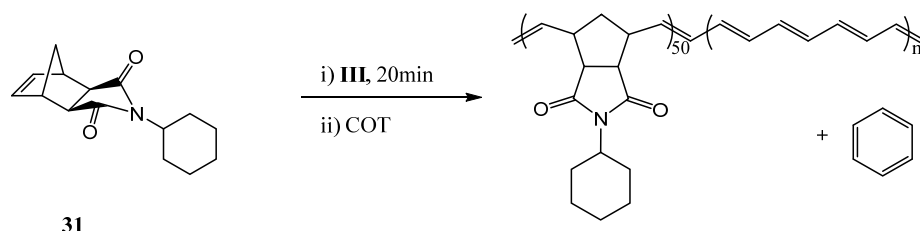
5.3.2 Insitu nanoparticlization of conjugated polymer (INCP)

Polyacetylene (PA) has attracted significant attention from both chemists and physicists because of its interesting electronic properties.⁹ For this reason, various synthetic methods have been developed, such as Ziegler–Natta polymerization of acetylene, ring–opening metathesis polymerization (ROMP) of cyclooctatetraene (COT), the Durham method, ROMP of benzvelene, and the use of poly(phenylvinyl sulfoxide) precursors.¹⁰ However, the synthesis and applications of PA are still challenging because of its instability in air and insolubility in any solvents, which arise from the strong $\pi-\pi$ interactions of the conjugated backbone. Chemists have tried to overcome the solubility challenge by preparing BCPs consisting of a soluble block and a PA block (PA BCP),¹¹ mostly via indirect syntheses that require temperatures above 100 °C for the thermal elimination of certain leaving groups from PA. Even though ROMP of COT is the simplest way to synthesize PA, block copolymerization via this direct method has been only partially successful because during ROMP of COT under dilute conditions or at elevated temperatures, an undesirable side reaction occurs that releases a large amount of benzene (over 50% based on consumed COT) and lowers the conversion to PA (Scheme 5–2).¹² Therefore, if a method to enhance COT conversion by suppressing benzene formation under mild conditions could be developed, ROMP would become the best method for the synthesis of BCPs containing a PA block.



Scheme 5–2. ROMP of COT and undesired benzene formation.

Table 5–2. ROMP of COT for PA BCPs.



entry	solvent	conc (M) ^a	temp (°C)	time (h)	conv (%) ^b	PhH (%) ^c	DP _{COT} ^d
1	THF	0.1	r.t.	16	85	23	20
2	toluene	0.1	r.t.	16	77	17	19
3	DCM	0.1	r.t.	16	93	12	25
4	DCM	0.01	r.t.	16	73	32	15
5	DCM	0.7	r.t.	16	>99	9	28
6	DCM	0.1	0	24	35	4	10
7	DCM	0.1	40	4.5	99	21	24
8	toluene	0.1	55	5	84	34	17

^a Based on [COT]. ^b Conversion of COT. ^c Yield of benzene formation calculated on the basis of the total number of double bonds from the converted COTs. ^d Degree of polymerization of COT.

To synthesize well-defined diblock copolymers containing a long PA block, we used the powerful and fast-initiating 3rd generation Grubbs catalyst (**III**) for the ROMP of COT. This catalyst is ideal for the direct synthesis of diblock copolymers because ROMP of low strained COT (2.5 kcal/mol)^{10a} is possible only with highly active catalysts. In addition, this highly active catalyst might promote the ROMP even at low temperature (< 25 °C), which would suppress the formation of benzene, the major problem in previous reports. To prepare a soluble PA BCP, a solubilizing first block was prepared by living ROMP of **31**. After 20 min, COT was added at desired temperature. The solution color immediately changed to red, implying that the conjugated polymer, PA, was being synthesized. To investigate the ROMP of COT, the polymerization was monitored in various deuterated solvents at various temperature in a closed

system, and the conversion of COT and the production of benzene were directly measured by ^1H NMR analysis (Table 5–2).

From these experiments, we observed that the solvent affected the COT conversion as well as the amount of benzene formation, and dichloromethane (DCM) was found to be the best solvent. The reaction temperature also proved to be another factor. As we expected, the ROMP of COT was much faster at 40 °C, resulting in complete conversion in 4.5 hours, whereas only 35% conversion was observed at 0 °C even after 24 hours (Table 5–2, entries 3, 6 and 7). Even using toluene, a relatively poor solvent for the ROMP of COT, the conversion reached 84% within 5 hours at 55 °C. However, higher temperature produced a large amount of undesired benzene (34% at 55 °C and 21% at 40 °C), resulting in relatively short PA incorporated into the diblock copolymer, while the least amount of benzene (4%) was formed at 0 °C (Table 5–2, entries 6–8). In short, the reactions at higher temperatures not only had a positive influence on the PA synthesis by increasing the COT conversion, but also a negative effect by promoting the depolymerization that released the benzene at the same time. Clearly the benzene formation was a thermodynamically driven process. Thus, the fact that benzene formation was minimized at 0 °C implied that the chain transfer reaction, another thermodynamically favored process, could be minimized at 0 °C as well. However, the polymerization rate was too slow and only 35 % conversion was obtained even after much longer reaction time than room temperature, showing higher conversion (93%) with small amount of benzene formation (Table 5–2, entries 3, 6). The effect of reaction concentration was also investigated to enhance the polymerization result at room temperature, which is the most manageable reaction temperature. The ROMP of COT at a

higher concentration resulted in higher conversion of COT and less benzene formation, while ROMP at a lower concentration gave the worst result (Table 5–2, entries 3–5). From the optimized condition (Table 5–2, entry 5, PA BCP (5)), we achieved the full conversion of COT and much lower benzene formation than in previous reports.

Various in–depth characterizations of the resulting polymer were performed to confirm its chemical structure. Although the polymer was completely soluble in various organic solvents such as THF, toluene, and chloroform, liquid ^1H NMR analysis of the final polymer revealed only peaks corresponding to the polynorbornene (PN) block. The dark–red solution was analyzed by UV/vis spectroscopy, which revealed a spectrum with $\lambda_{\text{max}} = 535$ nm and two sets of distinguishable onset points at 630 and 800 nm (Figure 5–8a). These two onset points translated into band gaps of 2.0 and 1.6 eV, respectively, in perfect agreement with the band gaps for *cis*–PA and *trans*–PA, respectively.¹³ Furthermore, cyclic voltammetry (CV) also revealed that two oxidation potentials for the diblock copolymer were related to the highest occupied molecular orbitals (HOMOs) of *cis*–PA (–5.49 eV) and *trans*–PA (–5.19 eV) (Figure 5–8b). The much deeper HOMO of PA BCP relative to pristine PA (–4.5 to –4.2 eV),¹⁴ is indicative of the improved stability in air, allowing for all of the characterizations in the ambient atmosphere. From these characterizations, we verified the integrity of the second PA block, which comprised polyenes with a mixture of *E* and *Z* stereoisomers, and this direct synthesis under mild conditions was the key to obtaining the PA block copolymer with high purity. The observation that liquid NMR spectroscopy showed signals only for the PN block led us to investigate the self–assembly behavior of PN–*b*–PA. Since the growth of the insoluble second PA

block during the copolymerization would promote the *in situ* formation of core-shell supramolecular structures, the core consisting of $\pi-\pi$ -stacked PA would not appear in the liquid NMR analysis.

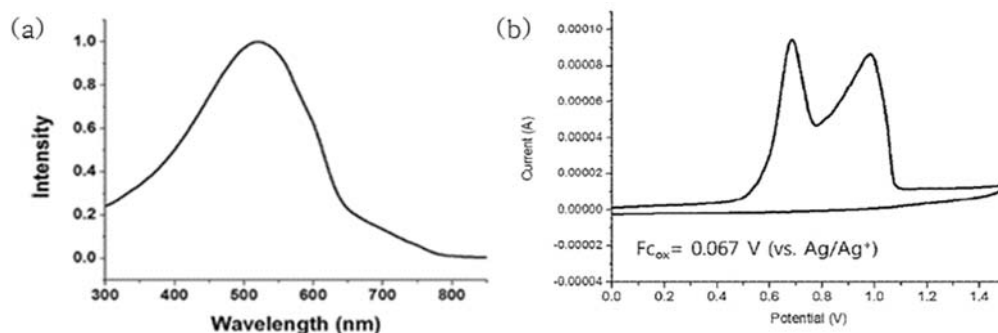


Figure 5-8. (a) UV/vis spectrum in chloroform and (b) Cyclic voltammogram of PA BCP(5).

The formation of supramolecules was also supported by chloroform GPC. GPC analysis of PA BCP showed two distinguished traces at high molecular weight (>389 kDa) and 14 kDa. The major peak at higher molecular weight part indicated the self-assembled aggregates, whereas the minor peak at 12 kDa corresponded to single chains of PA BCP containing relatively shorter PA chains, which were disassembled as a result of the shear pressure under the GPC conditions (Figure 5-9).

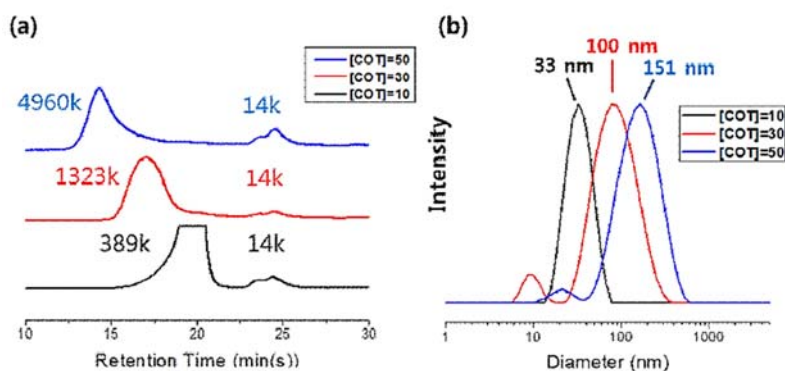


Figure 5-9. Size comparison of PA BCPs containing various lengths of PA block. (a) CHCl_3 GPC traces and (b) DLS profiles of nanostructures.

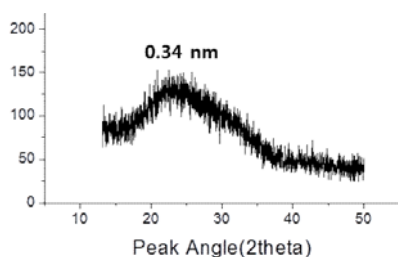


Figure 5–10. Wide Angle X–ray Scattering (WAXS) plot of PA BCP(5) indicating that there is $\pi - \pi$ stacked PA block (although the peak at 3.4 Å is broad due to low crystallinity in the core).

X–ray diffraction analysis showed a signal at 0.34 nm on average (Figure 5–10), implying that the $\pi - \pi$ interaction within the PA core blocks was very strong and these supramolecular adducts were stable enough to maintain the self–assembly under the shear pressure of the GPC conditions. Thus, this *in situ* supramolecular formation did not require any additional processes to induce self–assembly.

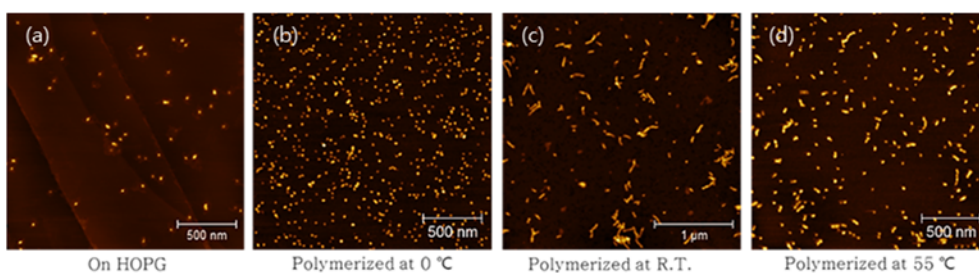


Figure 5–11. AFM images of the nanostructures from PA BCPs synthesized at various temperature.

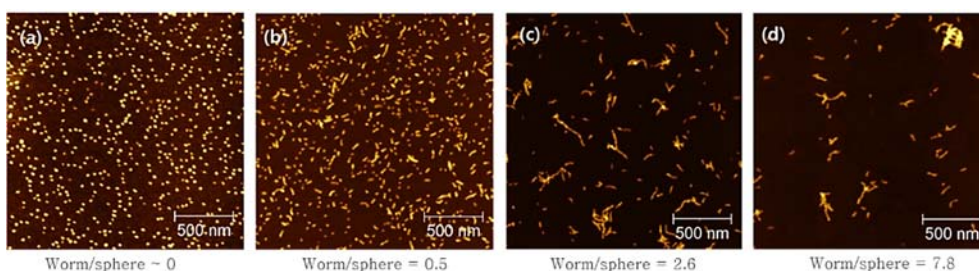


Figure 5–12. AFM images of the nanostructures self–assembled on mica from PN–b–PA with various lengths of PA block. PN:PA ratios of (a) 50:40, (b) 50:80, (c) 50:120, and (d) 50:200.

Detailed information on the nanostructure was obtained by AFM. Spin-coated PA BCPs on mica showed various kinds of structures with the ROMP temperature (Figure 5-11b-d), but no big difference with substrate (Figure 5-11a,b). The sphere shape nanostructure and wormlike micelles was observed from the 0 °C and higher temperature, respectively. We assumed that this structural difference came from the different length of PA block. Also, broader PDI of PA block can cause the irregularity of nanostructure like in Figure 5-11d. A series of PA BCPs with different length of PA block was synthesized under the optimized condition to figure out the effect of PA block length on nanostructure; 0.07 M concentration at room temperature. The PN₅₀-*b*-PA₄₀ having shortest PA block revealed spherical nanostructures having a diameter of 31 nm and a height of 2 nm with a highly uniform size distribution (Figure 5-12a). As the PA block was lengthened from 10 to 50 equiv of COT (40 to 200 for DP of PA), the heights and hydrodynamic volumes of the supramolecules increased (Figure 5-12), and structural evolution was observed as the PA block lengthened. For PN₅₀-*b*-PA₈₀, some portion of the nanospheres began to transform into wormlike micelles (Figure 5-12b), and the ratio of the populations of the wormlike and spherical micelles increased (0.5, 2.6, and 7.8; Figure 5-12b-d) as the amount of COT increased. Even though the wormlike micelles were as long as 500 nm (Figure 5-12d), 11% of the supramolecules were still spheres. We believe that because of polydispersity in the PA block, these spheres in figure 5-12c,d contained PA cores with an insufficient block size preventing them from transforming into wormlike micelles.

Surprisingly, high resolution AFM images of PA BCP(5) revealed the obtained wormlike structure to be very different from

the ordinary ones. The magnified image (Figure 5–13a inset) clearly shows a highly undulated supramolecule resembling a caterpillar. The side-view image also supports the formation of supramolecules interconnected by the spheres (Figure 5–13b). More insights into the structure of this intriguing supramolecule were obtained by TEM analysis, where no staining with the sample was necessary because the electron density difference between the PN shell and electron-rich PA core provided sufficient contrast for TEM imaging. Magnified images revealed that despite existing as one supramolecule, the PA cores were not connected at all (Figure 5–13c). Nevertheless, these nanocaterpillar structures were surprisingly stable, as the integrity of the nanostructure was still maintained even when the polymer solution was heated at 100 °C for 20 min or the sample was sonicated for 30 min right before the spin-coating for AFM imaging. These results further demonstrate that the supramolecular adducts are thermodynamically stable under heating and mechanical and shear forces. In addition to the solid-state imaging, further structural information on PA BCP(5) in solution was obtained using cryogenic TEM (cryo-TEM) and DLS. The cryo-TEM images vividly showed the presence of the same nanocaterpillars containing PA cores with an average diameter of 8 nm (Figure 5–13d), confirming the unique nanostructure in the solution state as well. In addition, the DLS analysis in chloroform revealed two distinct populations with average hydrodynamic diameters of 17 nm (minor) and 100 nm (major). This also proved the coexistence of the nanocaterpillars (100 nm) and the smaller nanospheres (17 nm) in solution, as already observed in the AFM and TEM images (Figure 5–9b).

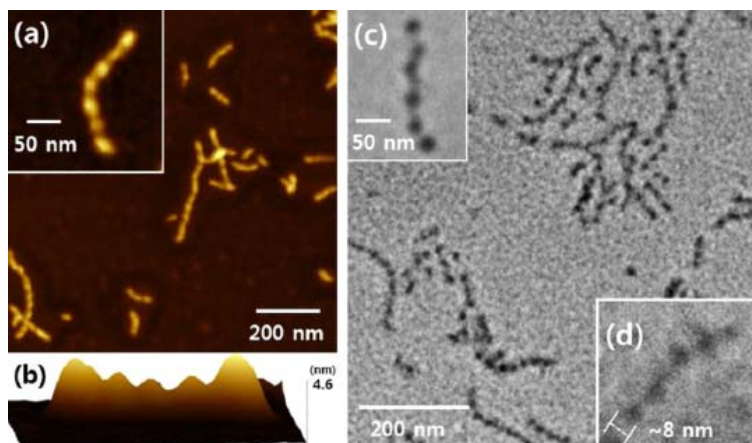


Figure 5-13. (a) AFM images of the nanocaterpillar structures from PA BCP(5) on mica substrate. (b) AFM 3D side view image. (c) TEM images of the nanocaterpillar structures on a carbon coated copper grid. (d) Cryo-TEM image in chloroform.

All these observations led to the conclusion that the diblock copolymers spontaneously self-assembled into highly stable nanocaterpillars in solution without any additional postsynthetic treatment. On the basis of the various analyses, the following model for nanocaterpillar formation is proposed. As the PA block grows to a certain size (Figure 5-14a), the produced diblock copolymer initially self-assembles into spheres, as expected (Figure 5-14b). As additional COT diffuses into the core, it expands until the PN shell block can no longer solvate the PA core as spheres (Figure 5-14c). This exposed PA core in the sphere then spontaneously clings to other spheres with extended PA cores (Figure 5-14d) forming the final nanocaterpillar by strong $\pi-\pi$ interactions to minimize the area of solvophobic PA cores (Figure 5-14e). Typical wormlike micelles were previously formed by the fusion of multiple spherical micelles¹⁵ or elongation from seed micelles.¹⁶ However, these nanocaterpillars with totally separated cores are uniquely shaped by individually isolated spheres that form loose contacts with others (Figure 5-14f). This unique assembly is markedly different from a

conventional self-assembly of block copolymers consisting of two flexible segments because the rigid and immobile conjugated PA core are held tight by $\pi - \pi$ interactions that are strong enough to endure heat and mechanical force. Lastly, this nanostructure in which the core is protected by the shell can provide the stable PA in solution and air with deep HOMO level than pristine PA.

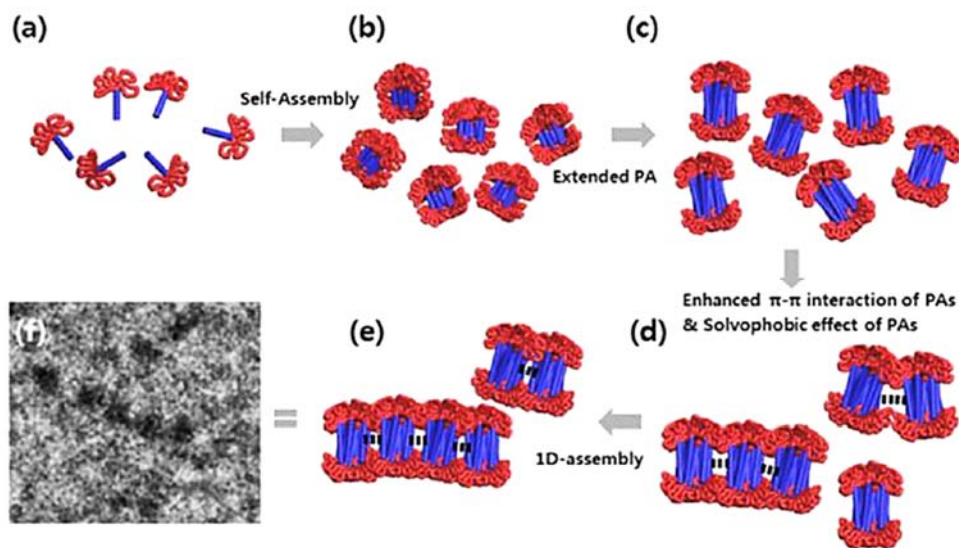
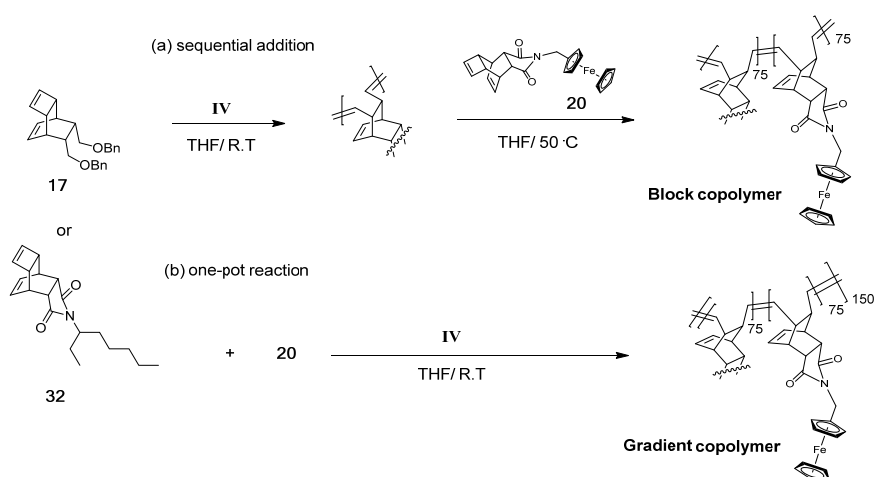


Figure 5-14. Proposed mechanism for *in situ* nanoparticulization of PN-b-PA into nanocaterpillars (INCP).

5.3.3 Self-assembly behavior of BCP containing ferrocene

Solubility of polyTDs containing metallocenes in common organic solvents (e.g. DCM, THF) at room temperature are not particularly good. Using this bad solubility, demonstration of another type of *in situ* nanoparticlization is possible. Here in, we introduced ferrocene (Fc), which is one of the most stable and useful organometallic compounds which used in broad range of applications including catalysis, biosensors.¹⁷ Moreover, reversibly controllable electronic state of ferrocene, leading the change of self-assembly structure and process of ferrocene-containing materials.



Scheme 5-3. Polymerization scheme for (a) block copolymer and (b) gradient copolymer containing ferrocene moiety.

The BCP containing ferrocene were prepared by two kinds of methods via ROMP (Scheme 5-3). The conventional block copolymer (Fc BCP) is synthesized from sequential addition method, and the reaction temperature needed to be heated up for second block copolymerization, because **20** is completely soluble only at high temperature in THF with ROMP concentration (0.4 M). On the contrary, gradient copolymer is synthesized at room temperature from one-pot reaction, because it dissolved gradually during the polymerization.

Table 5–3. Molecular weight information of copolymers containing ferrocene.^a

entry	polymer	M_n (CHCl ₃) ^b	PDI (CHCl ₃) ^b	M_n (THF) ^c	PDI (THF) ^c	area ^d
1	poly(17)– <i>b</i> –poly(20)	35 k	1.09	347 k 37 k	1.16 1.02	42/58
2	poly(32)– <i>b</i> –poly(20)	80 k	1.44	798 k 59 k	1.08 1.21	35/65
3	poly(17)– <i>g</i> –poly(20)	65 k	1.12	71 k	1.02	–
4	poly(32)– <i>g</i> –poly(20)	38 k	1.11	43 k	1.03	–

^a The ROMP was done for 30 min and 4h for each block. [M1]/[M2]/[I]=75/75/1. ^b The numbers were determined by chloroform–GPC calibrated by PS standards. ^c The numbers were determined by THF–GPC calibrated by PS standards. ^d The area ratio between two signal from single chain and aggregates from THF–GPC.

The micelle formation was confirmed from THF–GPC analysis first. Two signal were measured from block copolymers; small molecular weight from single chain and larger molecular weight from micelle. This large molecular weight was not observed from chloroform–GPC or gradient copolymer (Figure 5–15). The clue for micellization was confirmed again by DLS. Nano–sized particles were observed from all the copolymers both in THF and chloroform. From these results, we assumed that the block copolymers formed strongly bind micelles in THF but not in chloroform whereas gradient copolymers form weakly bind micelles with smaller size.

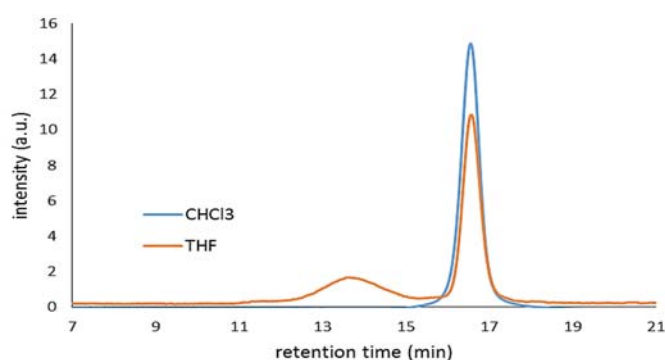


Figure 5–15. GPC traces of poly(17)–*b*–poly(20) from THF and CHCl₃.

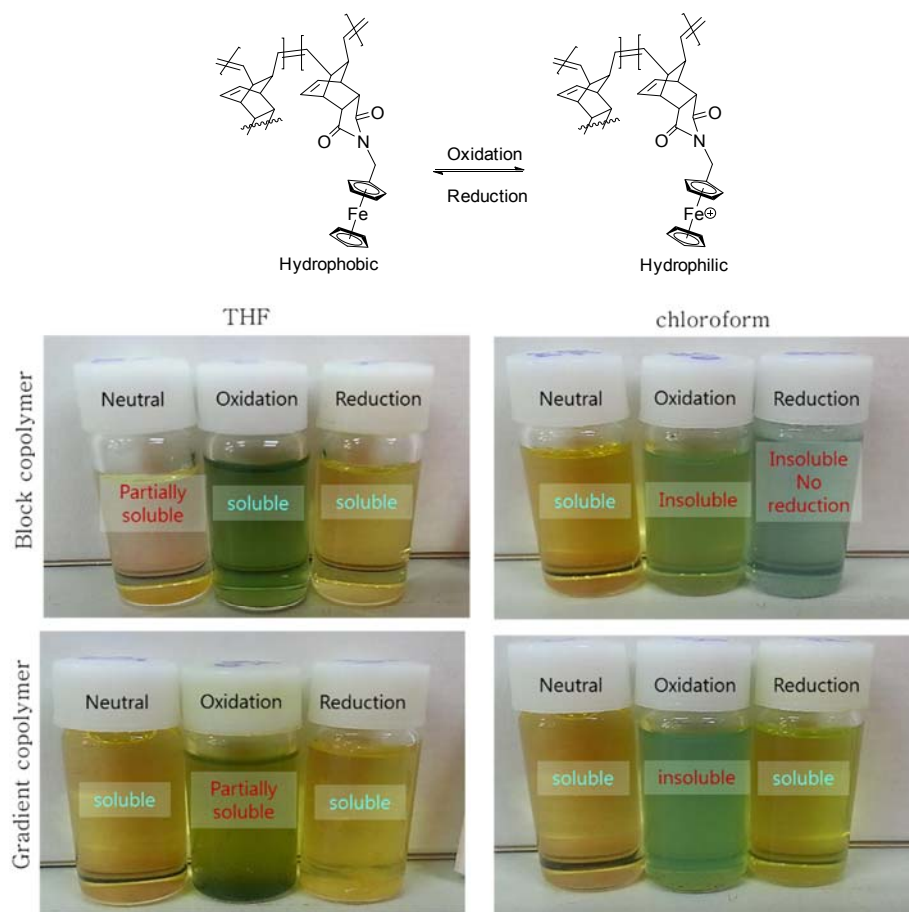


Figure 5–16. Oxidation and reduction of ferrocene moiety.

With the block copolymers, relationship between electronic state of ferrocene and nanostructure was investigated in THF. The FeCl_3 and NaBH_4 were used for oxidation and reduction, respectively. The color of polymer solution changed dramatically and reversibly with redox reaction of ferrocene, from yellow to green and to yellow again (Figure 5–16). This change is also affected to the UV/vis absorption; the absorption around 450 nm from Fc is quenched and new absorption around 640 nm from Fc^+ arises after oxidation. The absorption at 640 nm is quenched after reduction due to the re-formation of Fc (Figure 5–17a,b).¹⁸ The solubility also changed. The solubility increased after oxidation due to the increased

hydrophilicity of Fc block, inducing more regular micelle formation. This increased solubility was maintained after reduction. However, the micelle size change was not remarkable in DLS (Figure 5–17c,d). On the other hand, the solubility decreased after oxidation, and reduction was not possible in chloroform (Figure 5–16). This is probably caused by solvent polarity difference. The hydrophilic core part can be swelled in polar THF medium but not in non-polar chloroform medium to avoid the unfavored interaction. In the case of gradient copolymers, the micelle size was much smaller than block copolymer and soluble in both solvents before oxidation. However, the solubility decreased largely after oxidation because of the formation of ionic ferrocenium (Fc^+), and solubility was recovered completely after reduction (Figure 5–16). From these results, we concluded that gradient copolymers can't form a well-defined micelles in both solvents, irregular aggregation with exposed ferrocene block was formed instead. An ambiguous TEM images also support that clear micelle was not formed (Figure 5–20).

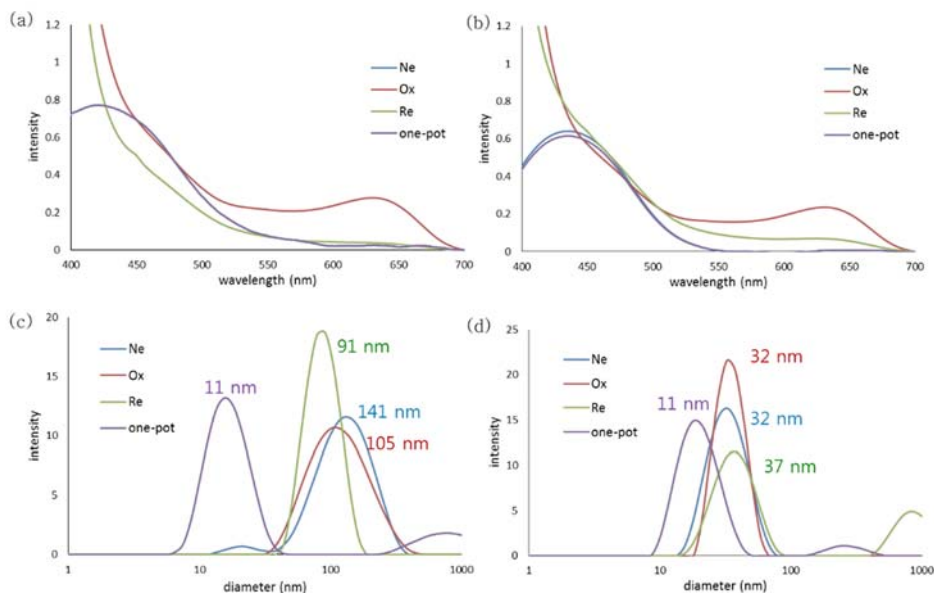


Figure 5–17. (a,b) UV/vis spectrum and (c,d) DLS profile of copolymers in THF. (a,c) poly(17)–*b,g*–(20) and (b,c) poly(32)–*b,g*–(20).

The nanostructure change of block copolymers with redox reaction in THF solution was visualized by AFM imaging technique on mica (Figure 5–18). Irregularly aggregated spheres were observed right after polymerization which induce the bad solubility. The detailed structure was investigated by high resolution AFM (Figure 5–19); one big sphere consist of many numbers of small spheres. After the oxidation, more well–defined micelle is formed due to the increased hydrophilicity of Fc block, and the nanostructure was changed again after reduction; longer and more densely packed cylindrical nanostructure was formed for both block copolymers. Hydrophilic Fc^+ induce tight aggregation of core part to minimize unfavored interaction with solvent and more undulated or sphere micelle is formed after oxidation. In contrast, Fc is recovered after reduction and loosely aggregated core can interact with another core from neighbor micelles, result in the formation of cylindrical micelles.

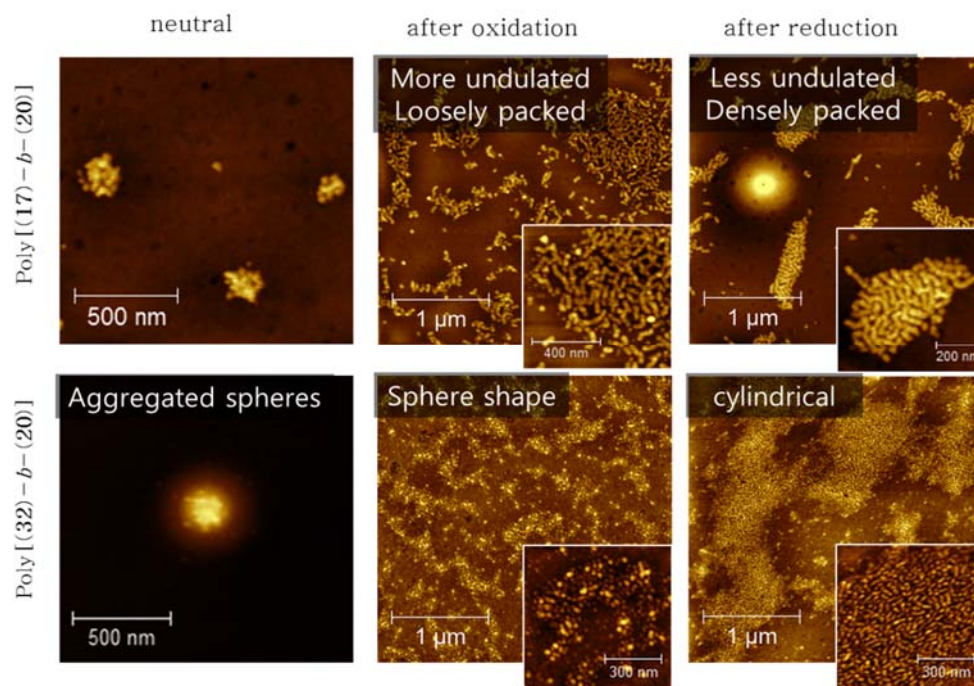


Figure 5–18. AFM image of Fc BCPs after redox reaction in the THF solution.

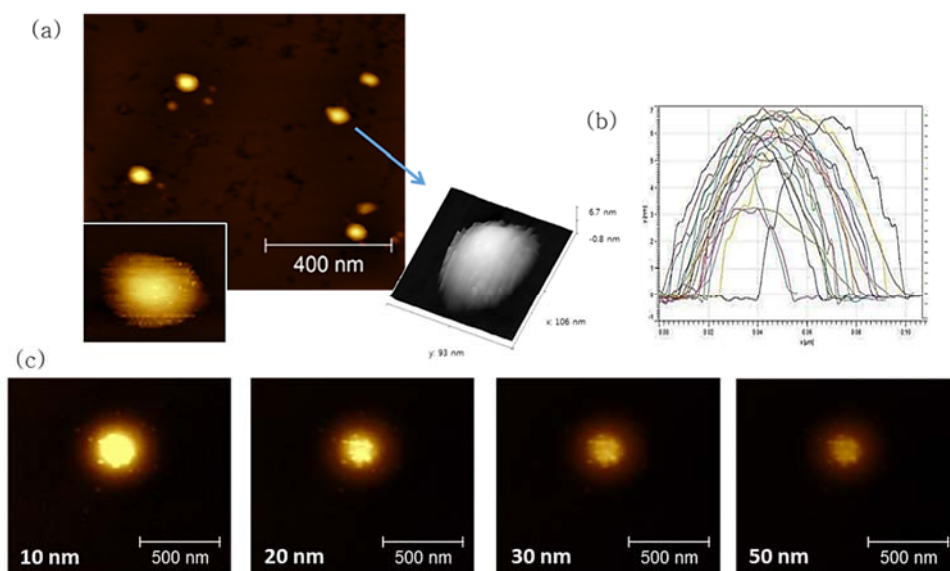


Figure 5-19. AFM image of poly(32)-*b*-poly(20) for detailed microstructure from the THF solution. (a) topography (b) 3D profile (c) image change with different maximum height.

The nanostructure change was observed more clearly by using TEM image on carbon coated copper grid. The shape of nanostructure was not completely same with AFM image owing to the different surface character between polar mica and nonpolar carbon coated copper grid substrate. The aggregated sphere and cylindrical micelle from poly(17)-*b*-poly(20) and poly(32)-*b*-poly(20), respectively, was divided in spheres after oxidation. This nanostructure shape returned to the cylindrical micelle after reduction reversibly. This result demonstrates that the self-assembly of block copolymer was controlled by redox reaction of ferrocene as a stimulus, which presumably enable us to develop a new redox-active functional polymer.

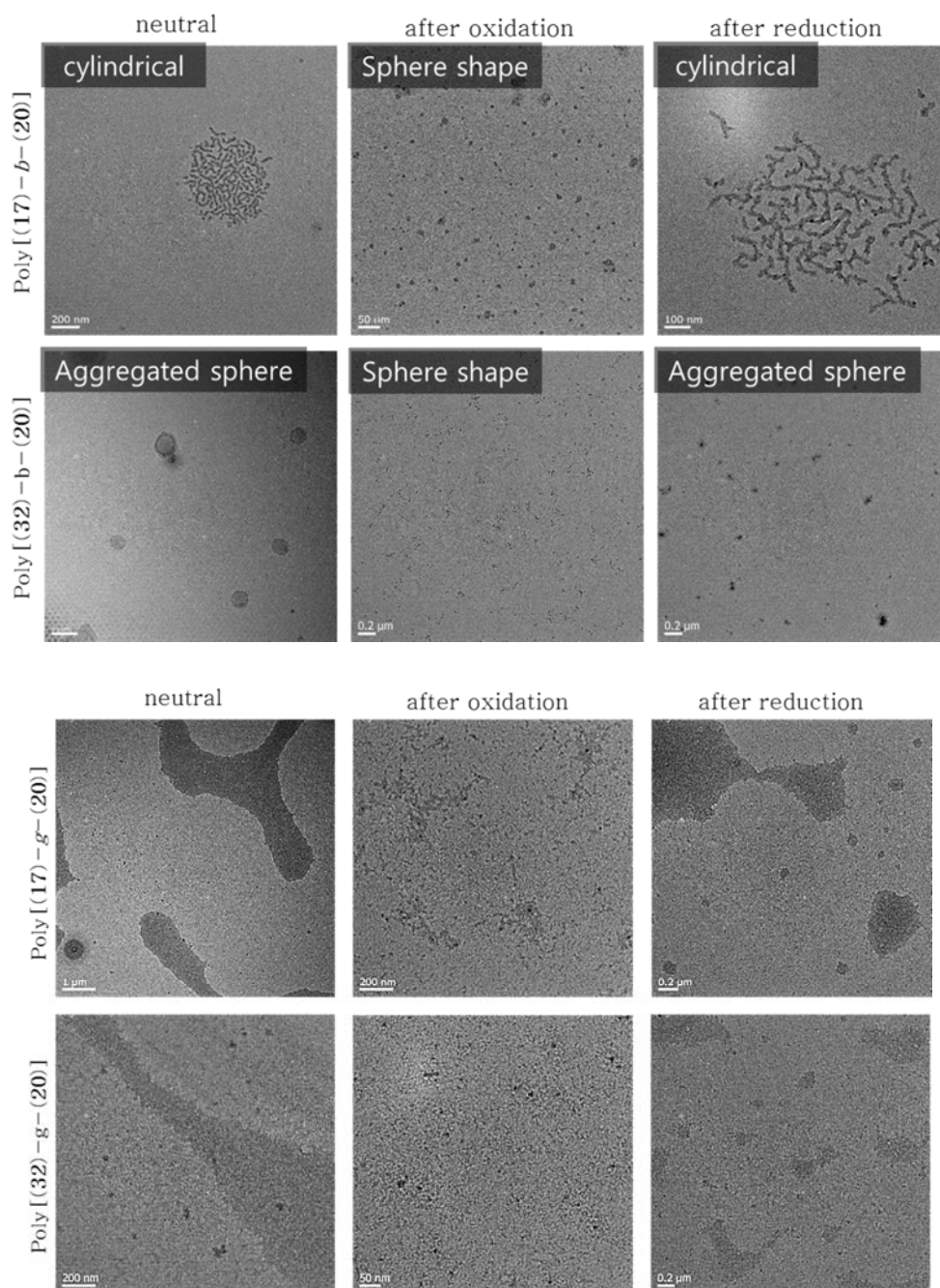


Figure 5-20. TEM image of copolymers containing ferrocene after redox reaction from the THF solution.

5.4 Conclusion

We prepared various kinds of block copolymers by ROMP including dendrons, polyacetylene, and ferrocene. All the polymerization were done in controlled manner, and the resulting polymer showed self-assembly behavior. Those self-assembled nanostructures were characterized by various techniques including ^1H NMR, DLS, and UV/vis spectroscopy. In the case of dendronized block copolymer having extended conformation and huge polarity difference between two blocks, sphere or cylindrical micelle was formed with solvent and substrate dependency. The size of structure was larger than common polymer self-assemblies due to the large dendrons, and the film morphology could be changed by thermal annealing under comparatively mild condition. In contrast, the self-assembly of block copolymer containing PA block didn't show solvent or substrate dependency, and thermally/mechanically stable nanostructure was formed. This self-assembly was achieved during the polymerization by *in situ* nanoparticlization of conjugated polymer (INCP). It started from the sphere shape and grew to the unique caterpillar structure (nanocaterpillars) with elongation of PA block length. Similarly, the block copolymer containing ferrocene moiety showed *in situ* nanoparticlization during the polymerization, but irregular assembly. However, more defined and reversible self-assembly was achieved after the redox reaction of ferrocene, as a stimulus, may provide a versatile tool to control the self-assembly. The detailed nanostructure of self-assemblies were investigated by using AFM and TEM imaging techniques.

5.5 References

- [1] (a) Nagarajan, R.; Ganesh, K. *Macromolecules*, **1989**, *22*, 4312. (b) Son, J. G.; Chang, J.-B.; Berggren, K. K.; Ross, C. A. *Nano Lett.* **2011**, *11*, 5079. (c) Ploetz, C. D.; Greer, S. C. *Langmuir*, **2009**, *25*, 13402.
- [2] (a) Mai, Y.; Eisenberg, A. *Chem. Soc. Rev.*, **2012**, *41*, 5969. (b) Luo, M.; Epps, T. H. *Macromolecules* **2013**, *46*, 7567. (c) Sanson, C.; Diou, O.; Thévenot, J.; Ibarboure, E.; Soum, A.; Brûlet, A.; Miraux, S.; Thiaudiere, E.; Tan, S.; Brisson, A.; Dupuis, V.; Sandre, O.; Lecommandoux, S. *ACS Nano*, **2011**, *5*, 1122. (d) Broz, P.; Driamov, S.; Ziegler, J.; Ben-Haim, J.; Marsch, S.; Meier, W.; Hunziker, P. *Nano Lett.*, **2006**, *6*, 2349.
- [3] (a) Braun, J.; Bruns, N.; Pfohl, T.; Meier, W. *Macromol. Chem. Phys.*, **2011**, *212*, 1245. (b) Zhang, L.; Eisenberg, A. *Science*, **1995**, *268*, 1728. (c) Cho, H. S.; Park, H. M.; Park, S. J.; Choi, H. Y.; Huang, H.; Chang, T. H. *J. Coll. Inter. Sci.*, **2011**, *356*, 1. (d) Cheng, C. X.; Tian, Y.; Shi, Y. Q.; Tang, R. P.; Xi, F. *Langmuir*, **2005**, *21*, 6576. (e) Koh, H. -D.; Park, J. -W.; Rahman, M. S.; Changez, M.; Lee, J. -S. *Chem. Commun.*, **2009**, *32*, 4824.
- [4] Miyake, G. M.; Weitekamp, R. A.; Piunova, V. A.; Grubbs, R. H. *J. Am. Chem. Soc.* **2012**, *134*, 14249.
- [5] (a) Cui, H.; Chen, Z.; Zhong, S.; Wooley, K. L.; Pochan, D. J. *Science*, **2007**, *317*, 647. (b) Li, Z.; Ma, J.; Lee, N. S.; Wooley, K. L. *J. Am. Chem. Soc.* **2011**, *133*, 1228. (c) Patra, S. K.; Ahmed, R.; Whittell, G. R.; Lunn, D. J.; Dunphy, E. L.; Winnik, M. A.; Manners, I. *J. Am. Chem. Soc.* **2011**, *133*, 8842. (d) Bhargava, P.; Tu, Y.; Zheng, J. X.; Xiong, H.; Quirk, R. P.; Cheng, S. Z. D. *J. Am. Chem. Soc.* **2007**, *129*, 1113.
- [6] (a) Li, Y.; Armes, S. P. *Angew. Chem., Int. Ed.* **2010**, *49*, 4042. (b) Sugihara, S.; Blanazs, A.; Armes, S. P.; Ryan, A. J.; Lewis, A. L. *J. Am. Chem. Soc.* **2011**, *133*, 15707. (c) Blanazs, A.; Madsen, J.; Battaglia, G.; Ryan, A. J.; Armes, S. P. *J. Am. Chem. Soc.* **2011**, *133*, 16581.
- [7] Ma, Q.; Remsen, E. E.; Clark, C. G.; Kowalewski, T.; Wooley, K. L. *Proc. Natl. Acad. Sci. U.S.A.* **2002**, *99*, 5058.
- [8] (a) Grayson, S. M.; Fréchet, J. M. J. *J. Am. Chem. Soc.* **2000**, *122*, 10335. (b) Hong, D. -J.; Lee, E.; Lee, J. -K.; Zin, W. -C.; Han, M.; Sim, E.; Lee, M. *J. Am. Chem. Soc.* **2008**, *130*, 14448.

- [9] (a) Shirakawa, H. *Angew. Chem., Int. Ed.* **2001**, *40*, 2574. (b) Etemad, S.; Heeger, A. *Annu. Rev. Phys. Chem.* **1982**, *33*, 443.
- [10] (a) Scherman, O. A.; Grubbs, R. H. *Synth. Met.* **2001**, *124*, 431. (b) Edwards, J. H.; Feast, W. *J. Polymer*, **1980**, *21*, 595. (c) Swager, T. M.; Dougherty, D. A.; Grubbs, R. H. *J. Am. Chem. Soc.* **1988**, *110*, 2973. (d) Wu, C.; Niu, A.; Leung, L. M.; Lam, T. *J. Am. Chem. Soc.* **1999**, *121*, 1954.
- [11] (a) Scherman, O. A.; Rutenberg, I. M.; Grubbs, R. H. *J. Am. Chem. Soc.* **2003**, *125*, 8515. (b) Mahmoud, A. *Synth. Met.* **1986**, *13*, 87.
- [12] Klavetter, F. L.; Grubbs, R. H. *J. Am. Chem. Soc.* **1988**, *110*, 7807.
- [13] Yoshino, K. *Synth. Met.* **1989**, *28*, 669.
- [14] Kaner, R. B.; Porter, S. J.; Nairns, D. P.; MacDiarmid, A. G. *J. Chem. Phys.* **1989**, *90*, 5102.
- [15] Jain, S.; Bates, F. S. *Science*, **2003**, *300*, 460.
- [16] (a) Gilroy, J. B.; Gaudt, T.; Whittell, G. R.; Chabanne, L.; Mitchels, J. M.; Richardson, R. M.; Winnik, M. A.; Manners, I. *Nat. Chem.* **2010**, *2*, 566. (b) Xiaosong, W.; Guerin, G.; Hal, W.; Yishan, W.; Manners, I.; Winnik, M. A. *Science*, **2007**, *317*, 644.
- [17] (a) Adhikari, B.; Kraatz, H. –B. *Chem. commun.*, **2014**, *50*, 5551. (b) Togni, A. “*Ferrocenes:homogeneous catalysis, organic synthesis, materials science.*” Wiley–VCH, **1995**. (c) Pauly, A. C.; Varnado Jr, C. D.; Bielawski, C. W.; Theato, P. *Macromol. Rapid. Commun.*, **2014**, *35*, 210.
- [18] Xiao, Z. –P.; Cai, Z. –H.; Liang, H.; Lu, J. *J. Mater. Chem.*, **2010**, *20*, 8375.

정확한 구조를 가지는 고분자 합성을 위한 제어된 고리개환복분해중합

김 경 오

화학과 유기화학 전공

서울대학교 대학원

고리개환복분해중합반응 (ROMP)은 정확한 구조와 다양한 작용기를 가지는 고분자 합성에 가장 널리 쓰이는 중합방법 중 하나이다. 이 반응의 장점 중 하나는 리빙/제어된 중합이 가능하다는 것이다. 이 점을 이용하여, 정확한 구조를 가지는 다양한 고분자 합성에 대한 연구가 많이 이루어져왔다. 그러나 합성 가능한 단량체 범위나 더 복잡한 구조를 가지는 고분자 합성과 관련하여 여전히 많은 부분에도전과제가 남아있다.

이 학위논문에서는 제어된 고리개환복분해중합반응을 이용하여 정확한 구조를 가지는 고분자를 합성하고 그들의 나노크기를 가지는 물질로서의 가능성을 설명하고 있다. 먼저, 덴드론화 고분자의 덴드론 크기, 연결부위, 주사슬 구조를 바꾸어 줌으로써 형태 제어를 시도하였다. 단일사슬의 구조는 다각도광산란 (MALLS)기법을 통해 분석하고, 원자간력 현미경 (AFM)을 통해 가시화 되었다. 그 결과, 5세대의 큰 덴드론이나 TD기반의 단량체가 사용되었을 때 막대형태의 구조가 관찰되었고, 모든 중합은 리빙중합의 성질을 띠었다. 이러한 NB와 TD 단량체들의 리빙중합을 이용하여, 블록공중합체와 그레디언트 공중합체의 중합이 각각 순차적인 단량체의 주입과 batch 방법을 통해 이루어졌다. 얻어진 두 공중합체는 경계선의 유무라는 분명한 구조적 차이점을 원자간력 현미경 이미지로부터 보여주었다. 이 결과는

고리개환복분중합반응과 batch 방법을 이용한 그레디언트 공중합체의 첫 번째 성공적 합성 예로, 두 단량체간의 반응성 차이 때문에 가능하였다. 반응속도론적 연구에 따르면, TD 단량체가 NB에 비해 빠른 개시속도와 느린 전파속도를 가지고 있다. 이는 개시속도와 전파속도 비율의 증가로 귀결되어 느린 개시반응을 하지만 더 안정한 촉매로 알려진 2세대 그럽스 촉매나 호베이다-그럽스 촉매로도 리빙중합이 가능하게 한다. 이 점을 이용하여, 3개의 팔을 가지는 별 형태 고분자의 합성이 core-first 방법과 고리개환복분해중합을 통해 처음으로 이루어졌다. 또한, 알카인 작용기를 가지는 단량체의 제어된 중합도 보호그룹 없이 이루어질 수 있었다. 마지막으로, NB와 TD를 기반으로 하는 단량체들과 리빙ROMP로 다양한 블록공중합체를 합성하여 고분자 나노구조를 형성하였다. 텐드론화 블록공중합체는 길게 펼쳐진 구조와 텐드론에 의한 큰 크기를 가지고 있어 넓은 영역을 가지는 구조가 비교적 온화한 조건에서 얻어졌다. 폴리아세틸렌블록을 가지는 공중합체는 컨쥬게이션된 고분자간의 $\pi-\pi$ 상호작용에 의해 형성된 열적/기계적으로 안정한 나노에벌레 구조를 보여주었다. 또한, 페로센 그룹을 가지는 블록공중합체로부터 산화환원반응에 반응하는 자기조립체를 얻을 수 있었다.

주요단어

고리개환 복분해 중합, 리빙중합, 텐드론화 고분자, 고분자 단일체인의 조, 고분자 나노구조

학번

2010-30089

Abstract in German

Kontrollierte ROMP für die Synthese von Polymeren mit genauen Strukturen

Ringöffnungsmetathese–Polymerisation (ROMP) ist eine der beliebtesten Methoden um definierte Polymere mit verschiedenen Funktionalitäten herzustellen. Ein Vorteil von ROMP ist, dass lebende Polymerisation (kontrollierte Polymerisation) möglich ist. In diesem Punkt wurde intensive Forschung betrieben um verschiedene Polymere mit genauen Strukturen zu synthetisieren. Jedoch müssen noch einige Hürden wie die Einführung neuer funktioneller Monomere oder die Entwicklung noch komplexerer Nanostrukturen überwunden werden.

Diese Arbeit beschreibt die Synthese von Polymeren mit definierten Strukturen durch ROMP, mit der Möglichkeit diese in Nanogröße herzustellen. Zuerst wurde die Konformation durch den Austausch der Generationen der Dendronen, der Linker Gruppen und des Polymerrückgrats der dendritischen Polymeren verändert. Die Konformation der Einfachkette wurde durch Mehrwinkel–Lichtstreuung (MALLS) analysiert und durch das Rasterkraftmikroskop (AFM) visuell dargestellt. Als Ergebnis wurde durch die Verwendung von Dendronen in einer höheren Generation (G5) und TD basierte Makromonomere steife, stäbchenförmige Konformationen erhalten. Des Weiteren zeigten die Homopolymerisationen typischen Charakter einer lebenden Polymerisation. Durch die Nutzung der lebenden ROMP der NB und TD Monomere konnte mittels der üblichen sequentiellen

Additionsmethode und dem Batch-Verfahren Block- und Gradientencopolymere synthetisiert werden. Die resultierenden Copolymere zeigten in den AFM Abbildungen deutliche strukturelle Unterschiede in der Existenz von Grenzflächen. Diese erfolgreiche und erstmalig durchgeführte Synthese von Gradientencopolymere mit dem Batch-Verfahren über ROMP war möglich aufgrund der verschiedenen Reaktivitäten zwischen den beiden Monomeren. Gemäß kinetischen Untersuchungen initiieren TD Monomere schneller und das Wachstum ist langsamer verglichen mit den üblichen NB Monomeren. Die TD Monomere erhöhen das k_i/k_p Verhältnis und ermöglichen somit die kontrollierte ROMP sogar mit dem langsam initiierenden aber stabileren Grubbs-Katalysator der 2ten Generation oder dem Hoveyda-Grubbs-Katalysator. Mit diesem Vorteil wurde erstmals mittels der „core first“ Methode über ROMP Drei-Arm Stern-Polymere synthetisiert. Ferner konnte ein Monomer welches eine Alkynylgruppe beinhaltet durch kontrollierte ROMP synthetisiert werden. Aufgrund der schnellen Initiation der TD Monomere war dies ohne Schutzgruppen möglich. Schließlich wurden verschiedene Blockcopolymere (BCP) durch lebende ROMP von NB und TD basierten Monomeren hergestellt, um polymere Nanostrukturen zu erhalten. Mit dendritischen Blockcopolymeren, synthetisiert unter verhältnismäßig milden Bedingungen aufgrund der ausgedehnten Konformation und Größe der Dendronen, wurden große Nanostrukturen erhalten. Im Fall von BCP mit einem PA Block wurden aufgrund der starken $\pi-\pi$ Wechselwirkungen zwischen den konjugierten Polymeren thermisch/mechanisch stabile „nanocaterpillar“-Strukturen erhalten. Des Weiteren konnte vom BCP mit Ferrocen als funktionelle Gruppe redoxsensitive Selbstorganisation gezeigt werden.

Publications

- [1] **K. O. Kim**, T. -L. Choi, *ACS Macro Lett.* **2012**, *1*, 445. "Synthesis of Rod-Like Dendronized Polymers Containing G4 and G5 Ester Dendrons via Macromonomer Approach by Living ROMP"
- [2] **K. O. Kim**, T. -L. Choi, *Macromolecules* **2013**, *46*, 5905. "Synthesis of Dendronized Polymers via Macromonomer Approach by Living ROMP and Their Characterization: From Rod-Like Homopolymers to Block and Gradient Copolymers"
- [3] **K. O. Kim**, S. Y. Shin, J. Y. Kim, T. -L. Choi, *Macromolecules* **2014**, *47*, 1351. "Living Polymerization of Monomers Containing *endo*-Tricyclo[4.2.2.0^{2,5}]deca-3,9-diene Using 2nd Generation Grubbs and Hoveyda-Grubbs Catalysts: Approach to synthesis of star polymer"
- [4] **K. O. Kim**, J. L. Kim, T. -L. Choi, *Macromolecules* **2014**, 10.1021/ma500877n. "Controlled Ring-Opening Metathesis Polymerization of a Monomer Containing Terminal Alkyne and its Versatile Post-functionalization via Click Reaction"
- [5] K. Y. Yoon, I. H. Lee, **K. O. Kim**, J. Jang, E. Lee, T. -L. Choi, *J. Am. Chem. Soc.* **2012**, *134*, 14291. "One-pot *in situ* Fabrication of Stable Nanocaterpillars Directly from Polyacetylene Diblock Copolymers Synthesized by Mild Ring-Opening Metathesis Polymerization"
- [6] K. H. Yoon, **K. O. Kim**, C. Wang, I. Park, Do. Y. Yoon, *J. Polym. Sci. Part A. Poly. Chem.* **2012**, *50*, 3914. "Synthesis and Structure-Property Comparisons of Hydrogenated Poly(oxa norbornene-imide)s and Poly(norbornene-imide)s Prepared by Ring-Opening Metathesis Polymerization"
- [7] K. H. Yoon, **K. O. Kim**, M. Schaefer, Do. Y. Yoon, *Polymer* **2012**, *53*, 2290. "Synthesis and characterization of hydrogenated poly(norbornene *endo*-dicarboximide)s prepared by ring opening metathesis polymerization"